UNIVERSIDADE DE LISBOA
FACULDADE DE CIÊNCIAS
DEPARTAMENTO DE FÍSICA

High accuracy absolute distance sensor

Nuno Miguel Cabecinhas Gonçalves

Mestrado Integrado em Engenharia Física

Dissertação orientada por:
Prof. Dr. Manuel Abreu
Dr. David Castro Alves

2020

Agradecimentos

Em primeiro lugar, gostaria de agradecer aos meus orientadores, Prof. Dr. Manuel Abreu e ao Dr. David Castro Alves, pela sua infinita paciência e disponibilidade para partilharem o seu imenso conhecimento acerca deste tema comigo. Adicionalmente, agradeço também, por terem sempre entendido o meu objetivo em relação a este trabalho e quando as coisas correram mal, conseguiram sempre me apontar no caminho certo. Por todos os ensinamentos que me deram em relação a este projeto, tiro também lições de como enfrentar o futuro que se aproxima, e por isso estar-vos-ei eternamente agradecido.

Gostaria também de agradecer a toda a equipa do Laboratório de Ótica Lasers e Sistemas do Departamento de Física da Faculdade de Ciências da Universidade de Lisboa. Em especial ao Sr. Fernando Monteiro e ao Sr. António Oliveira, que sempre estiveram presentes para me ajudar nas alturas mais difíceis e frustrantes deste trabalho. Como por exemplo quando o primeiro laser se estragou e foram imensos os esforços para o recuperar. Destaco também a ajuda do Prof. Dr. Alexandre Cabral que esteve sempre disponível para discutir e dar uma segunda opinião, a quem deixo o meu obrigado. Adicionalmente destaco também o Cédric Pereira pela imensa paciência em ler este documento diversas vezes e ajudar-me sempre a melhorá-lo.

Não poderia deixar de agradecer todo o apoio dado pela minha família, em especial à minha mãe, Teresa Cabecinhas, irmã Ana Gonçalves e ao Manuel e Ricardo. Sem o vosso apoio, paciência e amor incondicional nada disto seria possível. Apoiaram-me nas horas mais difíceis e sempre me permitiram seguir os meus sonhos. Agradeço-vos eternamente e incondicionalmente por isso.

Agradeço em especial à Natália Marques, por todo o seu amor, carinho e ajuda dada durante a escrita desta tese. Foste o meu porto de abrigo quando tudo parecia que não estava a correr bem, no entanto tiveste sempre a paciência e compreensão para me incentivar a ir pelo caminho certo. Sem ti cumprir os objetivos deste trabalho teria sido muito mais difícil. Gostaria também de destacar e agradecer toda a ajuda da família Marques neste processo, muito obrigado.

Por último, mas não menos importante, agradeço a todos os meus amigos que de uma forma ou outra contribuíram para me ajudarem a realizar este trabalho. Este contributo passou por me darem motivação e permitirem-me desabafar quando mais precisava, até me fazerem companhia nas imensas noites passadas na faculdade a trabalhar neste documento. O meu obrigado.

Abstract

Optical measuring systems offer new ways to determine absolute or relative distance measurements, dubbed as ADM, or RDM, respectively. These systems allow the determination of distances, deformations, or vibrations through accurate and high resolution optical techniques. These techniques are non-contact processes that can have a wide array of applications, from industrial measuring devices to aerospace equipment.

Therefore, the goal of the present dissertation was to develop and test a high accuracy absolute distance sensor, based on optical processes that could perform an ADM within a [10, 20] m range with an expanded uncertainty, $U_D < 100$ μm.

In this work, an assessment of the state of the art of the different optical measuring techniques was conducted to evaluate which method allow reaching the established requirements. After this analysis, the phase shift continuous wave time of flight technique was chosen.

To measure a distance using this method, a coherent light source is continuously amplitude modulated by a sinusoidal signal. The difference in the phase angle of the signal in the source and its reflection on a target contains the time of flight information. Therefore, the ADM between source and target can be obtained by a phase shift measurement. Due to the cyclical properties of the phase angle, the position information is contained within an ambiguity interval. To perform distance measurements, we must consider the number of times the ambiguity interval is repeated, N, plus the fraction part of this interval given by the unwrapped phase shift.

It has been already reported by several authors referenced in this document that this technique can achieve distance measurement accuracies in the order of 100 μm for modulation frequencies in the GHz range. However, to perform an ADM with these frequencies, the ambiguity integer, N, in a phase measurement has to be obtained.

In this context, we developed an adaptation of the Vernier method to remove the ambiguity in a phase shift measurement. It consists of performing a dual phase shift measurement for two different modulation frequencies. However, to measure its ambiguity integer correctly, one must determine it with an expanded uncertainty of $U_N < 0.5$.

We performed Monte Carlo and analytical computational simulations to evaluate the maximum magnitude of the uncertainty contributions for an ambiguity integer and ADM in a [10, 20] m range. To verify the validity of the proposed Vernier approach for ADM an experimental setup was devised and built whilst satisfying the established uncertainty requirements.

Finally, the method was tested by performing ADM at a short and mid range, [0, 100] mm and [4.808, 4.818] m, respectively and with a "blind measurement", where the target was placed at ≈ 2 m. We were able to verify that for the different test ranges, the developed sensor was able to correctly measure most of the ambiguity integer correspondent to the tested positions. Additionally, the N measurements in the short range prove that the presented method can detect a change in the ambiguity integer.

However, these tests reveal that in some situations the sensor was not able to measure the correct

ambiguity integer for the tested position, which leads to an incorrect ADM. By considering the erroneous N measurements as an outlier in our evaluation, it is possible to extract a calibration curve that corrects the scale and offset in our results. When performing a correction of the measured values, for the short and mid range tests, we obtained an average experimental absolute error of 126 μm and 256 μm, respectively, computed for a 1.8 GHz modulation. These results are within an expanded uncertainty of $\approx$ 600 μm with a coverage factor of k = 2, this means a confidence interval of 95 $\%$.

Keywords: absolute distance measurements, time of flight, phase shift, optical metrology, high accuracy, heterodyne.

Resumo

Os sistemas de metrologia baseados em processos ópticos oferecem novas formas de determinar distâncias absolutas ou relativas, apelidadas de ADM ou RDM, respetivamente (do inglês *Absolute/Relative distance measurements*). Estes sistemas permitem a determinação de distâncias, deformações, ou vibrações com elevada exatidão e resolução. As técnicas ópticas são processos sem contacto que abrangem uma vasta gama de aplicações, desde dispositivos de medição industrial a equipamento aeroespacial.

O objetivo deste trabalho de dissertação é desenvolver e testar um sensor de medição de distâncias absolutas com elevada exatidão, baseado em processos ópticos, de modo a realizar uma ADM dentro de um alcance de [10, 20] m, com uma incerteza expandida de $U_D < 100$ μm.

Neste trabalho foi realizada uma apreciação do estado da arte das diferentes técnicas de medição óptica para avaliar quais as que permitem alcançar os requisitos estabelecidos. Os três métodos mais comuns utilizados em sistemas de medição de distâncias absolutas ou relativas são: triangulação, tempo de voo e interferometria. Os alcances máximos e a sua relação com a incerteza da medição foram analisados para cada um dos métodos referidos. Decorrente desta apreciação, foi escolhido um método baseado no tempo de voo no qual um sinal óptico é continuamente modulado em amplitude.

Para medir uma distância utilizando este método, uma fonte de luz coerente é continuamente modulada em amplitude por um sinal sinusoidal. A diferença no ângulo de fase do sinal na fonte e na sua reflexão sobre um alvo contém a informação do tempo de voo. Portanto a ADM entre a fonte e o alvo pode ser obtida através de uma medição da diferença de fase entre ambos os sinais. Devido às propriedades cíclicas do ângulo de fase, a informação da posição está contida dentro de um intervalo de ambiguidade. Ao realizar medições de distâncias superiores a este intervalo, devemos considerar no resultado o número de vezes, N, em que este se repete mais a parte fracionária que é dada pela diferença de fase.

Já foi relatado por vários autores, referenciados neste documento, que esta técnica pode atingir incertezas de medição de distâncias na ordem dos 100 μm, para frequências de modulação na gama dos GHz. No entanto, para realizar uma ADM com estas frequências, é necessário obter o número inteiro de ambiguidade, N, numa medição de fase. Caso contrário estaríamos limitados a realizar medições absolutas num intervalo na magnitude do cm.

Neste contexto, e para remover a ambiguidade numa medição de diferença de fase, desenvolvemos uma adaptação do método de Vernier. Esta adaptação consiste em realizar duas medições de diferença de fase para duas frequências de modulação diferentes. Estas frequências estão separadas por um Δf que é correspondente ao intervalo de distâncias em que é suposto o sensor operar. Contudo e para medir corretamente o número de ambiguidade, que é um número inteiro, é necessário determiná-lo com uma incerteza expandida de $U_N < 0.5$.

Para avaliar a magnitude máxima das contribuições para o balanço de incertezas da medição do número de ambiguidade e ADM num intervalo de [10, 20] m, realizámos simulações computacionais

de Monte Carlo e analíticas. Com o resultado destas verificámos que utilizando uma frequência de modulação de 3 GHz e um $\Delta f = 14.8$ MHz, seria possível atingir o requisito de incerteza para uma ADM com $U_D < 100$ μm, no intervalo pretendido.

Para verificar a validade da abordagem de Vernier proposta, foi concebida e construída uma montagem experimental, que consegue satisfazer os requisitos de incerteza estabelecidos. De forma a conseguir detetar o sinal com uma frequência de modulação na ordem dos GHz, deve ser utilizada instrumentação apropriada que consiga lidar com estas taxas de repetição de sinal. Esta aumenta a complexidade e o custo da montagem experimental, o que apresenta uma desvantagem no uso destas frequências.

No entanto, existem formas de contornar este problema de instrumentação. A solução mais eficaz é utilizar a técnica de heterodinagem, que permite misturar dois sinais elétricos de frequências diferentes. O output deste processo será um sinal com a soma e a subtração das frequências dos sinais originais. Apesar desta característica ser alterada, a informação da fase dos sinais originais é mantida. Desta forma, filtrando as altas frequências no sinal de output é possível obter um sinal em que a sua frequência seja a diferença das originais com a informação de fase das mesmas.

Esta técnica torna possível o uso de um oscilador local (LO, do inglês *Local Oscillator*) de frequência bem definida. Ao utilizar dois processos de heterodinagem, o LO é misturado com um sinal de radio frequência (RF, do inglês *Radio Frequency*) responsável por modular a fonte de luz e novamente com o sinal medido pelo fotodíodo. Ao comparar a fase dos sinais resultantes destes processos de mistura, é possível medir a diferença de fase entre o sinal que modela o laser e a sua reflexão num alvo. O facto de a frequência destes sinais ter uma magnitude mais reduzida permite que instrumentação facilmente acessível no laboratório possa ser utilizada para aplicar o método desenvolvido.

Inicialmente pretendíamos utilizar um laser díodo que tolerasse uma modulação em amplitude de 3 GHz. No entanto, ocorreu um acidente com a fonte de luz modulável a 3 GHz, que não permitiu que a utilizássemos na montagem experimental. Em consequência, tivemos que recorrer a uma outra fonte de luz coerente disponível no laboratório. Todavia, esta tinha uma frequência de modulação inferior à original, pelo que a montagem experimental teve que ser adaptada a esta nova fonte. Repetimos as simulações computacionais e verificámos que não iria ser possível atingir o requisito de $U_D < 100$ μm.

Adicionalmente, estava planeado utilizar um carril de ar com deslocamentos calibrados de forma a testar o sensor para o intervalo de [10, 20] m. No entanto não conseguimos utilizar este instrumento e, por isso, com o material disponível no laboratório realizámos medições num intervalo de [0, 5] m.

O método proposto foi testado executando ADM num intervalo de curto e médio alcance, [0, 100] mm e [4,808, 4,818] m, respetivamente. Inclusive realizámos uma "medição às cegas", onde o alvo foi colocado a ≈ 2 m. Conseguimos verificar que para os diferentes intervalos de teste, o sensor desenvolvido foi capaz de medir corretamente a maior parte dos valores de ambiguidade correspondentes às posições testadas. Além disso, as medições de N no intervalo de curto alcance provam que o método apresentado consegue detetar uma alteração do número de ambiguidade.

Contudo, os testes realizados revelam que em algumas situações o sensor não foi capaz de medir o número de ambiguidade correto para a posição testada, o que leva a uma ADM incorreta. Ao considerar as medições erradas de N como um *outlier* na nossa avaliação, é possível extrair uma curva de calibração que permite corrigir a escala e compensar os nossos resultados. Ao realizar essa correção dos valores medidos, obtivemos, em média, um erro experimental absoluto de 126 μm e 256 μm, calculados para uma modulação de 1.8 GHz nos testes de curto e médio alcance, respetivamente. Estes valores estão contidos num intervalo de incerteza expandida de magnitude ≈ 600 μm, com um factor de expansão de $k = 2$, o que corresponde a um intervalo de confiança de 95 $\%$.

Palavras-chave: Medição de distâncias absolutas, tempo de voo, diferença de fase, metrologia óptica, heterodinagem.

Contents

List of Figures

List of Tables

List of Abbreviations and Symbols

List of Abbreviations

ADM	Absolute Distance Measurement
RDM	Relative Distance Measurement
TOF	Time of Flight
PS	Phase Shift
PS CW TOF	Phase Shift Continuous Wave Time of Flight
RF	Radio Frequency
LO	Local Oscillator
IF	Intermediate Frequency

List of Symbols

c = 3 $\times 10^8$	Speed of light in vacuum
n = 1.000268148	Air refractive index calculated with the NIST metrology toolbox [1] with Ciddor Equation and the parameters: λ_{vac} =1550 nm, $T_{ambiente}$ = 20 ºC, P = 101.325 kPa, $RelativeHumidity$ =50%.
$\Delta\phi$	Phase shift
N	Ambiguity integer

Chapter 1

Introduction

Optical measuring systems offer new ways to determine absolute or relative distance measurements, ADM, or RDM, respectively. These systems allow the determination of distances, deformations, or vibrations through accurate and high resolution optical techniques. These can have a wide array of applications, from industrial measuring devices to aerospace equipment.

On the industrial side, high precision engineering RDM and ADM are used to measure a machine's axis positions in an assembly line or to measure a product dimension or shape with μm accuracy for targets in the [10, 100] m scale [2]. Being optical techniques non-contact processes, they are highly attractive to be used in an industrial context for control and maintenance reasons.

There is also a need for accurate distance measurements in several space missions, either for internal measurements in the spacecraft or for formation flying, where the satellite's relative position is actively controlled. As an example, the European Space Agency (ESA) DARWIN mission consisted of four to five satellites with telescopes flying in formation, separated in distances up to 200 m [3].

The study of this type of system was natural to occur in the Laboratory of Optics, Lasers, and Systems (LOLS) in the Department of Physics of the Faculty of Sciences of the University of Lisbon. Since its integration with the Instituto de Astrofísica e Ciências do Espaço, it has been involved in several projects related to astronomical instrumentation, where ADM and RDM systems are required. Therefore, the theme for this dissertation was suggested with the aim to develop and test an optical measurement system for contactless ADM that could operate in a mid range, [10, 20] m, with an uncertainty ≤ 100 μm, with potential use in space application.

To carry out this work, a comparison of the state of the art of different optical measuring methods was conducted. This was crucial to understand the trade-offs of the different methods and also balance the feasibility of each of them with the available material in the laboratory. From this process, a phase shift continuous amplitude modulation time of flight (PS CW TOF) method was chosen. However, to perform ADM, the ambiguity in a phase measurement needed to be removed.

Therefore, a dedicated approach based on the Vernier method was applied to the PS CW TOF method, which lead to the development of a dual frequency method that allowed the removal of the phase shift ambiguity. Furthermore, an uncertainty analysis was performed based on the developed method, to understand what would be the maximum accuracy requirements in phase measurements and frequency stability, to achieve the goal of this work.

In this context, and to verify the validity of the proposed Vernier approach for ADM an experimental setup was devised and built. We verified that it was possible to achieve the established requirements, by performing the uncertainty budget for an ADM with the setup.

The developed Vernier approach was reported to the scientific community in the form of an oral

presentations at the *European Optical Society Annual Meeting* in September of 2020. Additionally, an article, appendix A, was published in the proceedings volume of the conference [4]

Despite not being possible to test the sensor in the [10, 20] m range, as we originally intended. We tested it in a [0, 5] m range with the available material in the laboratory.

However, while characterizing the experimental setup, our original light source suffered an accident and broke and a back up one had to be used. Due to the latter having a smaller modulation frequency than the original, the setup had to be modified to comply with it.

Due to the mentioned setbacks in the experimental work, we still tried to validate the presented mathematical model. Hence, ADM were carried out in a short range [0, 100] mm, in a mid range [0, 10] mm with an offset of ≈ 4.8 m and with a "blind measurement" of ≈ 2 m.

Due to the time limitation to perform this work, a brief evaluation of the noise sources was performed. In the performed measurements several erroneous ambiguity integer measurements were obtained, which leads to conclude that a more intensive characterization of the experimental setup was needed. Despite the measured ranges, the sensor's response to ADM in a full meter range sweep ([0, 5] m) was left undone.

Nevertheless, with the constructed sensor we were able to validate the proposed method by performing ADM that could accurately determine the test positions.

This dissertation is organized in 6 different chapters:

Ch. 1 - **Introduction** - Presents the motivation, the objectives, and the chosen approach for the dissertation work.

Ch. 2 - **Optical Measurement Techniques** - Provides the state of the art of optical measurement techniques, as well as the trade-off analysis between them.

Ch. 3 - **Phase Shift Time of Flight** - Shows an in-depth explanation of the Phase Shift Time of Flight method. Approaching the different methods to remove the ambiguity and explaining our developed solution for the problem. Additionally, two different uncertainty simulations methods were performed and their results were compared.

Ch. 4 - **Experimental Setup and Equipment** - Description of the built experimental setup and the technique on which it is based. Also, a characterization of the different used instruments is presented.

Ch. 5 - **Uncertainty Budget and Experimental Results** - Analysis of the uncertainty budget for a phase measurement and frequency stability with the built experimental setup. Also, the obtained results are presented and analyzed.

Ch. 6 - **Conclusions** - Summary of dissertation work, giving the final remarks and pointing some future work.

Chapter 2

Optical Measurement Techniques

Optical measurement techniques can be used for the determination of distances, deformations, or vibrations through accurate and high resolution optical techniques. These techniques are widely used in many fields and applications, and comprehensive reviews of the topic can be found in [5], [6], [7], [8] and [9].

The principle in optical range-finding techniques is to project a light signal that can efficiently propagate through a medium onto an object and analyze the reflected or scattered signal. For that purpose, electromagnetic waves in optical, infra-red, and radio regimes are used, due to their known characteristics and their predictable behaviour in a medium. Optical distance techniques can be found operating in different ranges: sub-meter ($<$ 1 m), mid-range [1, 100] m, and long-range ($>$ 100 m), although only a few can achieve a dozen of μm of accuracy in their corresponding ranges. There are three main techniques: triangulation, time of flight, and optical interferometry.

2.1 Triangulation

The triangulation technique is essentially a geometrical way to determine distances with an angular measurement, it is usually used to measure displacements. A light source projects a spot onto an object surface. The reflected light is collected by some optics and focused in a light position sensitive device (PSD), figure 2.1. The object displacement is measured along with the light source optical axis. If an object is displaced, then the light in the PSD will change its position proportionally.

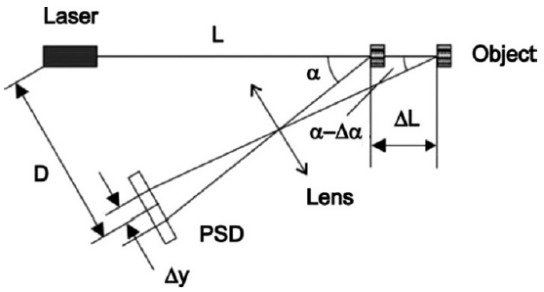

Figure 2.1: Triangulation technique typical scheme. **[10]**.

Commercially available sensors use a laser diode as the optical source and charged coupled devices (CCD) like the PSD, these are compact devices able to measure in a range from 10 mm to 1 m [5]. The resolution will depend on the laser beam size, the detection pixel size, and the target distance. Most commercially available sensors of this type operate in a range $<$ 1 m. State of the art sensors based on this technique, like the *Sick-DT20* close range sensor ($<$ 1 m), can achieve 1 mm resolution for its highest operating range [11].

Different variants of this method can be found in an assortment of contexts. For example, to measure the cantilever displacement, in the context of atomic force microscopy, a four-section photodiode is used

as the PSD and an 8 nm resolution has been reported [12]. These sorts of accuracies can be achieved for displacements in the magnitude of the unit of mm.

For ranges, $>$ 100 m, the triangulation method has accuracy problems due to the light source spot and the PSD resolution. The fact that the working ranges are directly proportional to the distance D, as seen in the figure 2.1, implies that the baseline will increase with the operating range, resulting in bulkier devices for mid and high-range applications [10, 100] m. This means that in applications where there is a limitation in space for the measuring device, this sensor has a substantial drawback.

2.2 Time of Flight

The Time of Flight (TOF) optical range-finders are based on the measurement of the time interval it takes for light to travel a given homogeneous medium from the source to detector. Since the light velocity depends on the medium's refractive index, n, one must consider the optical path length (OPL). In this work, we will always consider n, the air refractive index, and throughout this document, it was considered constant and equal to 1.000268148 for a wavelength in ambient air of 1550 nm, with an air temperature of 20 ºC, the atmospheric pressure of 101.325 kPa and relative air humidity of 50% – in accordance to the "Engineering Metrology Toolbox" provided by NIST [1].

The OPL between points A and B, in a medium with an index of refraction n, is defined as the distance a wave in a vacuum travels during the time interval Δt it takes light to travel from A to B in the actual medium, as described in [13]. Therefore, it is a proportion between the refractive index of the medium and the geometrical distance, D_{geo}, between the source and detector.

$$OPL = n \times D_{geo} = c \times \Delta t \tag{2.1}$$

Being c the speed of light in vacuum. The quantity of interest for distance measurements is D_{geo}, the euclidean distance between source-target. Hence, the TOF method can be performed with different techniques to quantify the time light takes to travel in a medium, all depending on how the electromagnetic wave is modulated. Based on this, one can roughly divide the TOF methods on whether the light source is pulsed or modulated continuously in frequency (FM) or amplitude (AM).

2.2.1 Pulsed TOF

A pulse TOF range-finder measures the time interval between two optical pulses to obtain an absolute distance measurement. A start pulse will trigger the start of a clock in a timing discriminator, then the detected signal in the target will stop it. If the target has a detection device then the distance is equivalent to the time it takes for the light to do a one-way trip from source to target. However, in most of the applications, the target has some sort of reflection device (a mirror or corner cube) that redirects the light to a detector that is aligned with the light source. So the light has to do a round trip as demonstrated in figure 2.2. By considering the OPL of the light pulse, eq. 2.1, one can obtain the geometric distance between source-target by the linear relation between the time interval Δt, obtained by the timing discriminators, and D_{geo}:

$$D = \frac{D_{geo}}{2} = \frac{c\Delta t}{2n} \tag{2.2}$$

The factor of two arises from the distance of interest being half of the light path when considering a reflection device in the intended target. For most terrestrial distance measurements, the refractive index

uncertainty is one of the limiting factors. Pulsed TOF is used for long distances (> 50m), considering that the minimum transit time must be longer than the pulse width [5]. The resolution is strongly dependent on the timing discriminator's capability of the electronics. This means that higher resolutions can only be obtained at the expense of a longer bandwidth.

High power Q-switched pulse lasers can be used for satellite positioning, measuring altitudes of several km. The best temporal resolution for a pulse detection falls in ≈ 3 ps corresponding to ≈ 1 mm in distance [2]. At distances in tens of meters, the time of flight measurements needs to take into account the pulse shape to correct the measured time delay, increasing the electronic complexity to process the pulse. A good example of this principle being applied is the International Laser Ranging Services, where they send a high energy pulse from Earth to various satellites to monitor their altitude with an accuracy in the hundreds of cm [14].

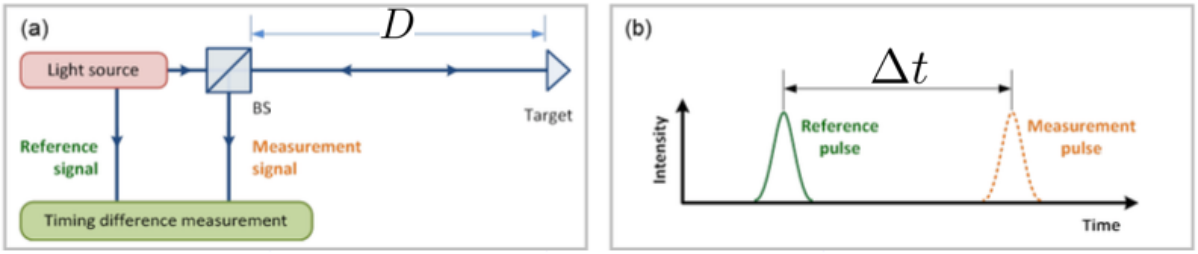

Figure 2.2: (a) Time of flight pulse scheme; (b) Reference and returned pulse signal. Adapted from [2]

2.2.2 Continuous TOF

Continuous wave modulated TOF (CW TOF) techniques use a coherent light source that is modulated in amplitude or in frequency to obtain absolute or relative distance measurements, figure 2.3.

2.2.2.1 Amplitude Modulation

In a phase shift (PS) CW TOF, a coherent light source is continuously modulated in amplitude with a sinusoidal signal with a given modulation frequency, f, and directed toward a target. The usual light source is a laser diode that can be directly modulated by its current [6]. Hence, when comparing the source optical intensity, eq. 2.3 to the one from the detected signal, eq. 2.4, there will be a phase shift, $\Delta\phi' = \phi' - \phi$, relative to the original signal.

$$I = Asen(2\pi ft + \phi) \qquad (2.3) \qquad\qquad I' = A'sen(2\pi ft' + \phi') \qquad (2.4)$$

Being A, A' the amplitudes, t and t' the time instants associated with the phases ϕ and ϕ', of the source and detected signals, respectively. However, a PS has two different components:

$$\Delta\phi' = \Delta\phi + 2\pi N \qquad (2.5)$$

The residual PS angle, $\Delta\phi$, is the local difference in the phase when comparing both signals, this is the quantity that one can measure with a phase meter device, illustrated in figure 2.3 a). On the other hand, N, the ambiguity integer, is due to the cyclical properties of the phase and it is the integer number of cycles necessary for the phase angle, at that given frequency, to reach the point it was detected. Furthermore, by measuring the PS between signals, one would be measuring the differences in optical

path length [13]. Therefore, to obtain the geometrical distance between the source and target, one must consider the relationship between the time interval and the PS:

$$\Delta t = \frac{\Delta \phi'}{2\pi f} \tag{2.6}$$

Thus, by using the relation described by eq. 2.1 one can obtain:

$$D_{geo} = \frac{OPL}{n} = \frac{c\Delta t}{n} = \frac{c\Delta \phi'}{2\pi n f} \tag{2.7}$$

When taking into account that the optical signal is reflected by the target, then the interest distance will be half of the geometrical distance. Additionally, by considering both components of the phase shift, eq. 2.5 the distance is given by:

$$D = \frac{D_{geo}}{2} = \frac{c}{2nf}\left(\frac{\Delta \phi}{2\pi} + N\right) \tag{2.8}$$

However, for a given modulation frequency, there will be a maximum target distance for unambiguous phase measurement, i.e, $\Delta\phi' = 2\pi$ rad and N = 0. This is referred as the ambiguity distance, given by:

$$\Lambda = \frac{c}{2nf} \tag{2.9}$$

Without solving the ambiguity, distance measurements will always be limited by the modulation frequency. This limits the technique's range. By using lower modulation frequencies, higher ambiguity ranges can be found, although there is a noticeable compromise in accuracy. Despite that, for displacements lower than the ambiguity range, high frequency (e.g, unit of GHz) modulated lasers have been used for ranges from 5 m to 100 m with a resolution of 1 μm and 3 μm, respectively [15]. By using this level of modulation, high-speed electronics must be used, increasing the complexity of this method. However, there are different methods to solve the ambiguity and they are described in [16]. Additionally, *Norgia et al* [17] was able to obtain ADM for a 30 m range with 100 μm uncertainty with this technique.

2.2.2.2 Frequency Modulation

Alternatively, one might use another variant of the TOF method, the frequency modulation continuous wave TOF (FMCW TOF). In that case, the optical frequency of a coherent light source is continuously modulated by a periodic saw-tooth profile, figure 2.3 b). This is usually done by controlling the emission wavelength of a tunable laser diode with a saw-tooth profile [6]. By applying a linear chirp in frequency to the optical source, the same property of the detected light signal in a target will differ from its reference [5]. The TOF in this method is measured by detecting the beat frequency, or intermediate frequency, f_{ij}, from both signals, eq. 2.10. Hence, the distance between the source and target will be related to the intermediate frequency by eq. 2.11, as shown in figure 2.3 b).

$$f_{ij} = \frac{\Delta f \Delta t}{T} \tag{2.10}$$

$$D = \frac{D_{geo}}{2} = \frac{OPL}{2n} = \frac{c f_{ij} T}{2n\Delta f} \tag{2.11}$$

Being Δt the delay of the round trip to a reflective target and its detection, T is the period and Δf the magnitude of the saw-tooth chirp. Depending on its period, beat frequencies in the dozens of kHz can be used, offering easy signal processing with relatively low-speed electronics, decreasing

the complexity of this technique. FMCW TOF can theoretically measure distances in the dozens of km without ambiguity. However, this method is limited by the non-uniform response of laser diodes when modulated in frequency. Additionally, the laser diode phase noise limits its spectral line widths, therefore the coherence length of the laser diode is limited to a dozen meters. Devices with narrower line widths for the modulation interval are ideal for larger ranges. Nevertheless, it has been reported that a distance measurement of 1 m with a chirp with a period of 10 μs a relative uncertainty of 4.3 $\times 10^{-5}$ was achieved [6].

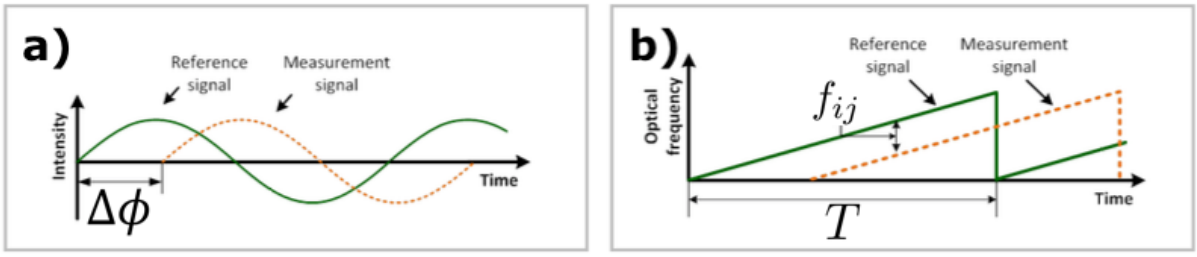

Figure 2.3: (a) Amplitude modulation. (b) Frequency modulation. Adapted from [2]

2.3 Optical Interferometry

Optical interferometry uses constructive/destructive interference to measure the difference in OPL traveled by light between a reference target and a measured one. Techniques with this principle have been used for distance and displacement measurements with a widespread set of applications, due to their wide dynamic range, fast scanning speeds, and good traceability to the meter [8].

The Michelson configuration, figure 2.4, uses a high coherency light source that is directed towards a reflector that acts like a target, and in the middle of its path, a beam splitter is placed. This device will allow for a part of the beam to pass and go to the moving reflector and the other to be deflected to a reference reflector. This creates two different arms in the two instruments, the reference (that is fixed) and the measuring arm, where the length of the latter is changed by displacing the reflector. The two beams, when returning from their targets will meet again in the beam splitter where the electromagnetic signal will interfere, resulting in an interference fringe pattern that is recorded by the detector. The two superimposed waves in the beam splitter are of equal frequency and amplitude because they were generated by the same light source. However, there is a constant phase difference between both signals, due to the difference in optical path length between both arms. This difference in phase angle results in constructive interference when the two waves are in the same phase. The detected signal has then a bright fringe pattern, i.e a maximum in intensity. This means that the phase difference will be 2πk, where k is the number of full phase cycles that both signals have between them. On the other hand, a minimum or dark fringe corresponds to destructive interference, where the phase difference will be 2π(k+1).

The base assumption for single-wavelength interferometry (SWI) is that it is possible to do phase measurements by counting the number of interference fringes. This method is ideal for displacement measurements, where it can achieve hundreds of nm in resolution [18]. For a SWI, the phase shift is given by:

$$\Delta\phi' = 2\pi f \Delta t \tag{2.12}$$

Being Δt the delay time interval between the reference and object, f is the light's frequency and λ its wavelength. Therefore, by considering the OPL, eq. 2.1 the geometrical distance for this method can

be written as:

$$D_{geo} = \frac{c \times \Delta t}{n} = \frac{\Delta \phi'}{2\pi} \frac{c}{fn} = \Big(\frac{\Delta \phi}{2\pi} + k \Big) \frac{\lambda}{n} \tag{2.13}$$

Like in the subsection 2.2.2, $\Delta\phi$ is the residual phase shift and k is an integer that represents the ambiguity in the phase measurement. However, single wavelength interferometry has a small unambiguous range, half of the optical wavelength (due to the round trip to the target). This condition limits its measuring range, therefore this method is used to measure relative distance measurements. Although, to measure absolute distances it is necessary to use incremental interferometry [19]. In this case, the phase is unwrapped over time starting in a well-known position. This always implies a precise device to move the target reflector with the requirement that the angle does not change more than $\pm\pi$ rad, and that the beam remains uninterrupted [20] [19] .

Additionally, more complex techniques like double-wavelength interferometry (DWI) can perform absolute measurements by increasing the unambiguous range [21]. This is possible by measuring the optical path length in the interferometer with two different wavelengths, λ_1 and λ_2, yielding two different phase shifts. Therefore, the phase difference will have a reduced sensitivity when the optical path length changes:

$$\Delta\Phi = \Delta\phi_2 - \Delta\phi_1 = 2\pi n D_{geo} \frac{\Delta f}{c} = 2\pi \frac{n D_{geo}}{\Lambda} \tag{2.14}$$

Where $\Delta f = f_2 - f_1$, creating a synthetic wavelength Λ:

$$\Lambda = \frac{c}{\Delta f} = \frac{\lambda_1 \lambda_2}{\lambda_1 - \lambda_2} \tag{2.15}$$

This allows for distance calculation through eq. 2.13.

Using this approach, uncertainty in the order of 30 μm for a (50-60) m range, has been obtained by [22]. Additionally, techniques like multiple wavelength interferometry increase even further the ambiguity range by mixing even more wavelengths, expanding its range limit where it can measure unambiguously. However, practical issues with this method, like using more than two different light sources, increase the complexity of the system.

Finally, frequency-sweeping interferometry is a special form of DWI. This is performed by using a tunable laser where there is a sweep in frequency and the phase of both wavelengths is measured along the sweep. This allows for a full unwrap of the phase, providing a phase difference with reduced uncertainty. Therefore, a 3 nm and 10 μm uncertainty have been reported for a 4 mm displacement and 1 m ADM, [18] [23], respectively. Additionally, by combining frequency sweeping and DWI, it has been reported a 12 μm uncertainty for a 20 m distance measurement [24].

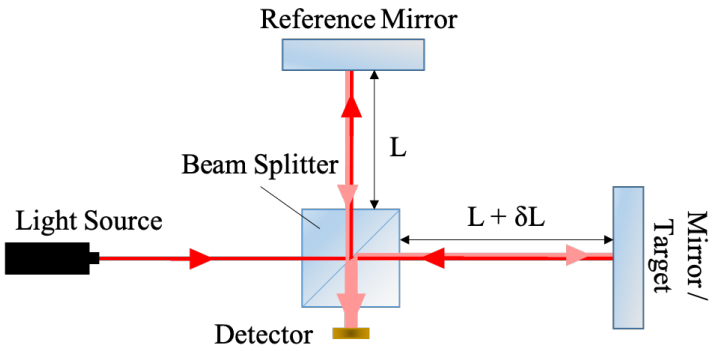

Figure 2.4: Basic Michelson interferometer configuration. Usually, a 50/50 beam splitter is used in order to split in half the intensity of the optical signal in the two different paths. The reference mirror is placed at a given distance, L, from the beam splitter while the target will have an additional distance ,δL, from the beam splitter.

2.4 Method Comparison

Different optical methods were analyzed and their performance was assessed in terms of range and accuracy. The results can be found in figure 2.5. For each of the presented techniques, different variations in the optical and electrical setup can translate to a bigger or smaller range and accuracy than those presented in the referred illustration. This is intended to give a general overview of the different methods and their characteristics.

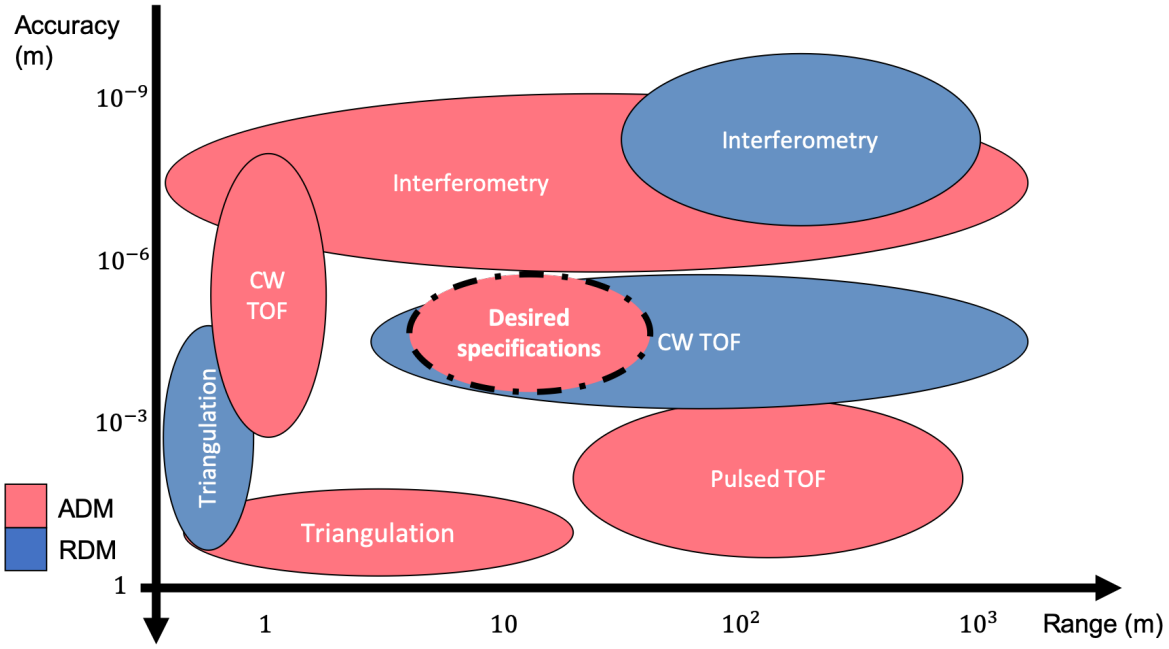

Figure 2.5: General comparison between the different range finding techniques and the desired specifications for this work. ADM - Absolute Distance Measurements; RDM - Relative Distance Measurements. Based on the reviews from [5], [6], [7], [8] and [9]

The triangulation technique, despite being simple and easy to implement, requires bulkier devices to operate in the mid-range [10, 100] m. State of the art devices can achieve mm accuracy for submeter ranges. Although, for RDM devices operating in the hundreds of mm range, μm displacements can be obtained, as shown in the cantilever example [12].

Interferometric methods usually have an accuracy in the dozens of nm or μm for ADM and can operate in the hundred meters range. Multiple-wavelength and frequency sweeping techniques can theoretically expand their unambiguous range and consequently reach high ranges ($>$ 100 m). However, these are complex methods and to achieve this sort of resolutions, it requires very stable equipment, increasing the component's price and operation complexity.

Depending on the optical source modulation, TOF techniques can be applied in an assortment of ranges with matching accuracy. ADM with pulsed TOF can achieve distances in the hundreds of meter to km range with a resolution in hundreds of mm and cm, respectively. CW TOF can be used for RDM in high and mid ranges, obtaining accuracies in the μm, although for km ranges the signal to noise ratio (SNR) will limit its capabilities.

After reviewing the presented methods, the conclusion is that the triangulation method, despite being simple, does not operate with the required accuracy $<$ 100 μm in a [10, 20] m range. On the other hand, interferometric methods can fulfill the specification, but due to its complexity and cost, it is not ideal for the intended work.

Overall, the PS CW TOF technique allows for the desired accuracy, operating within the intended range with off the shelf optical and electrical components. However, despite fulfilling the requirements for the intended range, this technique usually only performs RDM. As it was explained in subsection 2.2.2, this method is limited due to the presence of ambiguity in phase shift measurements. Nevertheless, there have been authors that succeeded in removing or bypassing the problem that the ambiguity in phase measurement presents. Different methods to do so are described in [16].

For example, *Norgia et al* achieved a 100 μm uncertainty for an unambiguous ADM of 30 m, with an application of the PS CW TOF [17]. Therefore, based on this author's work, it is clear that this technique for our desired range of [10, 20] m can perform ADM with an accuracy $<$ 100 μm. Thus, in this work, a measuring method was developed based on the PS CW TOF technique, which can remove the phase shift ambiguity, making it possible to achieve the desired operating range and accuracy goals.

Chapter 3

Phase Shift Time of Flight

In the previous chapter, a method for absolute distance metrology was selected. This was based on the requirements we established beforehand, a [10, 20] m measuring range with a < 100 μm accuracy. By comparing different optical measuring techniques and performing critical trade-offs, the PS CW TOF method was chosen. This method allowed for the desired accuracy and ADM in the range goal, as long as the ambiguity in a phase shift was removed. Hence, in this chapter we will present different methods to do so.

As mentioned in chapter 2, an absolute distance using the PS CW TOF method is obtained by considering the OPL, so that the geometrical distance between source-target (considering a round trip) is given by eq. 3.1. However, this method only allows ADM within an unambiguous range, where the ambiguity integer N is equal to zero, eq. 3.2.

$$D = \frac{c}{2nf}\left(\frac{\Delta\phi}{2\pi} + N\right) \tag{3.1}$$

$$\Lambda = \frac{c}{2nf} \tag{3.2}$$

Since there is an inverse relationship between the distance, D, and the modulation frequency, f, to achieve an accuracy in the hundreds of μm, a GHz modulation must be used. At the same time, by using a frequency in this magnitude, the ambiguity range is reduced to the cm span. Thus, for the intended range and accuracy, this method will perform a RDM, due to the aforementioned limitations. To achieve ADM with these conditions, one must be able to remove the ambiguity whilst maintaining the accuracy that a GHz modulation offers.

Hence, in section 3.1 we will analyze different solutions for the ambiguity problem and in section 3.2 we will suggest the one that is best suited for our application. Additionally, in section 3.3, we will theoretically study the behaviour of an ADM uncertainty (the different uncertainty contributors and how they propagate over a distance) with the chosen methodology. This allows us to determine the phase and frequency uncertainties that our instruments must achieve so that the distance measurements fulfil the established goals.

3.1 The ambiguity problem

The different approaches to solve the ambiguity problem usually rely on increasing the ambiguity range or to use auxiliary measurements to remove it. The easiest method is just to decrease the modulation frequency so that the ambiguity covers the system's operating range. For example, a 15 MHz

frequency can have an unambiguous range at 10 m order of magnitude, but the resulting accuracy will be roughly in the tens of mm reach.

Additionally, one might use a pair of modulation frequencies. The ambiguity distance of the smaller frequency of the pair determines the method operating range. Whilst the higher one is used so that within a smaller unambiguous range, a finer distance accuracy is obtained. This was suggested in [25] where they used a 10 MHz and 240 MHz modulation, allowing for measurements in the 15 m range with an accuracy in hundreds of μm.

However, to achieve a mid-range solution with this method, it would require to modulate the light source at dozens of MHz, followed by a second frequency in the dozens of GHz range. The first would remove the ambiguity and the latter allowed for a μm accuracy to be obtained. This means that different electronic interfaces would be needed to process the signals with both a fast and slower modulation. Since a GHz modulation would require fast electronics, then there is no guarantee that the same devices can operate correctly in the MHz domain. Hence, two different electronics would have to been made to process the two signals, increasing the complexity and cost of the setup.

3.1.1 Frequency Multiplexing

Silvano Donati in his book [16], suggested a different method to overcome the ambiguity problem - the multi-frequency method - in this case, a frequency, f_{Low}, low enough to avoid ambiguity, is chosen together with its multiples by a factor of ten, $10 f_{Low}$, $100 f_{Low}$, etc. The ingenuity of this method consists that each frequency will reveal an additional significant digit of the absolute source-target distance.

For instance, if one considers three different frequencies with a 100 factor between, then each frequency supplies two decades of digit information. By using three frequencies we cover 3 $\times$ 2 = 6 decades in a distance measurement. With a maximum frequency of f_1 =1.5 GHz, that corresponds to Λ_{f_1} =10 cm, the information of the 1-mm and 100-μm digit is obtained. Then, by considering $f_2 = 15$ MHz, with $\Lambda_{f_2} = 10$ m, the 1-m and 10-cm digit of the target distance is revealed. Finally, by performing a $f_3 = 150$ kHz, this means $\Lambda_{f_3} = 1000$ m, supplying the 100-m and 10-m digit. With each measurement, at a different frequency, it is possible to progressively obtain information regarding the absolute distance and with finer accuracy.

However, this method has the disadvantage that the electrical devices that could withstand a GHz modulation would have to operate properly for a slower wave in the kHz magnitude, increasing the complexity of the setup. An electrical scheme suggested in [16], makes the three phase measurements by multiplexing the modulation waveforms to the laser in sequence. However, even that setup would only have a maximum frequency of 15 MHz, two orders of magnitude smaller than what we intend to use. Despite this, and by using this method, an 100 m range was measured with 1 MHz, 10 MHz, and 100 MHz frequencies that obtained a 0.12 mm uncertainty [26].

3.1.2 Auxiliary Methods

Another approach is to use auxiliary measuring methods to overcome the ambiguity problem, such as using a pulsed TOF system to obtain a coarse measurement of the absolute distance and the CW PS TOF method to obtain a finer accuracy in the measurement. *F. Gueuning et al* [27] in 1997 obtained a 1 mm uncertainty for distance measurements in the hundreds of mm range, by combining pulsed and phase shift TOF. However, by using this concept with modern techniques, it allows measurements in a range of dozens of km with 2 $\times 10^{-6}$ relative uncertainty [28].

Despite being attractive due to the ease that the ambiguity is removed, when using two different measuring methods the complexity of the system as a whole would also increase. Since this dissertation work is limited to a specific time frame and by the available material, this option could not be considered.

3.1.3 Other Methods

Moreover, the PS CW TOF method is widely used for imaging cameras to capture three-dimensional images with an accuracy in the hundreds of μm [29]. These systems are different from the laser based ones that one might use for high accuracy absolute distance metrology. Despite this field being a different discipline of this method, inspiration can be drawn from the techniques they use to remove ambiguity.

TOF range imaging cameras operate similarly to a traditional video camera, using a CCD as its detector and white light as its source [30]. In the same way, this TOF imaging method also relies on the removal of the ambiguity to perform ADM. Comprehensive and comparative reviews of the different methods can be found in [30], [31] and [32]. In particular, the dual frequency method is explained in [30]. This method stated that by measuring the phase shift for a target at a fixed distance with two different modulation frequencies, slightly shifted from each other, there could only be one common distance for both phase results. Hence, the ambiguity in the phase measurement is removed.

Surely, if it is possible to remove the ambiguity by measuring the phase with two slightly different modulation frequencies, then by doing so with a GHz frequency, the ambiguity is removed and the accuracy that one desires could be achieved. Additionally, it would not be needed changes in the electrical setup to process both signals, due to both frequencies being in the same order of magnitude. Therefore, understanding this method served as an inspiration for a possible solution for the ambiguity and accuracy problem in our scenario.

3.1.4 Summary

Using two different frequencies lead to thinking about the PS CW TOF method as one would do with a physical and common ruler. This way, one could visualize measuring the same distance with two different frequencies as being equivalent to measuring with two different rulers.

By applying this dual frequency approach to some known metrology techniques, such as the Vernier method [33] [34], one can develop a technique for ADM. This approach uses the dual frequency modulation technique and allows the determination of the ambiguity integer N whilst achieving the desired accuracy.

Instead of trying to increase the unambiguous range or recover digit information like the previous methods, we tried to measure the number of phase cycles, as it will be presented in the next section.

3.2 An application of the Vernier method for the ambiguity measurement

An absolute distance with the PS CW TOF method is given by eq. 3.1. When solving this equation for the residual phase shift, as presented in section 2.2.2, one gets eq. 3.3. Also, by considering a constant modulation frequency, and plotting the residual phase against the absolute distance, one would obtain figure 3.1. The saw-tooth profile of the figure appears due to the residual phase shift only going from [0, 2π] and every time the phase completes one of these cycles, the ambiguity integer increases.

$$\frac{\Delta\phi}{2\pi} = \frac{2nf}{c}D - N \tag{3.3}$$

In figure 3.1, one can visualize that for the marked distance there will only be one residual phase shift and one N, that can fully pin-point that position. Meaning that with these two values we can fully characterize any distance.

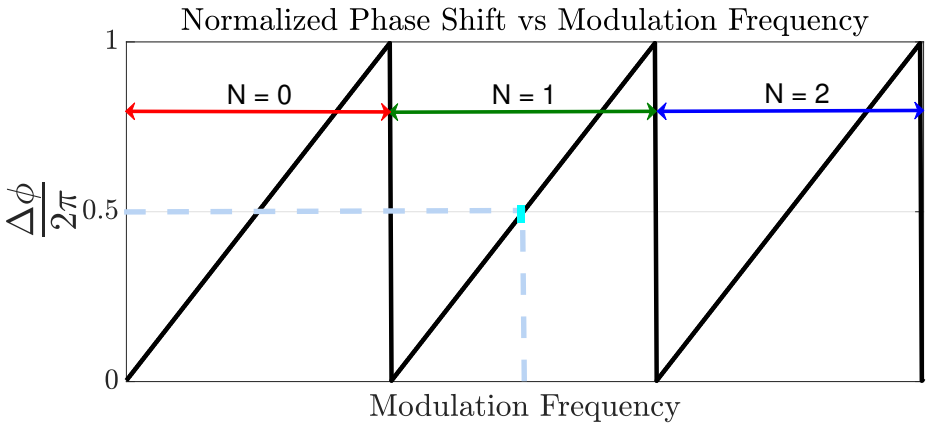

Figure 3.1: Residual normalized phase shift with the saw-tooth profile. This occurs due to the phase shift only going from [0, 2π]. The marked point represents a given distance that can be completly pin-pointed by knowing that N = 1 and $\Delta\phi/2\pi$ = 0.5.

One can think of the residual phase shift and the ambiguity integer as two metrics that correspond to the primary and secondary marks of a common ruler. Yet in a common ruler, both scales have discrete marks, but by using these two metrics of the PS CW TOF method, there will be one discrete mark (the ambiguity integer, N = 0, 1, 2, ...) and a continuous one that operates in between N's, the residual phase shift. This is possible to visualize when these two metrics are used to construct a ruler, figure 3.2.

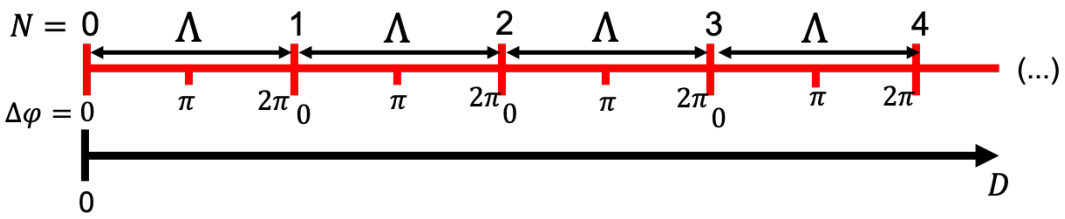

Figure 3.2: Graphical example of the ruler created by the PS CW TOF. Being Λ given by eq. 3.2 and it governs the distance between primary marks.

Hence, one can describe the distance given by this ruler in eq. 3.4. Clearly, the factor that is multiplying both metrics, Λ, will rule the spacings between marks. Since the ambiguity range is inversely proportional to the modulation frequency, then this is the parameter that ultimately governs how a given

ruler with the PS CW TOF method is constructed.

$$D = \Lambda \frac{\Delta\phi}{2\pi} + \Lambda N \tag{3.4}$$

Therefore, by using two different modulation frequencies to measure the same distance, it is equivalent to measuring the same position with two different rulers, figure 3.3. The differences in both rulers lead to different residual phases and ambiguity integers.

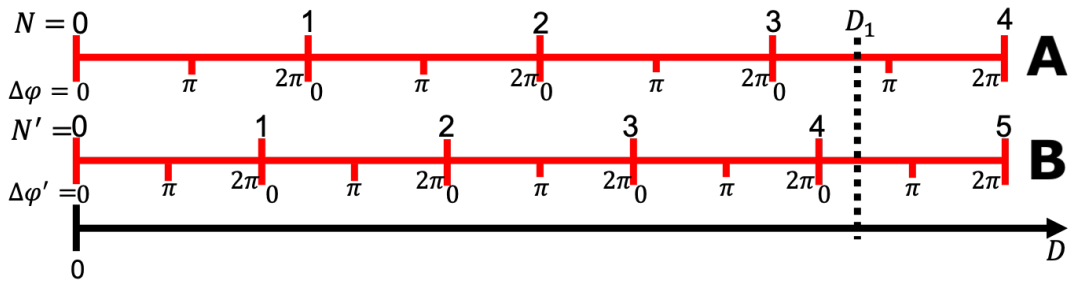

Figure 3.3: In the ruler A the distance between marks is determined by f and in B by $f + \Delta f$. As one can easily see by measuring the same distance with both rulers it corresponds to different residual phase shifts and ambiguity integers.

3.2.1 The differences between both rulers

To understand what occurs when the scale of the rulers is changed, it is necessary to quantify the differences between them. This can be done by defining a value Δx_N, eq. 3.5, that is intended to describe the difference in the position of the primary mark of both rulers, as shown in figure 3.4. This quantity is the product of the index of the primary marks of both rulers, and the differences in ambiguity ranges. By the definition of Δx_N the variation in the position of the marks with index '1' is the same as the difference in ambiguity range, hence Δx_1, eq. 3.6.

$$\Delta x_N = N \Delta x_1 \tag{3.5}$$

$$\Delta x_1 = \Lambda - \Lambda' = \frac{c\Delta f}{2nff'} \tag{3.6}$$

We define $\Delta f = f' - f$ as a real number always greater than zero , meaning that $f' > f$. This represents the difference in frequency for both scales and will rule the relative variation in the position of the primary marks. Additionally, in figure 3.4, when Δx_N reaches N = 4 then $\Delta x_4 = \Lambda'$. When this happens it means that both primary marks of the ruler coincide, and since $\Lambda > \Lambda'$, then in that point $N' = N + 1$.

In order to characterize even further the distinctions between both rulers, one must also take into account the secondary mark, i.e the residual phase shift. The difference in this quantity can be written as:

$$\frac{\Delta\Phi}{2\pi} = \frac{\Delta\phi'}{2\pi} - \frac{\Delta\phi}{2\pi} \tag{3.7}$$

Additionnally, by taking into account eq. 3.3, one can write:

$$\frac{\Delta\Phi}{2\pi} = \frac{2nf'}{c} D - N' - \left(\frac{2nf}{c} D - N\right) = D\frac{2n\Delta f}{c} + \Delta N \tag{3.8}$$

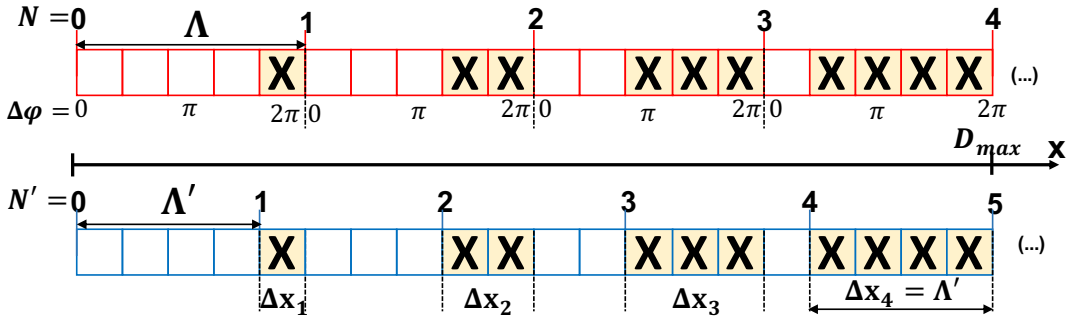

Figure 3.4: In this figure one can observe the difference in position of the primary marks of both rulers, Δx_N. Additionally, it is easier to understand that as long as N increases, so does the difference in marks. Here ruler A was determined by a modulation frequency f and ruler B by $f + \Delta f$.

Where $\Delta N = N - N'$, which represents the difference in ambiguity integers for a given distance. This can be seen as the variation of the primary marks indexes of both rulers, not to be mistaken with Δx_N that quantifies the change in position of that marks. Due to the way one defined the difference in phase shift and frequency, since $f'>f$ it leads to $\Lambda>\Lambda'$, consequently $N' \geq N$, for any given distance. This means that $\Delta N \leq 0$ and an integer.

By rewriting eq.3.8, one obtains a way to calculate the distance through the difference in frequency, phase shift, and ambiguity integer, resulting in eq. 3.9.

$$D = \frac{c}{2n\Delta f}\left(\frac{\Delta\Phi}{2\pi} - \Delta N\right) \tag{3.9}$$

Finally, by using the latter equation with eq. 3.1 and considering a fixed distance, it is possible to solve it for N and obtain an expression to calculate the ambiguity integer, eq. 3.10.

$$N = \frac{\left(\frac{\Delta\Phi}{2\pi} - \Delta N\right)}{\Delta f} - \frac{\Delta\phi}{2\pi} \tag{3.10}$$

Therefore, by measuring a distance with two known different modulation frequencies, one can measure both residual phase shifts. This means, that for the four different variables in the equation, it is possible to measure three. The only one left is ΔN that we cannot measure. However, it is possible to predict its behaviour by restricting some of the other variables.

If one can do so, then N can be measured and the ambiguity removed.

3.2.2 Understanding ΔN

To understand how ΔN will evolve, one must understand how N will behave for different rulers. For that reason, considering a fixed distance and plotting eq. 3.3 against the frequency, a sawtooth profile is revealed, just like when it was plotted against the distance in figure 3.1. However, if one takes a closer look at the graphical representation, it is possible to notice multiple linear parts, that range from 0 to 1, as marked in different colors in figure 3.5.

By considering a single and arbitrary frequency-PS point in this profile, like the one corresponding to frequency f in figure 3.5, the corresponding N can be found by intercepting the line on which the point is included with the $\Delta\phi/2\pi$ axis. However, for a pair of arbitrary and different frequency-phase shift points, the ΔN between them can be 0,-1,-2,-3... depending on the Δf spacing.

For different frequencies (or different rulers), sometimes the position is measured in the same primary

mark, and for that particular distance, both frequencies have the same N, for example, the scenario correspondent to frequencies f and f_1, on figure 3.5. On the other hand, when the variation in frequency is large enough, the phase shifts will not have the same ambiguity integer as the reference one, for example, the pairs f and f_2 or f_3. Essentially, knowing how ΔN will behave is dependent on the magnitude of Δf and the measuring distance. Meaning that if one can restrict the magnitude of Δf based on some conditions, then by measuring a pair of frequency-phase shift points, a given value for ΔN can be ensured. By having an initial estimate of what value this variable might assume, then one is able to calculate N through eq. 3.10 and with that information obtain the ADM through eq. 3.1.

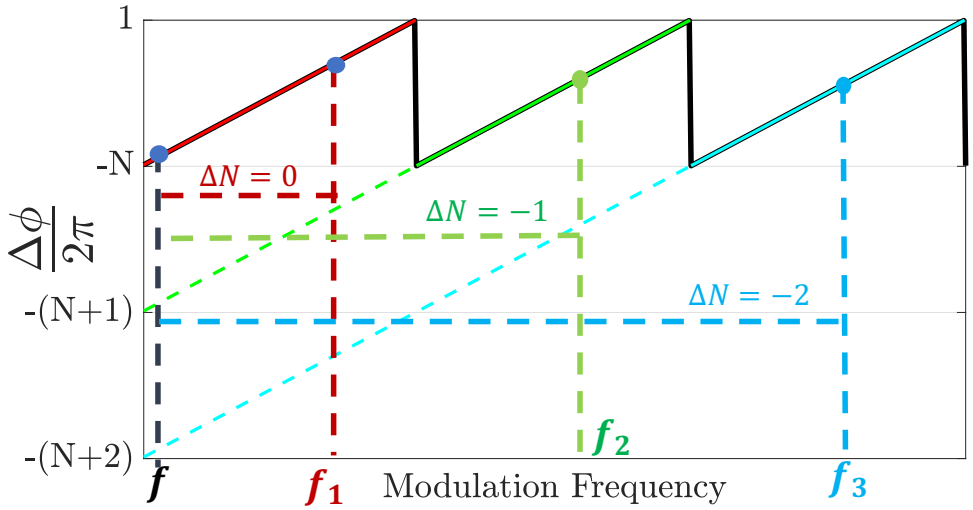

Figure 3.5: Comparison of the ambiguity integers of the frequencies f_1, f_2 and f_3 relative to f for a fixed distance. Showing that depending on the frequency shift relative to f different ΔN can be found.

3.2.3 Limiting Δf

The easiest way to limit Δf is by using the phase shift, the secondary scale of the rulers. The coincidence of these scales in both rulers can give us information regarding the difference in ambiguity integer ΔN. In metrology, when information is drawn by the coincidence of two different scales, this methodology is called a Vernier Method [33], [34]. It is the same method that mechanical callipers use to achieve greater accuracy in measurements.

In this case, we are using the Vernier method to limit the different ΔN one might obtain in a phase shift measurement. Instead of using it to obtain a finer displacement accuracy.

So with this in mind, in figure 3.6 two residual phase shifts measurements are represented at frequencies f and $f' = f + \Delta f$, that correspond to $\Delta\Phi = 0$. This means that there is a frequency shift of such magnitude that the full phase shift (as it is described in eq. 2.5) is moved 2π rad from the referenced one. Another interpretation is that the secondary marks on both rulers coincide. Hence, one is measuring the residual phase shift in two different ambiguity intervals, i.e the distance is measured in two different primary marks in each ruler. Since the residual phase shift is moved only 2π rad, one is measuring a phase in the following ambiguity integer, meaning that $N' = N + 1$, hence $\Delta N = -1$.

Therefore, there is a given frequency shift, Δf_{max} for when the residual phase shift is shifted to exactly 2π rad. Also, for frequency shifts with magnitude smaller than Δf_{max}, one might find a situation where the corresponding phase shift has the same or the next ambiguity integer when compared with the reference one.

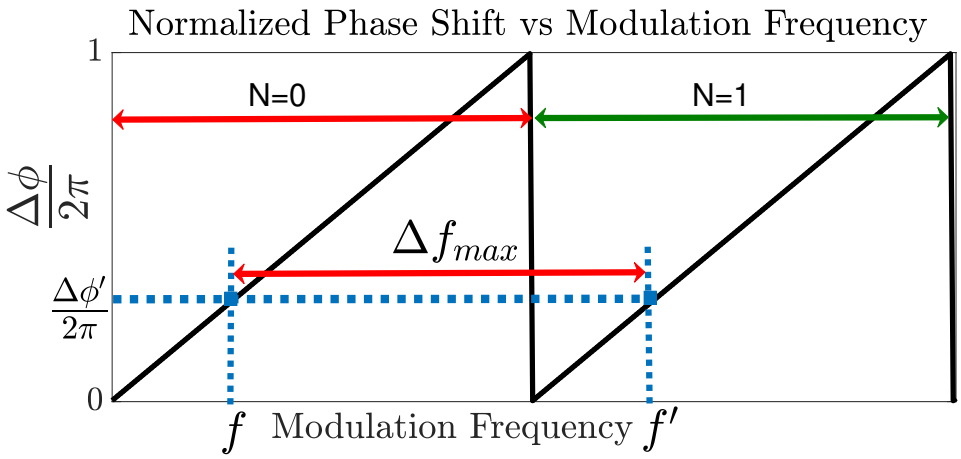

Figure 3.6: For a fixed distance, when comparing two frequency-phase shift points with frequencies f and $f' = f + \Delta f_{max}$, the correspondent residual phase shifts are equal to each other. This reveals that the full phase shift has been shifted by 2π, meaning that the measurements have different ambiguity integers, hence $\Delta N = -1$.

This indicates that, for any $\Delta f \leq \Delta f_{max}$, one can find $\Delta N = 0 \bigvee \Delta N = -1$.

Even though the showed example was for a fixed distance, by knowing that $\Delta\Phi = 0$, this would imply $\Delta N = -1$. By using eq. 3.9 one can find the relation between the maximum frequency shift and the target distance:

$$D_{max} = \frac{c}{2n\Delta f}(0 - (-1)) = \frac{c}{2n\Delta f_{max}} \tag{3.11}$$

This means that for a maximum distance of D_{max}, by assuming a frequency spacing of Δf_{max}, one can find $\Delta N = 0 \bigvee \Delta N = -1$. The relation between D_{max} and Δf_{max} can be found in figure 3.7. This would mean that, one can obtain $\Delta N = 0 \bigvee \Delta N = -1$ for any absolute distance, assuming a correspondent shift in frequency Δf_{max}.

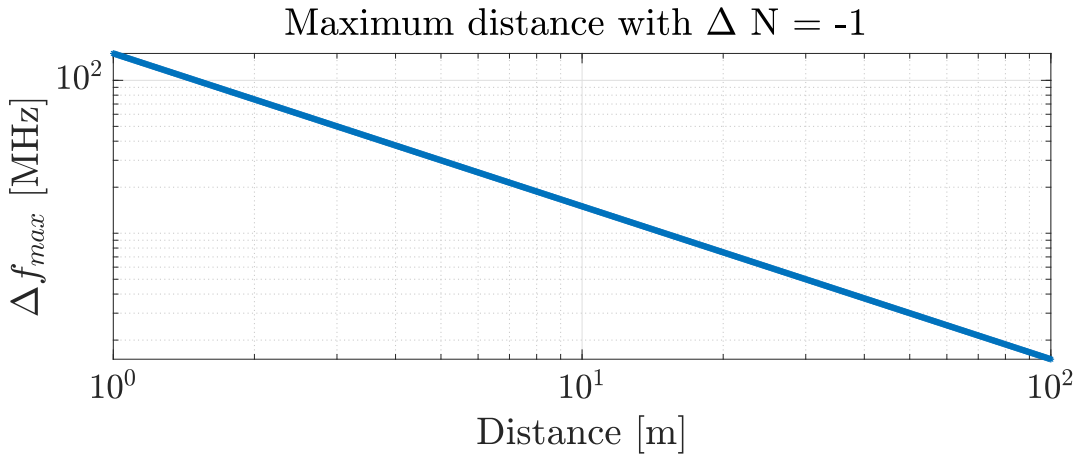

Figure 3.7: Maximum absolute distance that for a given Δf_{max}, one can find $\Delta N = -1$. For any $\Delta f < \Delta f_{max}$, one can find $\Delta N = 0 \bigvee \Delta N = -1$.

3.2.4 Method

Taking into consideration the limitations that were shown in the previous subsections, it is possible to obtain $\Delta N = 0 \bigvee \Delta N = -1$ for a given distance by performing two phase shifts measurements at

frequencies f and $f' = f + \Delta f$ with $\Delta f < \Delta f_{max}$. Nevertheless one must know when to use $\Delta N = 0$ or $\Delta N = -1$. This can be easily explained by analysing figure 3.8, where in this case our reference is the phase shift associated with the frequency f, $\Delta\phi$.

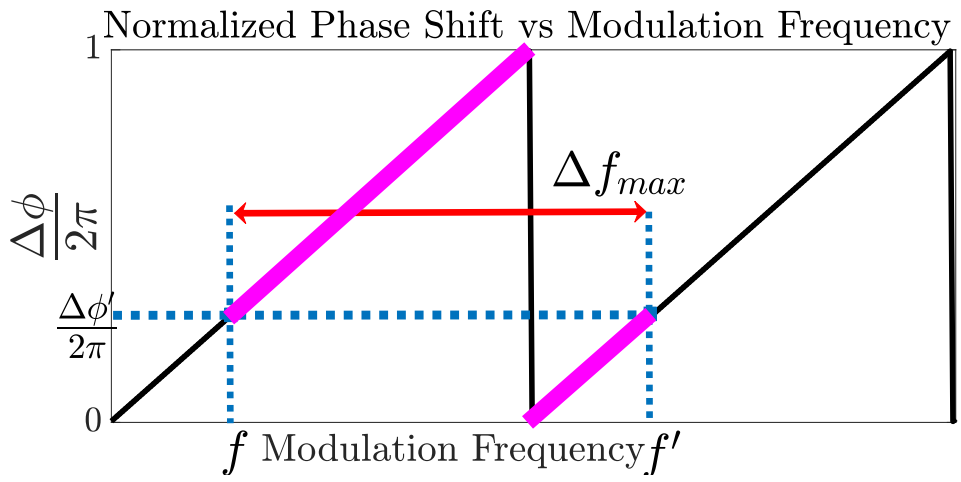

Figure 3.8: The marked coloured areas of the trace are associated with residual phase shift measurements for any frequency shifted by a Δf relative to f, with $\Delta f < \Delta f_{max}$. it is clear to see that all the phase shifts that are above the blue doted line are greater than $\Delta\phi$ and have $N' = N$, hence $\Delta N = 0$. On the other hand, when they are bellow the blue doted line all the phase shifts are smaller than $\Delta\phi$ and $N' = N + 1$, therefore $\Delta N = -1$.

For any frequency $f' > f$, that is associated with a phase shift $\Delta\phi'$, when $\Delta\phi' > \Delta\phi \rightarrow \Delta\Phi > 0$ this indicates that both phases are in the same ambiguity integer, $N = N'$, hence $\Delta N = 0$. Likewise, when $\Delta\phi' \leq \Delta\phi \rightarrow \Delta\Phi \leq 0$, it means that the residual phase shift $\Delta\phi'$ is in the next ambiguity integer, $N' = N + 1$, therefore $\Delta N = -1$.

However, this method is not limited by finding $\Delta N = 0 \bigvee \Delta N = -1$. Evidently, Δf_{max} is just the step in frequency so that a phase shift is moved 2π rad in relation to a reference. When comparing both residual phases it leads to $\Delta\Phi = 0$, allowing to determine $\Delta N = 0 \bigvee \Delta N = -1$ and a distance in the range $0 \leq D \leq D_{max}$.

Nevertheless, all the same relations can be found for when the difference in total phase shift is moved by 4π, 6π rad and so on, meaning that the spacing in frequency is $2\Delta f_{max}$ and $3\Delta f_{max}$ respectively. Although, as long as the frequency shift interval increases, so does the relation with ΔN. For example, if a frequency shift of magnitude $\Delta f_{max} < \Delta f \leq 2\Delta f_{max}$ is performed, one would obtain $\Delta\Phi > 0 \rightarrow \Delta N = -1$ and $\Delta\Phi \leq 0 \rightarrow \Delta N = -2$, leading to a scenario where $\Delta N = -1 \bigvee \Delta N = -2$, allowing a measurement of a distance in the range $D_{max} \leq D \leq 2D_{max}$. Clearly, in this sittuation it is impossible to determine $\Delta N = 0$ according to our method, therefore absolute distance measurements are limited to the range $D_{max} \leq D \leq 2D_{max}$.

To sum it up, by using the dual frequency PS CW TOF method it is possible to measure the ambiguity integer. However, this can only be done if one knows the maximum distance a target might be from its source. By knowing this information one can use the associated maximum frequency shift Δf_{max} so that $\Delta N = 0 \bigvee \Delta N = -1$. The indicated relation is valid for any reference modulation frequency one might choose, it is only important that $f > \Delta f$. Therefore, by performing a phase measurement at f and another at f', one might obtain $\Delta\Phi > 0 \rightarrow \Delta N = 0$ or $\Delta\Phi \leq 0 \rightarrow \Delta N = -1$.

With this information, it is possible to solve eq. 3.10 and determine the ambiguity integer. Moreover, with one of the frequency-phase shift measurement by using eq. 3.1, one can obtain an ADM.

3.3 Theoretical uncertainty analysis

In the last section, we established the measuring method. Now one must search for its practical limitations. This means understanding the uncertainty limitations that one must fulfil to achieve the ADM for a mid range target [10, 20] m with an accuracy $<$100 μm.

To perform an ADM with the purposed method it is required to measure the ambiguity number, N, and one must determine it with an expanded uncertainty $<$ 0.5. This limitation is critical because it is necessary to guarantee only one integer number in the measurement result interval. Additionally, the proposed method also states that in order to obtain an N measurement, the maximum distance where $\Delta N = 0 \bigvee \Delta N = -1$ is limited by Δf_{max}. Therefore, several constraints need to be taken into consideration to obtain a distance value and an N with the desired uncertainties.

For the uncertainty analysis, we choose to do it with two different methods, by using a Monte Carlo simulation and an analytical propagation of uncertainties. The latter is based on the law of uncertainty propagations and is made by expanding the measurand model in a Taylor series and only considering the first order terms, as described in [35]. However, this method can suffer from some limitations, for example, it assumes that all the variables are independent of each other and they have an insignificant non-linearity, which in some of the cases may not be irrelevant.

On the other hand, numerical methods like the Monte Carlo method, allow considering variables as probability distributions. Hence, by simulating error propagation with this method, the input variables are probability distributions and the output result is the convolution of the input quantities. Therefore, this type of analysis carries more information then when compared with the law of uncertainty propagation. In figure 3.9 a good visual comparison between both methods is presented, and in [36] both methods are discussed using practical examples.

On a practical side, by using a Monte Carlo simulation, one can evaluate the different uncertainty components for a given distance and due to the usage of probability distributions, the results can be closer to reality. Whereas with the analytical simulations, it can give us a notion of how the uncertainty behaves along with a distance and how the different components influence the uncertainty of the distance and ambiguity integer.

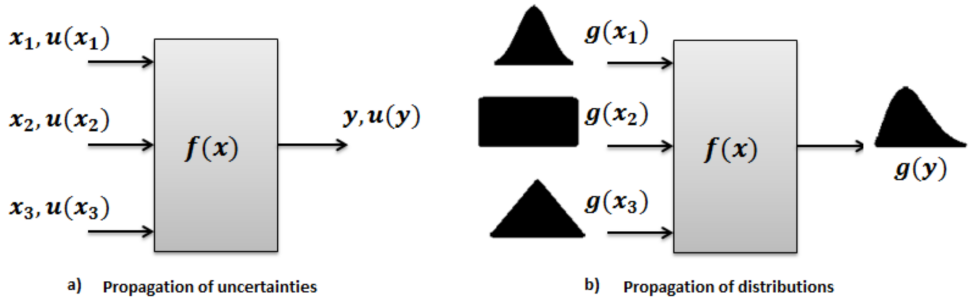

Figure 3.9: (a) x_1,x_2 and x_3 are the input variables and $u(x_1)$, $u(x_2)$ and $u(x_3)$ their respective uncertainties, while y and $u(y)$ are the output and its standard uncertainty obtained through the propagation of uncertainties. (b) on the other hand $g(x_1)$, $g(x_2)$ and $g(x_3)$ are probability distributions of the input variables, and as a result $g(y)$ the output is also a distribution. [36]

3.3.1 Monte Carlo Simulations

In appendix B there is a full description of the *Matlab 2017a* code used for this evaluation and the chosen parameters for it. By using the Monte Carlo method we intend to simulate the distance and N expanded uncertainty, U_N and U_D, with a coverage factor of k = 2, which means a 95% confidence

interval. Hence, one must analyse not one, but two different mathematical models, eq. 3.1 for the distance and eq.3.10 for N. To obtain the desired confidence with this method we performed 200 000 runs for each variable, as reported in [35] and [36].

Before we can measure absolute distances, we must obtain N with an expanded uncertainty, U_N, smaller than 0.5. Despite the fact that eq.3.10 has five different variables $\Delta\phi$, $\Delta\Phi$, Δf, f and ΔN, it has only three independent ones. Since ΔN is a factor that one will determine depending on $\Delta\Phi$, its contribution to the uncertainty can be ignored. The equation only has, in reality, two independent variables, $\Delta\phi$ and f. Therefore, one must adjust their respective standard uncertainty components $u_{\Delta\phi}$ and u_f , in order to obtain $U_N <$ 0.5.

The distance measurement brings the second requirement: U_D needs to be smaller than 100 μm. From eq.3.1, one notices that besides the speed of light c, we will consider N an integer with no uncertainty associated, that is considered a constant. The air refractive index, n, was calculated with the NIST Cidor equation calculator [1] with an expanded uncertainty, $U_n = 2.3 \times 10^9$ and a confidence interval of 95 % (2σ). The only parameters left are $\Delta\phi$ and f, the same requirements as the ambiguity integer requirement. Meaning that to obtain $U_D <$ 100 μm and $U_N <$ 0.5, the parameters $u_{\Delta\phi}$ and u_f had to be balanced.

The aforementioned variables were considered as Gaussian probability functions centred in the simulated value for each parameter with a coverage factor of k = 2, meaning a confidence interval of 95 %. We will assume that the phase uncertainty is the same for measurements at different frequencies, thus $u_{\Delta\phi} = u_{\Delta\phi'}$. Also, the modulation frequency uncertainty is considered a fraction of its value. By using a 3 GHz modulation frequency, we will assume that one knows its value with an uncertainty better than 1 ppm, consequently $u_f = f/10^x$ and $u_{f'} = f'/10^x$ with $x = 6, 7, 8, 9$. Hence, we will change the magnitude of the uncertainty contributors for each variable and calculate U_N and U_D to verify if the requirements can be fulfilled.

We used the maximum distance of 20 m for the Monte Carlo simulation. If the uncertainty requirements for this position are achieved, then for all the other smaller distances they will also comply. We used eq. 3.11 or figure 3.7, to obtain the correct Δf for ADM at that range. For a target in a interval of [0, 20] m, to obtain $\Delta N = 0 \bigvee \Delta N = -1$ the frequency shift needs to be $\Delta f_{max} = 7.498$ MHz. For simplicity we used $\Delta f = 7.4$ MHz and the results are presented in figure 3.10.

The results in figure 3.10 lead to a required phase shift standard uncertainty of $<$ 0.15 °. This corresponds to a phase measurement close to the limit of the available instrumentation. It is clear to see that the distance expanded uncertainty was well below the required accuracy, revealing that the uncertainty in N was the limiting factor in this scenario. Additionally, the contribution of the frequency uncertainty were only noticeable in the kHz domain.

Nevertheless, since our goal is to achieve the aforementioned requirements in a [10, 20] m range, it is not necessary to measure absolutely from [0, 20] m. Hence, instead of using a Δf_{max} for $\Delta N = 0$ or $\Delta N = -1$, by using a maximum frequency shift of $2\Delta f_{max} = 14.996$ MHz, meaning $\Delta N = -1$ or $\Delta N = -2$, the phase shift accuracy requirements could more easily be achievable. This will only allow for ADM in the [10, 20] m range. We ran another Monte Carlo simulation with the same parameters but changed the frequency shift to $\Delta f = 14.8$ MHz. The results can be found in figure 3.11.

When analysing figure 3.11 it is clear to see that the requirements in the phase shift standard uncertainty are broaden when compared to the results in figure 3.10, almost doubling in magnitude. The maximum obtained value for the phase shift standard uncertainty was $u_{\Delta\phi}$ =0.31 °. Even when considering $u_f = 3$ kHz, it lead to a maximum value of $u_{\Delta\phi}$ =0.26 °, much greater than when compared with the same point at $\Delta f = 7.4$ MHz.

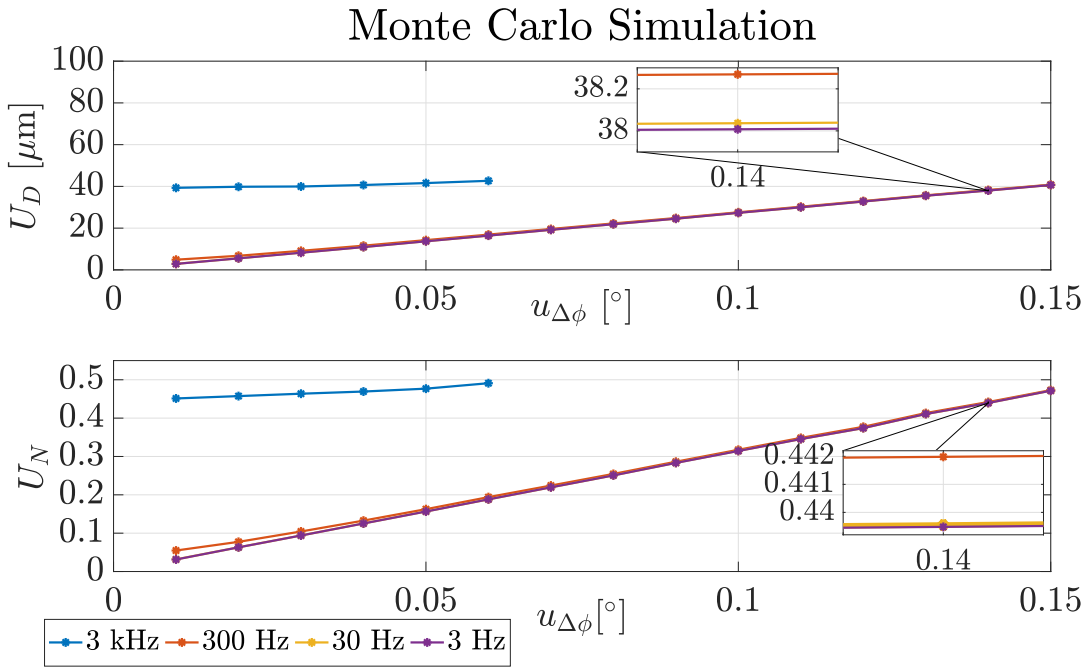

Figure 3.10: Results of the Monte Carlo simulations for the parameters: D= 20 m, $\Delta f = 7.4$ MHz and f= 3.0 GHz. The $u_{\Delta\phi}$ sweep was in the interval [0.01°, 0.8°] with a step of 0.01° and $u_f = f/10^x$ with $x = 6, 7, 8, 9$. It is clear to see that because the expanded uncertainty in N needs to be <0.5, it is limiting the values that u_f and $u_{\Delta\phi}$ could achieve for U_D<100μm.

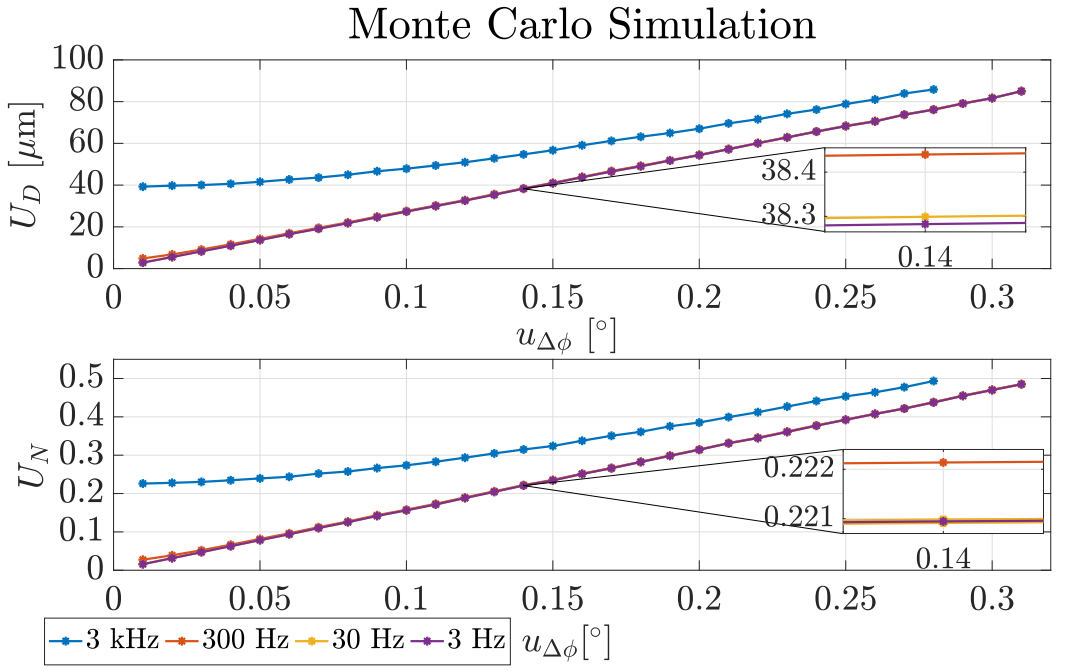

Figure 3.11: Results of the Monte Carlo simulations for the parameters: D= 20 m, $\Delta f = 14.8$ MHz and f= 3.0 GHz. The $u_{\Delta\phi}$ sweep was in the interval [0.01°, 0.8°] with a step of 0.01° and $u_f = f/10^x$ with $x = 6, 7, 8, 9$. it is clear to see that the change in frequency shift from $\Delta f = 7.4$ MHz to $\Delta f = 14.8$ MHz almost doubled the phase standard uncertainty when compared with the results from figure 3.10 .

The only difference between simulations was Δf, this means that this value must have a direct influence in the phase shift standard uncertainty. If one considers eq. 3.10, N is inversely proportional to Δf. This is also perceived when comparing the inlets of U_N in figures 3.10 and 3.11, for $u_{\Delta\phi} = 0.14$ ° the ambiguity integer uncertainty result almost doubles in magnitude.

To validate this we fixed $u_f = 3$ kHz and performed the same Monte Carlo simulations and changed Δf. The results are in figure 3.12 and they verify our assumption.

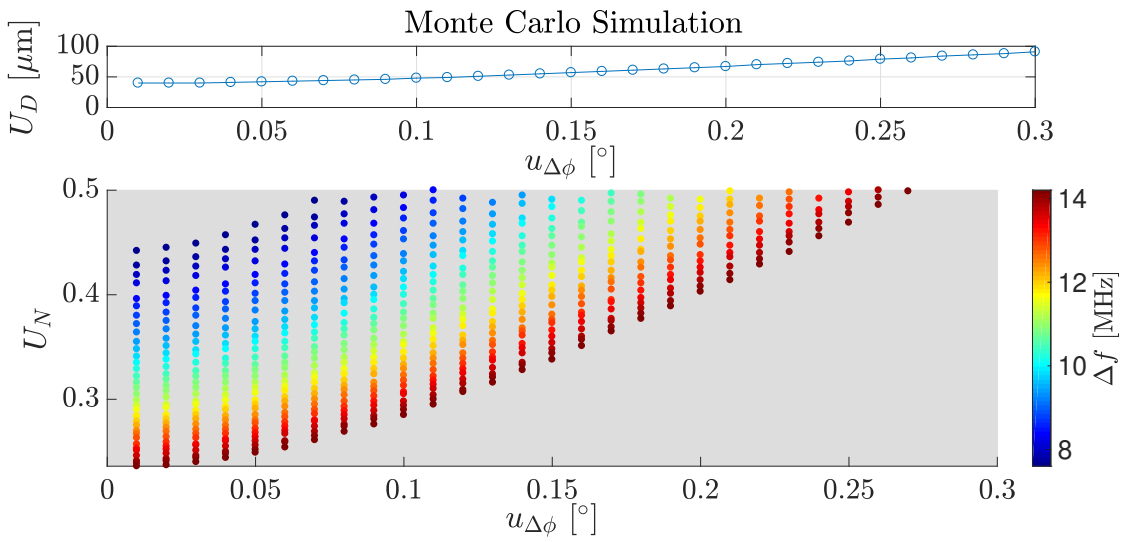

Figure 3.12: Results of the Monte Carlo simulations for the parameters: D= 20 m, $u_f = 3$ kHz and f= 3.0 GHz. The $u_{\Delta\phi}$ sweep was in the interval [0.01 °, 0.8 °] with a step of 0.01 ° and Δf [7.6, 14.8] MHz with a step of 0.1 MHz.

3.3.2 Analytical Simulations

To consolidate the obtained results with the Monte Carlo approach we performed analytical simulations based on the law of uncertainty propagations, as described in [35]. Additionally, in the appendix C, the full *Matlab 2017a* code and the different parameters description is available.

To perform the law of uncertainty propagations, the measurand mathematical model is expanded in a Taylor series. If there is no correlation between each variable, only the first term of this expansion is considered. Thus, the ambiguity integer N and the distance as a function of its variables are in eq.3.12 and eq.3.13, respectively.

$$D = f(\Delta\phi, f, n) \qquad (3.12) \qquad\qquad N = g(\Delta\phi, \Delta\Phi, f, \Delta f) \qquad (3.13)$$

In this scenario it is the same to consider $\Delta\Phi$ and Δf as variables, rather than $\Delta\phi'$ and f', like in the Monte Carlo simulations. This happens because one can just apply the propagation of uncertainties to $\Delta\Phi = \Delta\phi' - \Delta\phi$ and $\Delta f = f' - f$ since they are a function of $\Delta\phi'$ and f', respectively. Hence, the expression for the combined standard uncertainty for all these quantities is:

$$u_D^2 = \left(\frac{\partial D}{\partial \Delta\phi}\right)^2 u_{\Delta\phi}^2 + \left(\frac{\partial D}{\partial f}\right)^2 u_f^2 + \left(\frac{\partial D}{\partial n}\right)^2 u_n^2 \qquad (3.14)$$

$$u_N^2 = \left(\frac{\partial N}{\partial \Delta\phi}\right)^2 u_{\Delta\phi}^2 + \left(\frac{\partial N}{\partial \Delta\Phi}\right)^2 u_{\Delta\Phi}^2 + \left(\frac{\partial N}{\partial f}\right)^2 u_f^2 + \left(\frac{\partial N}{\partial \Delta f}\right)^2 u_{\Delta f}^2 \qquad (3.15)$$

Considering u_f, $u_{\Delta\phi}$, $u_{\Delta\phi}$, $u_{\Delta f}$ the standard uncertainties for their respective quantities, which are being multiplied by their correspondent sensitivity coefficient. For the purpose of this simulation, one will consider that all standard uncertainties have a type B evaluation, meaning they have a normal distribution with a coverage factor of k =2, which means a 95 % confidence level. The same considerations

regarding the frequency and phase standard uncertainties are done as in the last section: $u_f = f/10^x$, $u_{f'} = f'/10^x$ with x = 6,7,8,9. Hence, one can write $u_{\Delta\phi}$, $u_{\Delta f}$ as :

$$u_{\Delta\Phi} = \sqrt{2}u_{\Delta\phi} \qquad (3.16) \qquad u_{\Delta f} = \sqrt{u_f^2 + u_{f'}^2} \qquad (3.17)$$

Based on the distance equation, eq.3.1, one can discriminate each component by writing the product of each sensitivity coefficient with its standard uncertainty:

$$e_f^D = \Big(\frac{\partial D}{\partial f}\Big)u_f = \frac{-c}{nf^2}\Big(\frac{\Delta\phi}{2\pi} + N\Big)u_f \qquad (3.18)$$

$$e_n^D = \Big(\frac{\partial D}{\partial n}\Big)u_n = \frac{-c}{fn^2}\Big(\frac{\Delta\phi}{2\pi} + N\Big)u_n \qquad (3.19)$$

$$e_{\Delta\phi}^D = \Big(\frac{\partial D}{\partial \Delta\phi}\Big)u_{\Delta\phi} = \frac{c}{4\pi f}u_{\Delta\phi} \qquad (3.20)$$

The same goes for the N, eq. 3.10, the product of each sensitivity coefficient with its standard uncertainty is written as:

$$e_{\Delta\Phi}^N = \Big(\frac{\partial N}{\partial \Delta\phi}\Big)u_{\Delta\phi} = \frac{-u_{\Delta\phi}}{2\pi} \qquad (3.21)$$

$$e_{\Delta\Phi}^N = \Big(\frac{\partial N}{\partial \Delta\Phi}\Big)u_{\Delta\Phi} = \frac{f}{2\pi\Delta f}u_{\Delta\Phi} \qquad (3.22)$$

$$e_f^N = \Big(\frac{\partial N}{\partial f}\Big)u_f = \frac{\Big(\frac{\Delta\Phi}{2\pi} - \Delta N\Big)}{\Delta f}u_f \qquad (3.23)$$

$$e_{\Delta f}^N = \Big(\frac{\partial N}{\partial \Delta f}\Big)u_{\Delta f} = \frac{-\Big(\frac{\Delta\Phi}{2\pi} - \Delta N\Big)f}{\Delta f^2}u_{\Delta f} \qquad (3.24)$$

By using eq. 3.14 and 3.15, one can obtain the combined uncertainties for the distance and ambiguity integer values, u_N and u_D. The expanded uncertainty of these variables is calculated with a coverage factor of k = 2, as seen in eq. 3.25 and 3.26. This means that the expected confidence interval for the measured value is of 95 $\%$, or in other words, a confidence interval of 2σ [35].

$$U_D = ku_D \qquad (3.25) \qquad U_N = ku_N \qquad (3.26)$$

With the uncertainty mathematical functions defined, we simulated two different scenarios, with $\Delta f = 7.4$ MHz and $\Delta f = 14.8$ MHz.

The results from the Monte Carlo simulation were used to verify that the calculated uncertainty for each contributor, u_f and $u_{\Delta\phi}$, would be consistent in the two types of evaluation.

The limit conditions were tested for $\Delta f = 7.4$ MHz, $u_f = 3$ kHz and $u_{\Delta\phi} = 0.06$ ° and the distance was swept from [0, 20] m with a step of 0.1 m, figure 3.13. They were also tested, for $\Delta f = 14.8$ MHz by using the limit parameters $u_f = 3$ kHz and $u_{\Delta\phi} = 0.27$ ° a [10, 20] m range with a step of 0.1 m, figure 3.14.

For distance measurements, the component with the highest impact is $e_{\Delta\phi}^D$. In contrast, the e_n^D contribution is almost negligible due to its small magnitude .

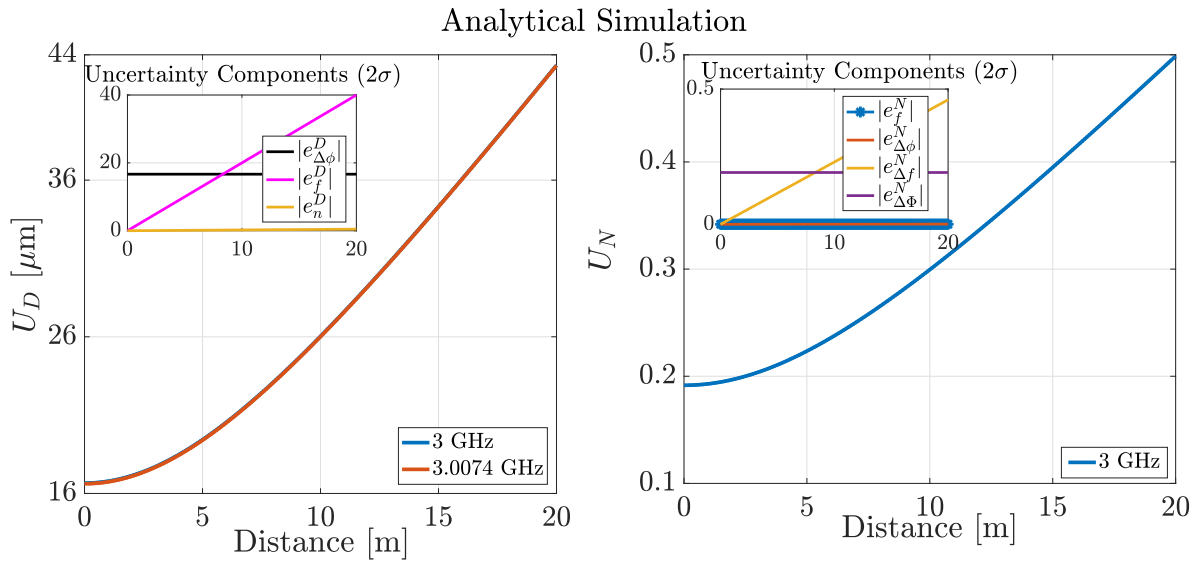

Figure 3.13: Analytical simulation of the expanded uncertainty of the ambiguity integer N and absolute distance, together with their different components. Parameters: D = [0 20] m with a 0.1 m step, $\Delta f = 7.4$ MHz, $u_f = 3$ kHz and $u_{\Delta\phi} = 0.06$ °

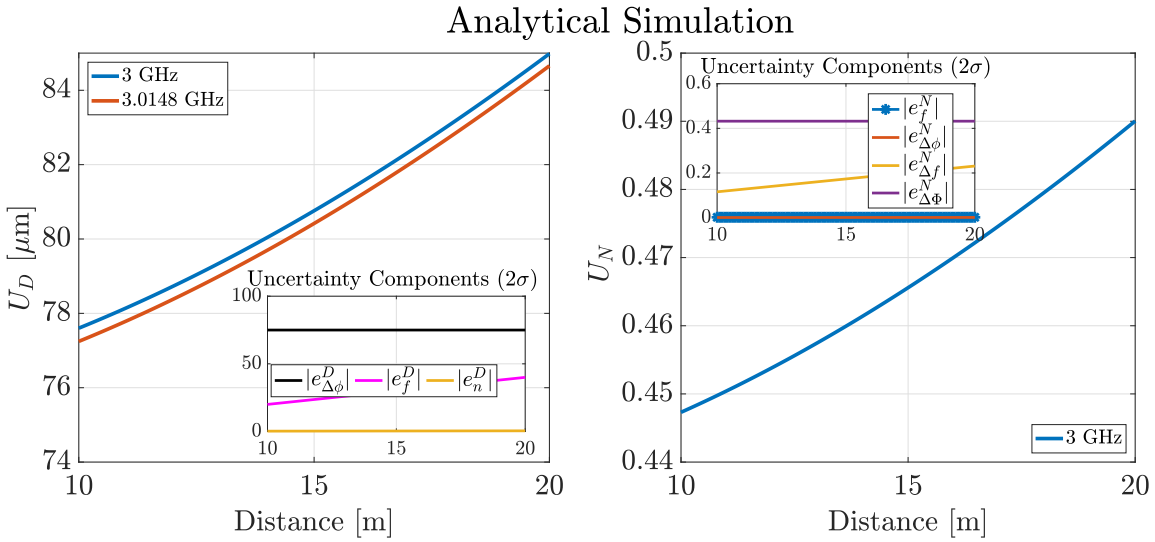

Figure 3.14: Analytical simulation of the expanded uncertainty of the ambiguity integer N and absolute distance, together with their different components. Parameters: D = [10 20] m with a 0.1 m step, $\Delta f = 14.8$ MHz, $u_f = 3$ kHz and $u_{\Delta\phi} = 0.27$ °

The contributions for the ambiguity integer uncertainty, that are dominant are $e^N_{\Delta\Phi}$ and $e^N_{\Delta f}$. The latter linearly grows with the distance, so by ensuring that the combination of these contributions is smaller than 0.5, then the ambiguity integer requirement is achieved. The obtained results in figures 3.13 and 3.14 are consistent with the ones from the Monte Carlo simulations.

3.4 Summary

In this chapter, a mathematical model was developed for ADM using a two frequency PS CW TOF method. This Vernier approach was also presented by the author in [4] (appendix A). This developed technique allows for ADM measurements in the [10, 20] m range through the measurement of the ambiguity number, N. An uncertainty analysis of this model was performed, so that the phase and frequency

uncertainty requirements could be defined to obtain $U_N < 0.5$ and $U_D < 100$ μm.

By taking into consideration the method's limitations and the desired goals, this technique was tested through Monte Carlo numerical error propagation and an analytical analysis using the law of uncertainty propagations. With these simulation results, one figured that by using the dual frequency PS CW TOF method, the phase requirements were too demanding for measuring a [0, 20] m range, so one stayed within a [10, 20] m interval.

In brief, it is possible to attain an ADM in a [10, 20] m range with $U_N < 0.5$ and $U_D < 100$ μm. For that reason, the instruments must achieve a standard uncertainty of $u_{\Delta\phi} = 0.27$ º and $u_f = 3$ kHz, when a 3 GHz modulation frequency and another shifted by $\Delta f = 14.8$ MHz are used.

Chapter 4

Experimental Setup and Equipment

In the last chapter, we identified and quantified the parameters that have a stronger impact on the measurement uncertainty. With this in mind, we were able to design an experimental setup that allows us to verify the measurement method and study its limitations. Different variations of optical schemes performing similar methods can be found in [5], [6], [7], [8], [9] and [16]. To obtain the desired $U_D < 100\ \mu$m, our method relies on the measurement of the phase shift between two signals in a GHz frequency. For frequencies in this magnitude, specific instrumentation must be used in order to cope with these limit electrical bandwidths. Techniques like heterodyne down conversion allow a way to bypass this problem.

4.1 Heterodyning

Heterodyning mixing is a technique that allows to downconvert or upconvert the signal of a carrier while maintaining the phase information. The result of the mixing process is a signal that contains two new frequencies, the sum and the subtraction of the original ones. For its implementation, one uses an instrument called a mixer. In this device, the signal of interest (the radio frequency signal, RF) is mixed with the one from a local oscillator (LO) that serves as a reference. By filtering the unwanted higher frequency, it is possible to only obtain its difference. The LO is fed with a signal with a well known frequency, to mix the RF signal. Its output is a signal with an intermediate frequency (IF) as seen in figure 4.1 . By using this technique, one can down convert the signal to a magnitude where it is easier to be analysed by the available instrumentation, whilst maintaining the phase information of the interest signal.

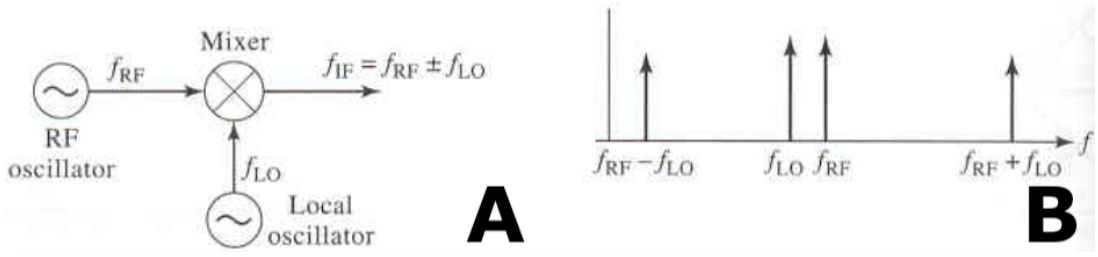

Figure 4.1: (A) Eletrical symbol of the mixer, being f_{RF} and f_{LO} the input signal frequencies and f_{IF} the output . (B) Frequency domain representation of the output signal, that contains the presence of the LO and RF signals and its sum and subtraction. Adapted from [37].

By adapting the equations from [37] one can quickly demonstrate the product of the heterodyning process. A reference oscillator signal LO can be described as eq. 4.1, likewise the RF signal can be seen

in eq. 4.2. The heterodyning process is based on the multiplication of these two input signals in a mixer. Hence, its output is the IF signal, eq. 4.3, where K is a constant accounting both signal gains and the conversion lost in the mixer device. Apart from that, by selecting the desired frequency $f_{IF} = f_{LO} - f_{RF}$ with a low pass filter, the phase information $\phi_{IF} = \phi_{LO} - \phi_{RF}$ has an offset due to the mixing process.

$$v_{LO}(t) = cos(2\pi f_{LO} t + \phi_{LO}) \qquad (4.1)$$

$$v_{RF}(t) = cos(2\pi f_{RF} t + \phi_{RF}) \qquad (4.2)$$

$$v_{IF}(t) = K v_{LO}(t) v_{RF}(t) = K cos(2\pi f_{RF} t + \phi_{RF}) cos(2\pi f_{LO} t + \phi_{LO}) =$$
$$= \frac{K}{2}\Big[\underbrace{\boxed{cos(2\pi(f_{LO} - f_{RF})t + \phi_{LO} - \phi_{RF}))}}_{\text{Low Frequency Component}} + \underbrace{\boxed{cos(2\pi(f_{LO} + f_{RF})t + \phi_{LO} + \phi_{RF}))}}_{\text{High Frequency Component}}\Big] \qquad (4.3)$$

One can think of a possible setup to retrieve the phase information for a round trip of a continuous amplitude modulated light signal, as the one from figure 4.2.

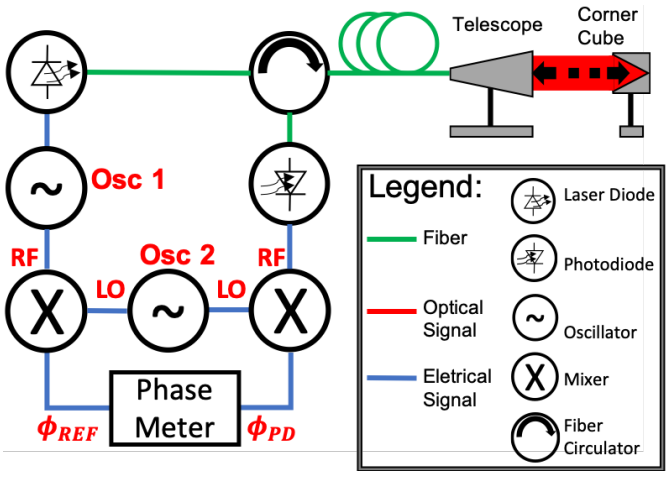

Figure 4.2: Simplified electro optic scheme for the detection of a phase shift difference between a reference signal and a detected one in a photodiode. Adapted from [17].

This setup consists of two oscillators that are involved in two different mixing processes This was achieved by mixing the RF signal modulating the laser source, with a local oscillator. The process is repeated with another mixer and the detected signal on the photodiode serves as the RF input in the mixer. In figure 4.2, *Osc 1* is the one responsible for amplitude modulating the laser diode. Additionally, an *Osc 2* is added to behave as the LO that will have the purpose to down-convert the reference signal from *Osc 1* and the one detected by the photodiode. This is the signal that contains the time delay information within its phase shift difference with regard to the reference.

The resulting IF signals from both mixing processes have a phase given by ϕ_{REF} and ϕ_{PD}, respectively. If one uses an instrument like a phase meter or a frequency counter, the phase shift difference between both signals can be given as eq. 4.4. The difference in both signals cancels the offset of the LO.

$$\Delta\phi = \phi_{PD} - \phi_{REF} = \phi_{LO} - \phi_{PD} - (\phi_{LO} - \phi_{REF}) = \phi_{REF} - \phi_{PD} \qquad (4.4)$$

Evidently, both oscillator and phase meter devices had to be disciplined by a master clock with a 10 MHz frequency. This needs to be done to be sure that there is no frequency drift or phase slippage between two different clocks. By using this setup with an oscillator, *Osc 1*, with an adjustable frequency, it is possible to perform a dual frequency phase shift measurements.

4.2 Experiment Assembly

4.2.1 Experiment Components

The following list of materials contains every equipment and component that was used in this dissertation work. They were used in different contexts to characterize and test different setups and equipments. Ultimately, this lead to the construction of an electro optic scheme that could perform within our desired needs. The list of used material is as follows:

- Eletro optic components
  - **Osc 1** - Anritsu MG3690C - RF/Microwave Generator 80 MHz - 70 GHz [38]
  - **Osc 2** - Atlantic Microwave Phase Locked Oscillators, a 3 GHz External Reference Clock and a 2 GHz Internal reference clock [39]
  - **Laser 1** - Thorlabs Pig Tailed Laser LPS-1550-FC $\lambda = 1550$ nm, $f_m = 1.8$ GHz [40]
  - **Laser 2** - Compound Semiconductor technologies $\lambda = 1550$ nm, $f_m = 3$ GHz 1550-FPL-2.5-X 1550 nm [41]
  - **Photodiode** - Ultrafast Photodetectors UPD-35-IR2-FC $<$ 10 GHz, (170 - 2600) nm spectral range [42]
  - **Mixers** - Mini Circuits Coaxial Frequency Mixer Level 7, ZAM-42 , (1500 - 4200) MHz [43]
  - **Low Pass Filter** - Mini Circuits Low pass filter SLP-200+, DC to 190 MHz [44]
  - **Power Splitter** - Mini Circuits Power Splitter / Combiner ZN2PD2-63-S+ (350 - 6000) MHz [45]
  - **Fiber** - Corning SMF-28 Ultra Optical Fiber $\lambda = 1550$ nm [46]
  - **Bias-Tee** - Mini Circuits Bias-Tee (0.1 - 6000) MHz [47]
  - **Amplifier 1** - Mini Circuits Low Noise Amplifiers ZX60-33LN+ (50 - 3000) MHz [48]
  - **Amplifier 2** - Mini Circuits Coaxial Amplifier ZHL-6A+ (0.0025 - 500) MHz [49]
  - **Amplifier 3** - Stanford Research Systems Sr445a 4 Channel 350 MHz [50]
  - **Fiber Circulator** - Fiber optic circulators 6015-3-APC [51]
- Mechanic Components
  - **Translation Table** - Thorlabs NRT Series Motorized Translation Stage [52]
  - **Controller Unit** - Thorlabs BSC103 Three-Channel APT Stepper Motor Controller [53]
  - **Telescope** -Thorlabs Optical Beam Expander BE20M-C (1050 - 1620) nm [54]
  - **Corner Cube** - Newport Hollow Retroreflector UBBR1-5S (450-10.000) nm [55]
- Measuring Devices
  - **Frequency Counter** - Agilent 53230A Series RF / Universal Frequency Counter 12 digits/s frequency resolution [56]
  - **Osciloscope** - Agilent MSO6054A 500 MHz [57]
  - **Power Detector** - Mini Circuits Power Detector ZX47-60+ (10 - 8000) MHz ZX47-55+ [58]
  - **Melles Griot** - Universal Power Meter 13 PDC 001 [59]
  - **Leica** - Leica DISTO D510 Laser Distance Meter [60]

4.2.2 Preparing the setup

Before starting the measurements one must know the performance of these instruments and how they operate. All of them deserve a closer look to obtain the maximum performance possible. All of the electro optic components were tested individually to check if they were operating as expected. Some devices are more important to understand when compared with others, due to our time limitations we decided to focus our attention in particular to three devices: laser, mixer and LO (*Osc 2*).

In order to achieve the accuracy requirements that were established in the last chapter, it was required to use a 3 GHz modulated laser, so *Laser 1* [41] was used with a bias-tee to add the RF signal with a DC bias, figure 4.4. The laser diode is the centrepiece of this setup, because of the frequency magnitude at which it can be amplitude modulated. This parameter constrains the frequency of the LO for the mixing process. So, to match the laser frequency, the *Atlantic Microwave* 3 GHz external reference clock oscillator was used as the LO input.

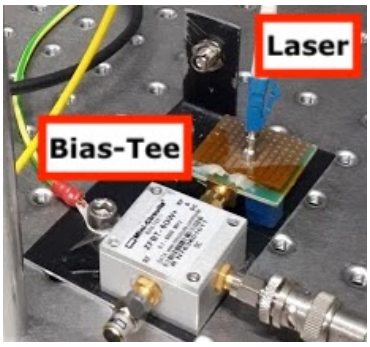

Figure 4.3: *Laser 1* [41], in its PCB holder connected to a bias-tee.

As it was referred earlier, both oscillators and measuring devices must have the same clock reference, to avoid frequency slippage. Since the RF device, the *Anritsu*, accepted an external clock reference and the LO needed one, it meant it was possible to set the same master clock for both oscillators. The equipment available with the best timing resolution, to serve as the reference signal, was the *Agilent 53230A* frequency counter, due to its 20 ps timer accuracy using a double oven-controlled crystal oscillator (OCXO) [56].

Unfortunately, an accident occurred with *Laser 1*. Due to connecting and disconnecting the fibre LC connectors, we broke its electrical terminals, turning the laser unusable. We still tried to salvage it, but it was in a state beyond repair with the available material.

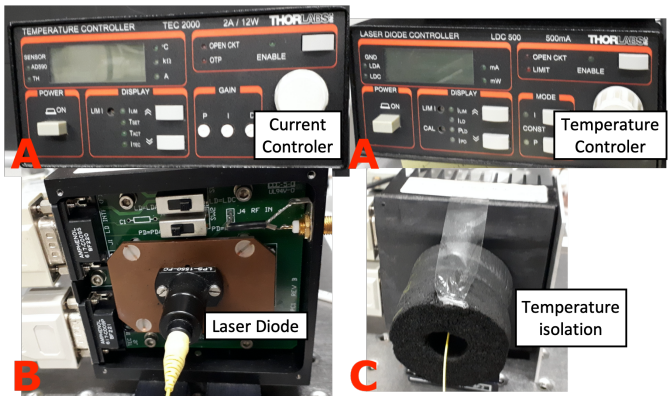

Figure 4.4: *Laser 2* [40], with their respective controllers, A. The pig tail laser on their support with and without temperature isolation, B and C, respectively.

Therefore, a backup laser had to be used, a Thorlabs pigtailed laser, *Laser 2* [40]. This device was mounted on a support that allowed temperature and current control, figure 4.4. However, to keep the setup simple, we did not explore the influence of this control on the overall device, so this was set to operate at 25 ºC. However, this laser was limited to a 2 GHz modulation frequency. This was verified by doing some frequency measurements of the detected signal on the photodiode for different modulation frequencies. It was determined that its ideal operating frequency was around 1.8 GHz. On the other hand, this also meant that the LO had to be changed so that when mixing with the RF, the resulting IF has a frequency smaller than 350 MHz. This was the signal limitation in terms of frequency for the *Agilent 53230A* in phase measurements [56].

The *Atlantic Microwave* 2 GHz internal reference clock oscillator available in our laboratory was chosen as the LO. Since it has its own internal reference, one cannot use the *Agilent 53230A* as a master clock as initially planned. So the timing reference for the whole setup had to be changed to the one

provided by *Osc 2*.

Due to the "accident" with *Laser 1*, the original setup had to be modified to be compatible with the lower modulation frequency of *Laser 2*. This laser was controlled in current by a control instrument, but the RF modulation frequency is provided by *Osc 1*. This meant that the signal from the *Anritsu* oscillator was our reference for the phase shift measurement.

Also, the whole setup needed to have the same time synchronization, this meant that all of the clocks on the oscillators and frequency counter must be synchronized, i.e operating in the same frequency. A basic consequence of asynchronism in clock times is, for example, tuning a given frequency in your RF generator and read it in the frequency counter with a given offset from the set value.

Additionally, the phase relation between *Osc 1* and *Osc 2*, is of critical matter in terms of a phase shift measurement between both signals. Hence, by foreseeing some necessary measurements of the phase difference between both oscillator, one calibrated the mixer as a phase detector.

4.2.3 Calibration of test equipment

4.2.3.1 Mixer phase calibration

To prepare for the measurement of the absolute phase roll between oscillators, one used the mixer as a phase detector. The absolute phase roll is the phase shift in the mixing process due to the phase noise in the RF and LO oscillators. This effect is intrinsic to the oscillators and it propagates to the mixing process as a drift in time of the phase shift, $\phi(t)$.

By using a mixing device, with $f_{RF} = f_{LO}$, the mixer output signal will be a function of the phase roll between oscillators. By considering eq. 4.3, one obtains the mixing output given by eq. 4.5.

$$v_{\Delta\phi}(t) = \frac{K}{2}\Big[cos(\phi_{LO} - \phi_{RF} + \phi(t)) + cos(\phi_{LO} + \phi_{RF} + \phi(t))\Big] \tag{4.5}$$

The $\phi_{LO} \pm \phi_{RF}$ components are the phase difference and sum between oscillators.

The calibration curve of the mixer ZAM-42 as a phase meter was performed. The idea behind this process is that the mixer will act as a transducer between phase and RMS output voltage. Hence, the *Anritsu* oscillator was set to 2 GHz and connected to the RF input, and the *Atlantic Microwave* 2 GHz oscillator to the LO while distributing the clock between devices, figure 4.5.

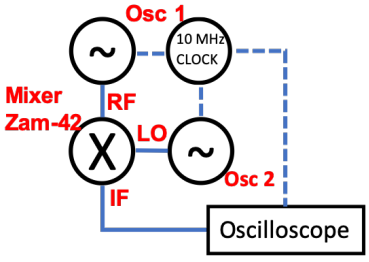

Figure 4.5: Eletric setup in order to measure the phase roll between setup with ZAM-42 mixer. The LO oscillator provided the master clock.

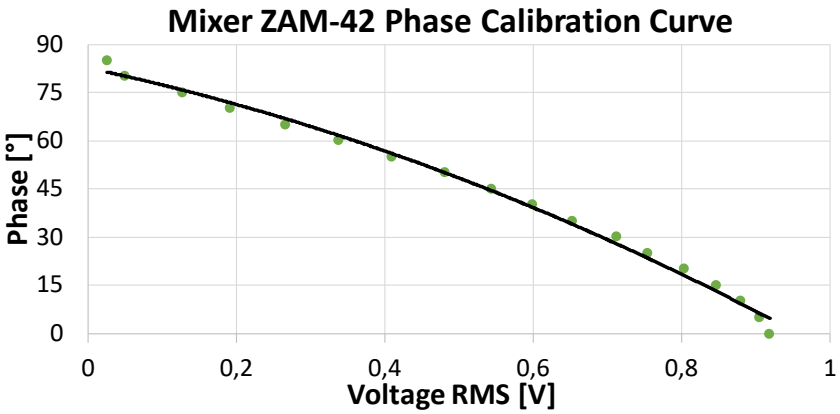

Figure 4.6: *Mini Circuits* ZAM-42 mixer calibration curve.

By using one of the characteristics of the *Anritsu* oscillator, a phase offset could be produced in the RF signal ϕ_{RF}, allowing the mixer to operate in a linear zone. When that region was found, its phase was swept with a 5 ° step for a total phase shift of [0, 90] °. This phase change was measured as a DC voltage

in the oscilloscope. This required some programming of the *Agilent 53230A*, so we developed a small *LabView* interface, that could control the acquisition time window of the measured signal voltage RMS. The calibration curve of the mixer as a phase detector can be found in figure 4.6 and the fit equation in eq. 4.6.

$$y = -39.075x^2 - 48,969x + 82.688 \tag{4.6}$$

4.2.3.2 Power detector calibration

Further, preparations were carried by performing the calibration curve of the RF power detector, *Mini Circuits* Power Detector ZX47-60+. With a calibration curve for this device, one would have a handy tool to measure the power output of the electrical devices. By connecting the power meter device to the RF oscillator *Anritsu*, one could adjust the signal level and read out the voltage RMS through a voltmeter, as seen in figure 4.7 . The resulting calibration curves, figure 4.8 were done for a set of frequencies that would be helpful for the characterization of the setup. Moreover, it is evident from the obtained results that the power meter had a different response for two different operating regions. So two different models were used to adjust the curves, which can be found in table 4.1.

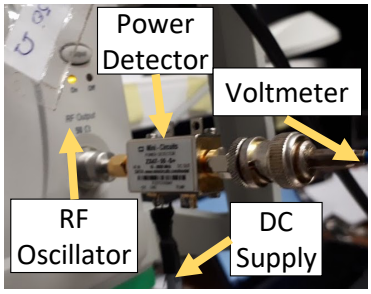

Figure 4.7: Photo of the calibration setup for the *Mini Circuits* Power Detector ZX47-60+ power meter.

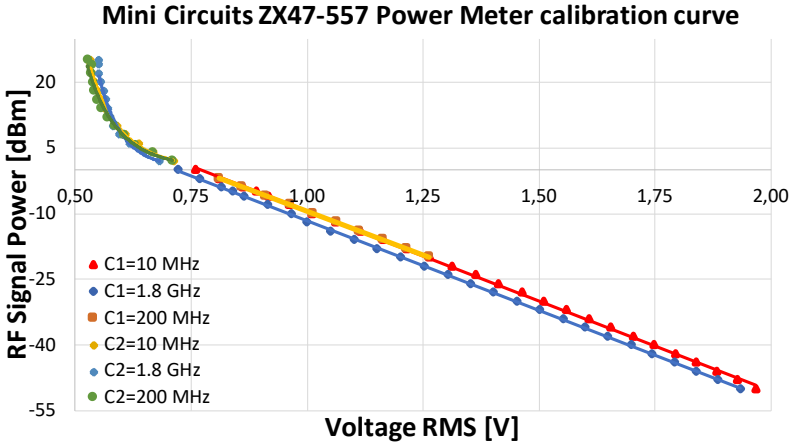

Figure 4.8: Calibration curves for the *Mini Circuits* Power Detector ZX47-60+. In total 6 different calibration curves two for each tested frequency. One can correspond two different regions to the curve region 1 for a measured RMS voltage between [0.5 0.75] V and region 2 for [0.5, 0.75] V

	10 MHz	**200 MHz**	**1.8 GHz**
Region 1	$y = -41.031x + 31.61$	$y = -40.924x + 30.095$	$y = -39.618x + 30.095$
Region 2	$y = 0.1377x^{-8.148}$	$y = 0.1412x^{-7.981}$	$y = 0.0263x^{-11.25}$

Table 4.1: Resulting calibration curves obtained for the different calibration regions. Region 1 for a measured RMS voltage between [0.5 0.75] V and region 2 for [0.5 0.75] V .

4.2.3.3 Mixer Conversion Loss

Afterwards, the mixer conversion loss was tested. This was important to understand because mixers have a given compression point where the IF signal power is proportional to the RF. So, to obtain the power budget of the whole setup, one should know the linear region of the RF power signal where the

mixer operates. Therefore, the *Anritsu* oscillator and *Osc 2* the 3 GHz oscillator were connected to the RF and LO input of the mixer, as seen in figure 4.9. The *Anritsu* oscillator served as the master clock.

According to its datasheet, *Osc 2* had a +16 dB output signal power. So, an -9 dB attenuation was used so that the LO input of the mixer was +7 dB. By setting the *Anritsu* in RF input with a 3.010 GHz frequency, an IF of 10 MHz was generated and selected using the 190 MHz low pass filter. The input power of the RF signal was then adjusted in the same device within an interval of [-25, 23] dB and a further -30 dB offset was made to increase the measuring range. The IF output signal was measured with the calibrated power meter. The conversion loss consists of a way to measure the difference in RF input signal and the IF ($P_{RF} - P_{IF}$). The results are in figure 4.10 and are what would be expected in the manufacturer's datasheet [43].

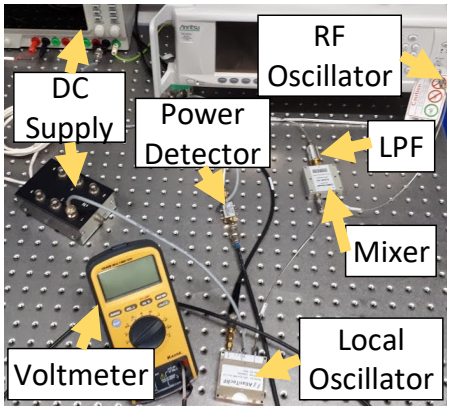

Figure 4.9: Photo of the setup using the *Atlantic Microwave* 3 GHz external reference clock oscillator and the *Anritsu* RF generator. Being that the device under test is the *Mini Circuit* ZAM-42 mixer. The calibrated power meter is used as a transducer of measured power in voltage.

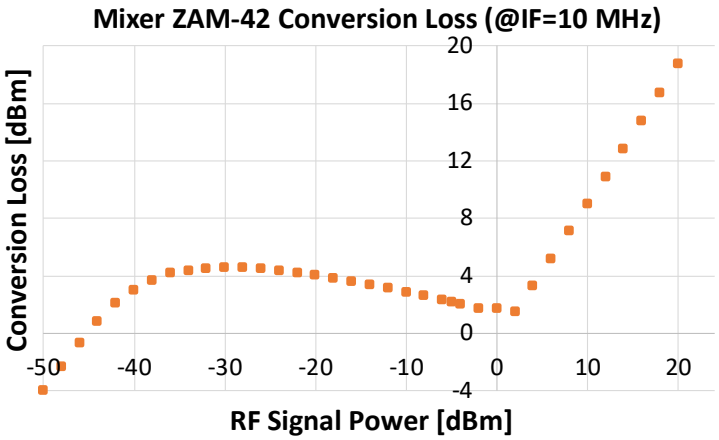

Figure 4.10: *Mini Circuits* ZAM-42 conversion loss curve.

4.2.3.4 Laser threshold current

To conclude the setup preparation, one performed the current characterization of both lasers. This was to understand how much gain can one allow the RF signal without happening the clipping of the light intensity. In our original setup with *Laser 1*, a DC signal was added to a RF with a given frequency using a bias-tee.

On *Laser 2* the laser holder has an integrated bias-tee, the difference is that the offset current is adjusted in its controller. This applied offset in both cases is done so that the laser device can operate in a stimulated emission regime for the entirety of the DC + RF signal. One would have to balance the amplitude of the RF signal with the DC one. The applied current allows for lasing emission without damaging the semiconductor device and the laser is in all condition over its threshold.

Therefore, the threshold currents from both lasers were performed, figures 4.11 and 4.12. The optical power of *Laser 1* and *Laser 2* were measured by using the *Melles Griot* universal power meter, whilst controlling the current flowing through the device, with no RF applied. From the obtained threshold curves, a linear fit was done in its linear region. By calculating the linear fits interception with the current axis, one can measure the threshold current. Starting from that specific drive current, stimulated emission of photons occurs and the laser diode achieves lasing emission.

The obtained results for *Laser 1* and *Laser 2* threshold currents are approximately $\approx$ 10.3 mA and

$\approx$ 11.9 mA, respectively. Despite the power meter not being calibrated, with these measurements one has a rough idea of the lasing currents one might expect from the laser. It is worth mentioning that for a current range of [20 - 25] mA, the optical power of *Laser 2* is twice that of *Laser 1*.

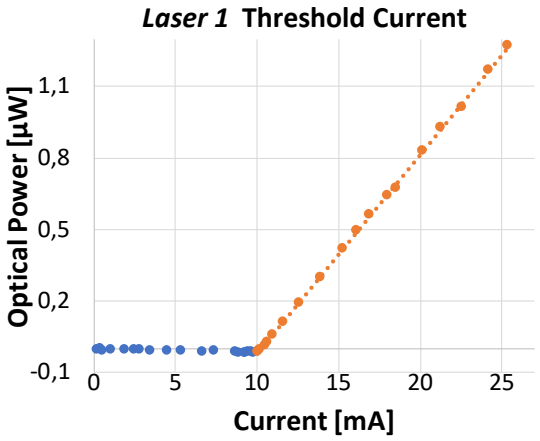

Figure 4.11: The *Laser 1* threshold current is approximately $\approx$ 10.3 mA.

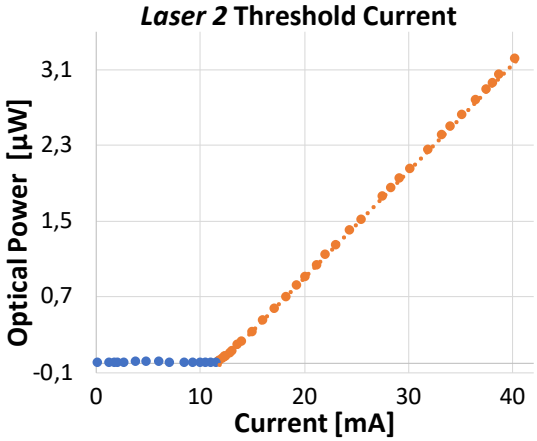

Figure 4.12: The *Laser 2* threshold current is approximately $\approx$ 11.9 mA.

4.2.4 Experiment Evolution

In this section, a brief explanation of the building process of the electro optic setup is presented. We started with the basic blocks that allowed a phase shift measurement with an adjustable frequency, then a moving target was added, so that different measuring distances could be adjusted. The setup noise sources were studied and the signal power adjusted in specific points. This way a phase shift measurement in the final setup could be performed with a SNR that allowed a correct ADM.

4.2.4.1 Preliminary Setup

After characterizing the relevant instruments one started to build the experimental setup. Firstly, its skeleton was constructed, figure 4.13. Initially, this was done with *Laser 1*, so the 3 GHz oscillator was used as *Osc 2*.

In terms of power adjustment, only the necessary gain adjustments for the mixers to operate properly were produced. The +16 dB signal from *Osc 2* was in first place attenuated -3 dB, due to the effect of the power splitters, and then attenuated -6 dB to achieve the necessary + 7 dB in the LO input.

Additionally, the laser drive current was set to 20 mA and the modulation frequency to 3 GHz in the *Anritsu* oscillator. The resulting output from both mixing processes, the reference and detected signals, were measured in the *Agilent* frequency counter.

A frequency shift in the RF oscillator was performed that lead to a change in the measure phase shift. This change in phase shift was detected by the frequency counter, verifying that the assembled setup was operating correctly.

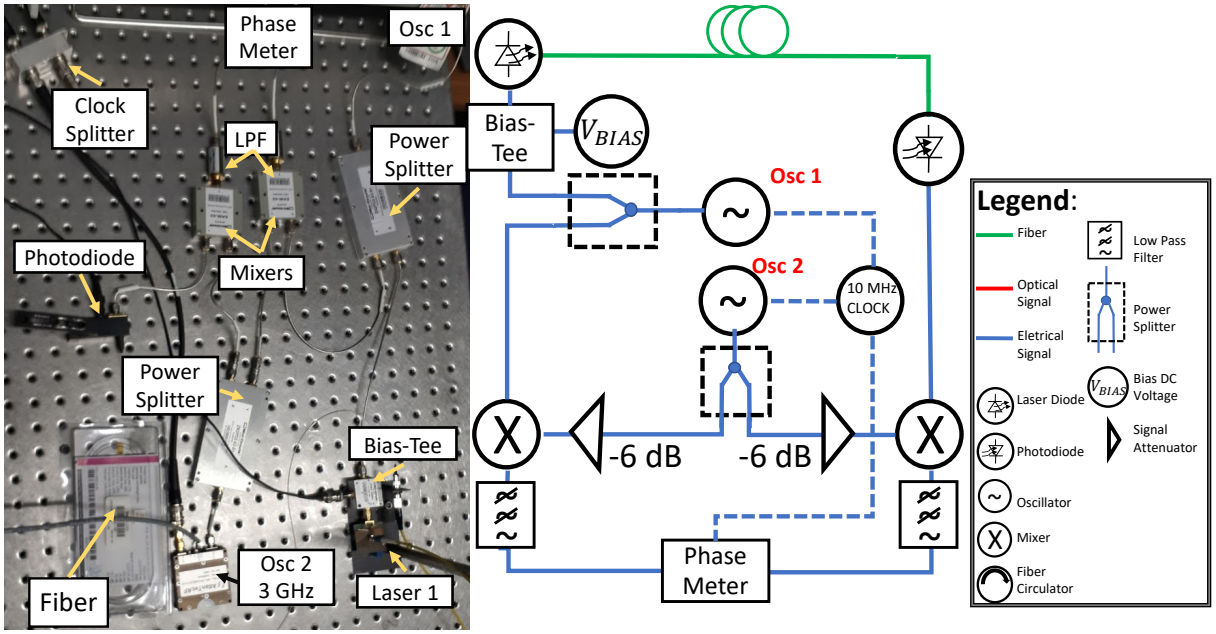

Figure 4.13: Preliminary setup using *Laser 1* with a 3 GHz amplitude modulation and the external reference clock 3 GHz oscillator.

4.2.4.2 Target Selection

Now with the concept of the setup verified, one started to arrange it in a way that distance measurements could be perform. This step consisted in choosing a target and designing how the light would be directed.

As the target one chose the *Newport* Hollow Retroreflector UBBR1-5S. By using a corner cube, one can ensure that the light reflected in it will be travelling in exactly in some direction. To use the reflector unit, a beam expander had to be mounted. For this purpose the *Thorlabs* Optical Beam Expander BE20M-C was used. This instrument allowed for a maximum beam expansion of 20x and a max output of beam width of 59 mm diameter.

A fibre optical circulator was used. This is a three port fibre device which can divert the beam in the output ports depending on its direction of propagation. As one can see from figure 4.14, the laser diode was connected to port 1, the beam would travel to port 2 and connected to the telescope. The reflected light on the corner cuber is collected by the telescope and it exits on port 3. This final port is connected to the photodiode for the optical signal detection.

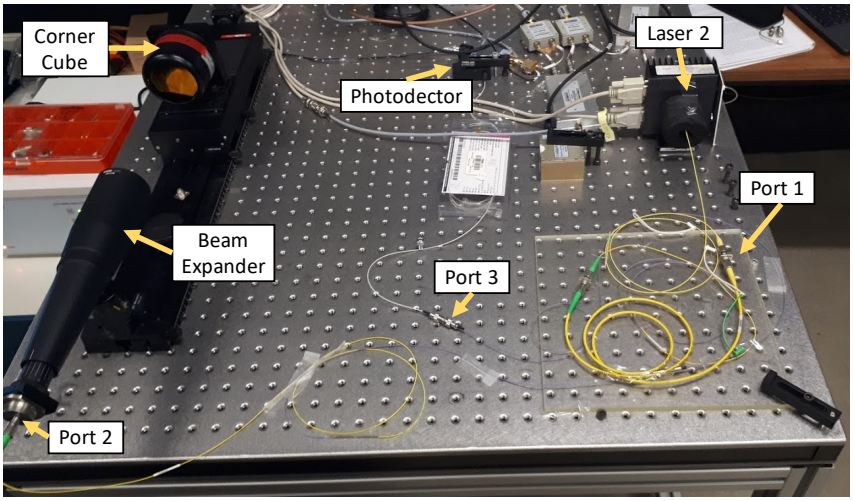

Figure 4.14: Photo of the optical components of the setup. Port 1, 2 and 3 refer to the inputs of the fiber circulator.

4.2.4.3 Power Balance

Now one could start doing the power balance of the setup. This was done by using the calibrated *Mini Circuits* Power Detector ZX47-60+, to measure the power in certain points of the setup. For example, the output power of the *Osc 2* at 2 GHz frequency was around +18 dB, after the splitters a -3 dB loss was expected, but still, a + 17 dB gain was measured. A -10 dB attenuation was set so that the LO input of the mixer had a + 7 dB input signal.

Also, when the time came for phase measurements, one would have to take into consideration the SNR of the interest signal. Thus, some fine tuning with the *Amplifier* 1,2 and 3, guaranteed that they were all operating in their linear regions and according to their maximum input power. This allowed to amplify the signal where it needed most so that the noise in the setup was kept to a minimum.

4.2.4.4 Noise Sources

The noise in our electro optic scheme can be generated from sources both external and internal to the measurement system. The induced external noise in the setup can arise from several reasons, that include their proximity to the main power supply cables or to radiofrequency equipment (like a Wi-Fi rooter that usually emits a signal with a bandwidth between [1, 6] GHz). Since our oscillator devices operate in that range, they are particularly susceptible to this noise and they can also be seen as noise sources. On the other hand, internal noise sources include thermoelectric potentials in the components and evidently shot noise in the semiconductor devices [61].

The main reason why external noise affects our electric components is due to electromagnetic interference (EMI), or radio frequency interference (RFI), that is, radiated or conducted electrical disturbances from electronic components, which can interfere with the operation of other electrical devices [62]. This effect can be seen as crosstalk between electrical components. This stray electromagnetic radiation will interfere with the operation of neighbouring devices, creating a mutual inductance and inducing in it undesired currents. Additionally, capacitive coupling, or electrostatic coupling, can arise between the signal wires and nearby power line conductors if they are not properly shielded. This is due to the charges in its outside mesh, which create an electric field between cables and consequently a coupling capacitance arises [61].

Finally, another noise source that can affect our setup is the existence of multiple ground loops. This effect happens when different components are connected to different references, meaning that there will be a difference in potential between them.

In summary, the sum of the mentioned noise sources is manifested in the transmitted RF signal through jitter, in the time domain and respectively phase noise in the frequency domain. This distortion of the signal affects the detection SNR. The influence of EMI has been tested and proven critical for the output signal of voltage controlled oscillators [62], [63]. Therefore, these noise sources must be reduced to a minimum, because the reduction of jitter is critical for an accurate phase shift measurement between signals.

4.2.4.5 Final Setup

Considering the mentioned noise sources, it was important to try to decrease the crosstalk between devices for the final setup. With this in mind, all of the equipments were referenced to the same ground plane. By using a star formation between all the electrical devices so that they are referenced to the same ground. Furthermore, the power supply was shielded as the best of our knowledge to avoid inductive

coupling to the signal. The components were as physically separated as possible to avoid this. The capacitive coupling was reduced by placing the cables as close as possible to the ground plane.

We had to ensure that the signal from the photodiode was in a power level were the conversion loss from the mixer, figure 4.10, was in its linear region. Hence, a +26 dB amplification with two different *Amplifier 1*, *Mini Circuits* Low Noise Amplifiers ZX60-33LN+ was set. This part of the setup was difficult to characterize because this signal was dependent on the gain of the RF device that modulated the laser device, the losses in light signal propagated through the air and the EMI noise. It was only possible to achieve a reliable setup through empirical testing, i.e trial and error. The final setup that one used for dual frequency phase shift measurements with a SNR ≈ 10, is the one presented in figure 4.15.

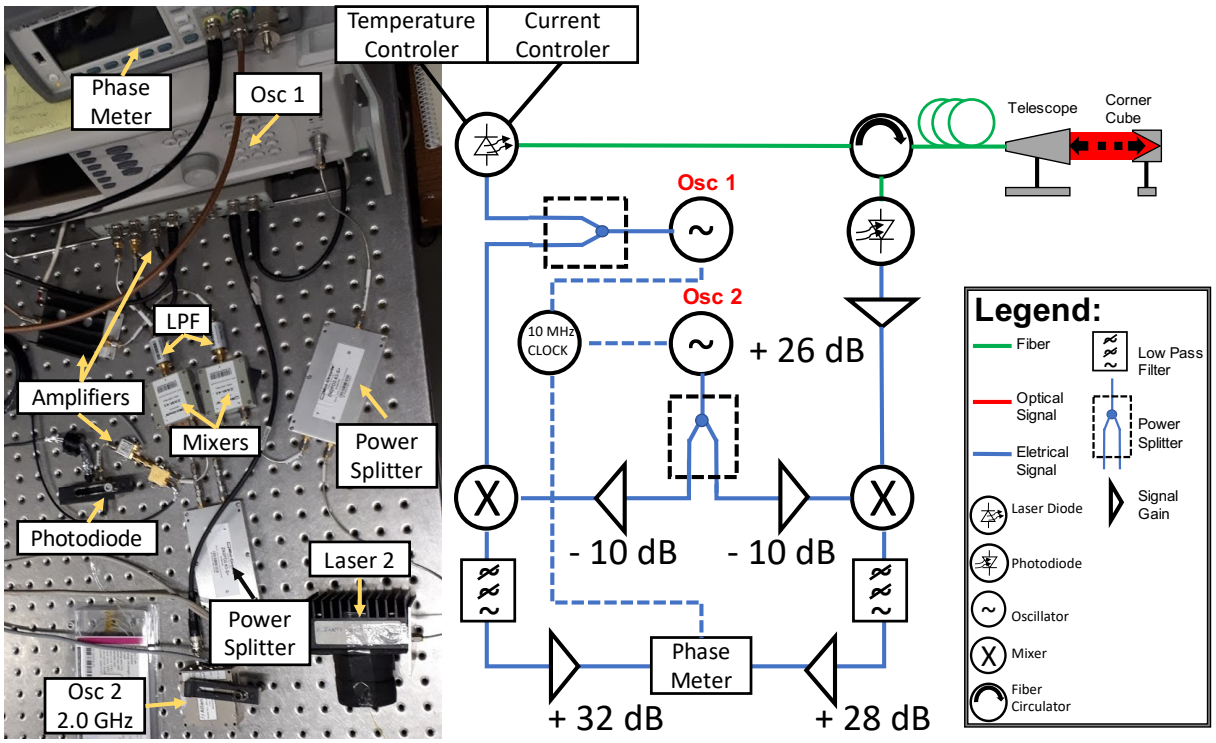

Figure 4.15: Final setup to implement the dual frequency PS CW TOF method. *Laser 2* with a 1.8 GHz modulation along with the *Osc 2* with a 2 GHz signal.

4.3 Impact of components changes in the experiment

The forced change of *Laser 1* for *Laser 2* led to a decrease in the achievable modulation frequency of the laser source intensity. This jeopardized this work's initial goal, the development of a setup to measure a [10, 20] m distance with an accuracy smaller than < 100 μm.

Due to these limitations, the *Atlantic Microwave* 2 GHz oscillator served as the LO to cope with the 1.8 GHz of the RF modulation. The mixing of these two signals provided an IF = 200 MHz. Moreover, as our method required a dual frequency and phase shift measurement, one other frequency had to be found to modulate the laser. In the sequence of the Monte Carlo simulation results on chapter 3, Δf should be maximized to decrease the expanded uncertainty of N. So, another modulation frequency of 1.825 MHz was found, that allowed to obtain an IF of 175 MHz.

The laser current and the RF signal gain were set to 20 mA and + 3 dB, respectively. With the established IF of 175 MHz and 200 MHz, a phase shift measurement was performed with a SNR ≈ 10 for both frequencies.

We planned to use a calibrated air rail to test the device by performing distance measurements in a [10, 20] m, however, that was not possible. So one had to use the available material in the laboratory. For that reason, the maximum range of our measurements was limited to 5 m, that were simulated by an optical fibre to extend the OPL of the light beam.

Now with our experimental constraints well defined, we redid the analytical simulations to see what would be the impacts of the changes in design in the overall performance of our method. Since a $\Delta f = 25$ MHz was achieved, this meant that the maximum range for unambiguous measurement was 5.998 m (meaning, measurements with $\Delta N = 0 \bigvee \Delta N = -1$), which worked for the new testing range. The simulation results can be found in figure 4.16.

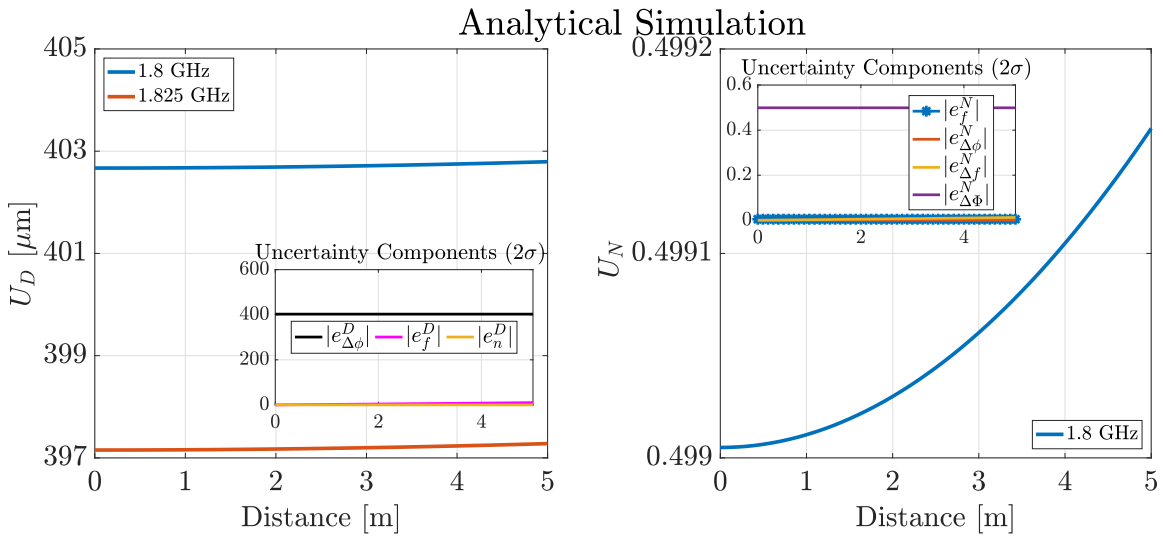

Figure 4.16: Analytical simulation of the expanded uncertainty of the ambiguity integer N and absolute distance, together with their different components. Parameters: D = [0, 5] m with a 0.1 m step, $\Delta f = 25$ MHz, $u_f = 1.8$ kHz and $u_{\Delta\phi} = 0.87$ °

As one notices from figure 4.16, the distance uncertainty requirements for that given range surpass by a factor of 4 the ones that we initially established. This is evidently a direct consequence of using a lower modulation frequency. Since the distance uncertainty requirement was clearly not possible to achieve, the only direct constraint that one must impose is the requirement to measure the ambiguity integer with $U_N < 0.5$. The phase shift uncertainty requirement loosens up to $u_{\Delta\phi} = 0.87$ ° when comparing with the

result for a 3 GHz frequency of $u_{\Delta\phi} = 0.31°$. In table 4.2 the trade offs between the experimental setups using *Laser 1* and *Laser 2* are presented.

The original setup with the 3 GHz modulated *Laser 1* and the 3 GHz *Osc 2* would make it easier to generate an IF that can match the operating bandwidths of the low pass filters and the amplifiers. Therefore, this setup would allow the usage of the adequate Δf to do ADM in the [10, 20] m range. Due to this laser modulation frequency, one could have probably obtained an $U_D <$ 100 μm, even if it was just for the [0, 5] m range. However, the phase accuracy requirements to achieve $U_N <$ 0.5 are stricter than when compared with a 1.8 GHz modulation.

The experimental setup with *Laser 2* modulated at 1.8 GHz, made it impossible to achieve the requirements of $U_D <$ 100 μm. Due to its limitations in modulation frequency adjustment, the ideal Δf to operate in the [10, 20] m was not reached. However, the change in the test range made possible the usage of a higher Δf, that contributed to the broadening of the phase uncertainty requirement, which is an improvement to achieve $U_N <$ 0.5.

By taking into consideration our mathematical model and the results obtained with the configuration the 1.8 GHz configuration, the initial ADM uncertainty goal would have been achieved if the laser frequency could reach the 3 GHz limit as it was though in our preliminary design.

	Modulation Frequency	Δf	**Maximum Range**	**Maximum** $u_{\Delta\phi}$	**Maximum** U_D
Laser 1	3.0 GHz	14 MHz	[10, 20] m	0.31 °	$\approx$ 80 μm
Laser 2	1.8 GHz	25 MHz	[0, 5] m	0.87 °	$\approx$ 400 μm

Table 4.2: Summarized trade offs between the experimental setups with *Laser 1* and *Laser 2*. The coloured green cells represent an advantages in one setup when compared to the other.

Chapter 5

Uncertainty Budget and Experimental Results

In chapter 3, we presented a method for ADM and evaluated its uncertainty requirements for a [10, 20] m measurement range. In chapter 4, we developed an experimental setup so that the suggested method could be tested. In this chapter, we will try to establish if the presented sensor can perform an ADM within the uncertainty limits that were established.

With the developed experimental setup we were limited in performing ADM in a range smaller than 5 m. By using a light source only modulated at 1.8 GHz the distance uncertainty requirement of $U_D <$ 100 μm could no be achieved. Despite not being able to test the sensor in the desired range and by knowing upfront that the distance requirements could not be met, we still tried to verify if our method could be used to obtain the correct ambiguity integer. For that reason, the established requirement of $U_N <$ 0.5 must be fulfilled.

To test the sensor, we performed an ADM of a target in a short and mid range, [0, 100] mm and at $\approx$ 4.8 m, respectively. Additionally, an uncertainty budget of the modulation frequency f, and the phase shift measurement, $\Delta\phi$, were performed. This was done to verify if the available instruments could achieve the phase shift and frequency requirements that were obtained in section 4.3.

Due to the complexity of the system and the available time for this work, the presented uncertainty analysis is a light approach. To fully characterize the experimental results, a more complete and thorough analysis of the uncertainty and error sources associated with an ADM needs to be performed. Nevertheless, in this work, the uncertainty contributors were overestimated, so that the preliminary results of the obtained ADM can provide an idea of the error and uncertainty that the suggested setup and method can achieve.

5.1 Variable uncertainty analysis

To implement our method it was determined that *Laser 1* was going to be modulated at 1.8 GHz and then shifted by $\Delta f = 25$ MHz. The analytical uncertainty analysis in chapter 4 revealed that to achieve the ambiguity integer uncertainty requirement, there is a limit standard uncertainty of 0.87 ° and 1.8 kHz for the phase shift measurement and the frequency stability. By taking into consideration the proposed setup, one had to determine the uncertainty contributions of these variables.

5.1.1 Frequency uncertainty

The uncertainty of the modulation frequency of the light source is associated with the degree of knowledge in the output frequency that the *Anritsu* Oscillator produces. Since the RF oscillator is responsible for modulating the laser in amplitude, its output accuracy will correspond to the frequency uncertainty of the modulation. The *Anritsu* oscillator in the continuous working mode, has two main uncertainty components, its resolution and clock uncertainty. Both components were considered with a type B evaluation, since this information was obtained in the instrument datasheet [38]. The resolution contribution to the budget was considered a rectangular distribution, and the clock uncertainty a normal distribution with a coverage factor of k = 1, meaning a confidence interval of 68 $\%$. With this information, one calculated the combined standard uncertainty, for a 1.8 GHz frequency output for this instrument. The results can be found in table 5.1.

Source of Uncertainty	**Value of Component [Hz]**	**Type of Evaluation**	**Squared Standard Uncertainty** $[u_{x_i}]^2$ **[Hz]**^{2}
Resolution	0.01	B/ Rectangular	$\left(\frac{0.01}{\sqrt{3}}\right)^2$
Clock	50	B/ Normal	$\left(\frac{50}{1}\right)^2$
		Combined Standard Uncertainty $[u_f]$ **[Hz]**	50

Table 5.1: Uncertainty balance for the generated frequency in the *Anritsu* oscillator.

5.1.2 Phase shift uncertainty

The phase shift between reference and detected signal on the photodiode was measured with the *Agilent 53230A* frequency counter. In this measurement, the expected error sources are associated with the instrument systematic and random uncertainty for a phase measurement. However, a phase roll between oscillators appears due to the frequency drift of the LO relative to the RF input. Depending on how much this intrinsic characteristic of the oscillators drifts in time, one might have to consider it in the phase shift uncertainty budget.

In summary, the impact of the measuring device, number of phase shift measurements per data set and the phase roll between oscillators, were considered in this evaluation. These contributions are related to the combined standard uncertainty as per eq. 5.1.

$$u_{\Delta\phi} = \sqrt{u^2_{Instrument} + u^2_{RU} + u^2_{PhaseRoll}} \tag{5.1}$$

5.1.2.1 Measuring equipment, the *Agilent 53230A*

The instrument responsible to measure the phase shift was the *Agilent 53230A* frequency counter. The datasheet [56] provides the equations for the random and systematic uncertainty components (RU and SU, respectively), associated with a phase shift measurement. So for a phase shift measurement with this instrument, the uncertainty components can be given as:

$$SU = 360(skew + 2T_{accu})f_{IF} \quad (5.2) \qquad RU = 360(T_{ss}^2 + T_E^2)f_{IF} \quad (5.3)$$

The parameters to calculate the uncertainty components can be found in table 5.2, being that f_{IF} is the measured frequency of the IF signal. This input will be the down converted frequency resulting from the mixing process.

Since our method requires a double frequency phase shift measurement, with the established LO of 2 GHz and RF of 1.8 GHz, one obtains the IF = 200 MHz. When the RF is shifted by 25 MHz, the result is an IF = 175 MHz. Since this uncertainty component is linearly related to the signal frequency, it is clear that this phase shift uncertainty component will not be the same magnitude for both frequencies.

Source of Uncertainty	**Value of Component**	**Description**
T_E	$\frac{500\times10^{-6}}{SR}$ s	Threshold error describes the input signal dependent random trigger uncertainty or jitter.
SR	$2\pi f_{IF}V_{pk-pk}$ V/s	Slew rate describes the input signal's instantaneous voltage rate of change
V_{pk-pk}	5 V	Limit peak to peak voltage
T_{ss}	20 ps	Timing resolution of a start/stop measurement event
$skew$	5 ps	Skew is the additional time error if two channels are used for a measurement.
T_{accu}	10 ps	The timming error is the device measurement error between two points in time.

Table 5.2: Parameters of the *Agilent 53230A* frequency counter for the uncertainty in a phase shift measurement. [56]

Finally, the SU component is a type B evaluation of measurement uncertainty with a coverage level of k = 2. Meanwhile, the RU is a type A, this can be seen as the random uncertainty, so it will reduce as $1/\sqrt{N}$, where N is the number of phase shift measurements [64]. Therefore, the instrument component of the standard uncertainty of a phase shift measurement can be given by eq. 5.4.

$$u_{Instrument}{}^2 = \left(\frac{SU}{2}\right)^2 + \left(\frac{RU}{\sqrt{N}}\right)^2 \quad (5.4)$$

5.1.2.2 Results dispersion

The *Agilent 53230A* was programmed to measure a given number of phase shifts. This measurement has a type A uncertainty, considered with a 68 % confidence interval (k = 1). This uncertainty source is associated with the results dispersion and it can be seen as a phase shift random uncertainty, u_{RU}. So this standard uncertainty component, is given by:

$$u_{RU} = \frac{\sigma}{\sqrt{N}} \quad (5.5)$$

Being σ the phase shift measurement standard deviation.

To test this component's influence, we programmed the frequency counter to acquire 10^6 phase shift measurements with the suggested setup, figure 4.15. The output data set was divided in bins with sizes of

$N = 10^j$ counts, j = 1, 2, 3, 4, 5, 6. For each bin, the standard uncertainty was calculated and averaged. The results are presented in figure 5.1.

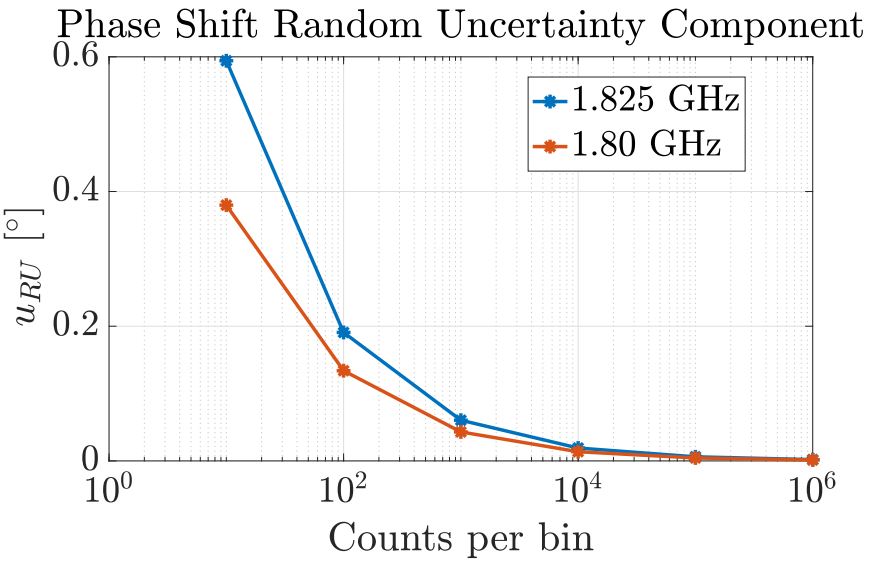

Figure 5.1: Phase shift random uncertainty component for a different number of measurements at RF= 1.8 GHz and 1.825 MHz.

As expected the magnitude of this component decreases with the measurement number. Additionally, for smaller sample size, there is a noticeable difference between this component magnitude for each frequency. With the increase in the sample size, the component contribution to the phase uncertainty budget will approach zero. However, with a large number of measurements the instrument's acquisition time will increase. Therefore, one must trade off the number of measurements with the magnitude that this uncertainty component can achieve to reach the desired goals.

5.1.2.3 Phase roll

The absolute phase roll is the phase shift in the mixing process due to the phase noise in the RF and LO oscillators. This effect is intrinsic to the oscillators and it propagates to the mixing process as a drift in time of the phase shift, $\phi(t)$. It's possible to measure it by using the mixing instrument as a phase detector, as it was explained in section 4.2.3.1.

The phase roll should be taken into account in the uncertainty budget if its overall contribution to it is significant. Therefore, one must quantify how $\phi(t)$ drifts in time to estimate its contribution to the budget. By using the setup presented in figure 4.5 with the *Anritsu* as the RF and the *Atlantic Microwave* 2.0 GHz oscillator as LO, both oscillators were connected to a mixer and the output RMS voltage was measured by an oscilloscope. The RMS was calculated through 5 $\times 10^5$ measurements of voltage potential and acquired by a time window of 0.1 s. By using the calibration curve obtained in section 4.2.3.1, the measured RMS was converted in a phase measurement.

A first measurement of the phase roll was performed with an acquisition time of 3600 s, the results can be found in figure 5.2. There is a slow drift in the phase measurement between oscillators before the phase rolls. These oscillations have a period of $\approx$ 2000 s. Since we intended to perform a phase measurements in a time window at least smaller than 180 s, then such slower variation of the phase should not influence the results.

Additionally, the phase roll measurement was performed for an acquisition time of 180 s, figure 5.3.

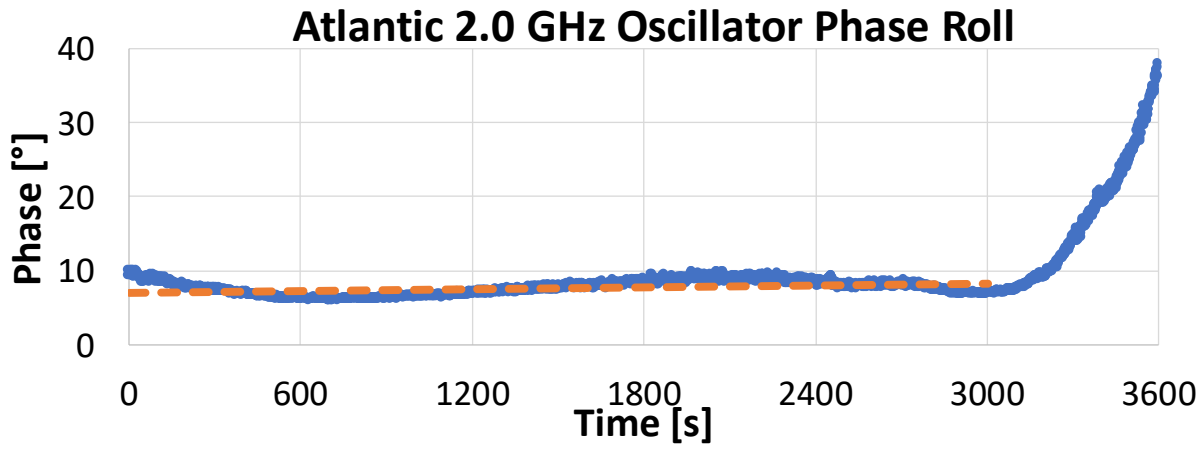

Figure 5.2: *Atlantic Microwave* 2 GHz oscillator phase roll measurement when compared with the *Anritsu MG3690C*. The presented results were measured with an acquisition time of 3600 s and the orange line represents a linear fit to the dataset. This is a linear fit in the region of [0, 3000] s with an equation : $y = 0.0004x + 6.97$.

To quantify how much the phase drifts in time, a linear fit of the data set was performed. With it, a phase offset and a change in phase rate was measure with a magnitude of ≈ 48.37 ° and $\approx 8.6 \times 10^{-5}$ °/s, respectively. Since we intend to perform a phase shift measurement with the output of two mixing processes with the same oscillators, then the offset contribution is cancelled out. However, the same does not apply for the change in phase per time.

Since the phase roll is a drift in time, a possible strategy to deal with this contribution to the overall budget is to reduce the phase shift measuring time. This is done by considering a measurement period short enough that this phase roll contribution can become negligible.

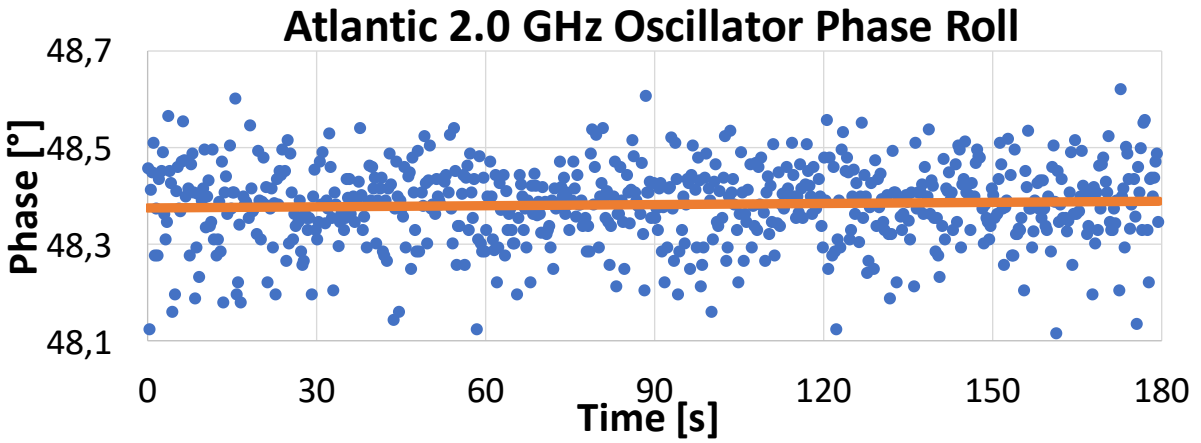

Figure 5.3: *Atlantic Microwave* 2 GHz oscillator phase roll measurement when compared with the *Anritsu MG3690C*. The presented results were measured with an acquisition time of 180 s and the orange line represents a linear fit to the dataset. Its equation is : $y = 8.6 \times 10^{-5}x + 48.37$.

5.1.2.4 Phase shift uncertainty budget

With the phase shift measurement's main contributors characterized, we performed its uncertainty budget. Since our method required a dual frequency measurement, the uncertainty budget was done for both IF of 200 MHz and 175 MHz, tables 5.3, 5.4 respectively.

Component	Source of Uncertainty	Value of Component [º]	Type of Evaluation	Squared Standard Uncertainty $[u_{xi}]^2$ [º]^2	Relative Standard Uncertainty
Instrument	Systematic	1.80	B/ Normal	$\left(\frac{1.8}{2}\right)^2$	95.5 %
	Random	$\left(\frac{1.44}{\sqrt{100}}\right)$	A / Normal	$\left(\frac{0.14}{1}\right)^2$	2.5 %
Result Dispersion	Phase Shift Measurement	0.13	A / Normal	$\left(\frac{0.13}{1}\right)^2$	1.9 %
Phase Roll	Drift in 180 s	$8.5 \times 10^{-5} \times 180$	A / Normal	$\left(\frac{0.016}{1}\right)^2$	0.03 %
			Combined Standard Uncertainty $[u_{\Delta\phi}]$ [º]	0.92 º	

Table 5.3: Phase shift uncertainty budget for an IF = 200 MHz, meaning a modulation frequency of 1.8 GHz.

Component	Source of Uncertainty	Value of Component [º]	Type of Evaluation	Squared Standard Uncertainty $[u_{xi}]^2$ [º]^2	Relative Standard Uncertainty
Instrument	Systematic	1.58	B/ Normal	$\left(\frac{1.58}{2}\right)^2$	91.6 %
	Random	$\left(\frac{1.26}{\sqrt{100}}\right)$	A / Normal	$\left(\frac{0.126}{1}\right)^2$	2.4%
Result Dispersion	Phase Shift Measurement	0.20	A / Normal	$\left(\frac{0.2}{1}\right)^2$	5.9 %
Phase Roll	Drift in 180 s	$8.5 \times 10^{-5} \times 180$	A / Normal	$\left(\frac{0.016}{1}\right)^2$	0.04%
			Combined Standard Uncertainty $[u_{\Delta\phi}]$ [º]	0.82 º	

Table 5.4: Phase shift uncertainty budget for an IF = 175 MHz, meaning a modulation frequency of 1.825 GHz.

This uncertainty budget was done for an ADM with 100 phase shift measurements for each modulation frequency. Evidently, the acquired number of samples has an impact on the budget. This component is different for each modulation frequency and it decreases with the number of samples, as seen in figure 5.1. The justification for having different values for each modulation frequency is based on the fact that the measurement is heavily dependent upon the SNR of the detected phase. This can be noticed by this component relative contribution of 1.9 % with an IF of 200 MHz and 5.9 % with 175 MHz. On the other hand, the random component of the measuring instrument, that also relies in the number of samples, has smaller and similar contributions of 2.4 % and 2.5 %, for each IF, respectively.

Additionally, with 100 phase shift measurement, the ADM could be performed in a short interval of time (hundred of ms). Hence, by reducing the measuring time, the phase roll component can be

overlooked. This is due to its small contribution for the phase measurement, of 0.03 $\%$ and 0.04 $\%$ for 1.8 GHz and 1.825 GHz, respectively. Even when considering an overestimated measuring time of 180 s.

With a large enough number of samples, all of the aforementioned contributors can be reduced to a negligible magnitude. The only relevant uncertainty component is going to be the SU of the measuring device. As it was mentioned in section 5.1.2.1, the SU of the instrument is directly proportional to the input frequency. This means that different IF will have different phase uncertainties. Due to this limitation, the best achievable phase shift combined uncertainty, only with the SU contribution, is ≈ 0.9 º and ≈ 0.79 º, for an IF of 200 MHz and 175 MHz, respectively.

Due to the trade off with the measuring time and by only doing 100 measurements, the SU component has an impact of 95.5 $\%$ and 91.6 $\%$, for each frequency budget. One figures that with a result dispersion of $u_{RU}(@1.8GHz) \approx 0.13$ º and $u_{RU}(@1.825GHz) \approx 0.20$ º, as in figure 5.1, a phase shift combined standard uncertainty of $u_{\Delta\phi}(@1.8GHz) = 0.92$ º and $u_{\Delta\phi}(@1.825GHz) = 0.82$ º should be expected.

5.1.3 Summary

As a conclusion, by considering the phase shift uncertainty results $u_{\Delta\phi}(@1.8GHz) = 0.92$ º and $u_{\Delta\phi}(@1.825GHz) = 0.82$ º along with the frequency uncertainty of $u_f = 50$ Hz, we determined that these parameters allowed for an $U_N < 0.5$, satisfying this work's goal.

Evidently, this is different from the expected results for the uncertainty analytical simulation of chapter 3. However, in that scenario, the phase shift uncertainty for each modulation frequency was considered the same, this did not correspond to reality.

The greatest contributor to the uncertainty budget of an ambiguity integer measurement is $e^N_{\Delta\Phi}$, eq. 3.22 as it is described in 3.3.2. In order to obtain $U_N < 0.5$, this component must be smaller than 0.5 as it is shown in the simulation results in figure 4.16, in chapter 4. Despite the phase shift uncertainty not being of equal magnitude, as it was considered in the analytical simulations, the $e^N_{\Delta\Phi}$ satisfies its requirement. Therefore, the ambiguity integer uncertainty requirement can be met.

This means that with the developed setup in chapter 4, the phase uncertainty requirement for an ADM can be achieved.

5.2 Absolute measurements

In order to test the developed sensor, one performed distance measurements with the corner cube positioned in a short and mid range. The short range consisted in a [0, 100] mm displacement interval with a 10 mm step. For the mid range measurements, one increased the OPL by approximately $\approx$ 4.8 m and performed displacements in an interval of [0, 10] mm with a 1 mm step. Also, the sensor was tested with a "blind measurement", where the target was placed at $\approx$ 2 m and its distance was measured.

Parameter	Value
RF Gain	+ 3 dBm
Laser Current	20.3 mA
Temperature Controler	10.098 kΩ
Measurements per set	100

Table 5.5: Experimental parameters for ADM.

In the experimental setup presented in figure 4.15, in chapter 4, we relied on the usage of the *Thor Labs NRT* translation stage with a corner cube attached to extend the OPL travelled by light. This design allowed for the target position to be displaced and consequently perform an ADM relative to a reference point D_0, as seen in figure 5.4. Considering that the *Thor Labs NRT* translation stage presents a 1 μm bidirectional repeatability [52], thus it has an error much smaller when compared with the expected ADM. The OPL measurement error can be considered to be only due to the phase shift measurement process.

Figure 5.4: ADM setup with the corner cube attached at the *Thor Labs NRT* translation stage. The scheme measures D_M by referencing the phase shift measurement of D_1 to D_0.

By fine tuning the experimental setup, one established the best parameter for the electrical components to obtain the highest SNR. These parameters can be found in table 5.5 and they are fixed throughout the measurements.

For the established ranges, we performed one set of 100 phase shift measurements per position and for each modulation frequency of 1.8 GHz and 1.825 GHz. The resulting raw data was then processed with a *Matlab 2017a* script, that is available in appendix D. This script is based on the model presented in chapter 3, where the ambiguity integer is determined with eq. 3.10.

Since the ambiguity integer is the number of cycles for a phase shift, this value must be determined without an uncertainty associated. Hence, the presented processing algorithm in the appendix D, searches for an integer number within the confidence interval of the measured ambiguity value. This resulting value is considered the ambiguity integer for that measurement. That is why it is crucial that $U_N < 0.5$ with a coverage value of k = 2, so that the confidence interval of the measured ambiguity integer only contains one integer value.

Additionally, the set of measurements has to be referenced to a given point in the setup at a distance of D_0. This point was set differently for each test ranges . For the reference position, the corner cube was always placed in the zero mark of the translation stage, as seen in figure 5.4.

In each set of measurement, the reference point is measured to obtain the phase shift $\Delta\phi_0$ for each modulation frequency. Consequently, the ambiguity integer N_0 for that position is determined. For all the other different corner cube positions, D_i, i = 1,2,3 ..., the phase shifts for each position were measured $\Delta\phi_i$ and the ambiguity integer calculated, N_i i=1, 2, ... By using eq. 5.6 and eq. 5.7 the phase shift and ambiguity integers were referenced to D_0, Δphi and N, respectively and the resulting ADM was calculated using 3.1.

$$\Delta\phi = \Delta\phi_i - \Delta\phi_0, i = 1, 2, 3... \quad (5.6) \qquad N = N_i - N_0, i = 1, 2, 3... \quad (5.7)$$

The combined uncertainty of the referenced phase shift is given by eq. 5.8. Since in the simulation in chapter 3 we did not account for this difference between phase shifts, it is expected that the resulting ADM uncertainties will have a higher magnitude than the calculated ones.

$$u_{\Delta\phi} = \sqrt{u^2_{\Delta\phi_i} + u^2_{\Delta\phi_0}}, i = 1, 2, ... \quad (5.8)$$

5.2.1 Short Range

The first ADM we performed with the sensor was done by displacing the corner cube in a [0, 100] mm range with a 10 mm step. Since the ambiguity range for the 1.8 GHz and 1.825 GHz modulation frequencies is $\approx$ 80 mm, to measure the target position, one would have to measure N. This set of measurements were done to verify if one could capture a change in the ambiguity integer. If one was able to do so, it meant that our method could be used to perform ADM as it was predicted.

By using a $\Delta f = 25$ MHz, the unambiguous measurement range is [0 5.998] m, i.e measurements with $\Delta N = 0$ or $\Delta N = -1$. However, the available unambiguous interval for ADM is only part of that range. Since our sensor's reference is not in $N = 0$ and $\Delta\phi = 0$, this means that an ADM relative to that point has an offset in the unambiguous interval. Due to the existing electrical and optical paths in the setup, one estimates that this offset is $\approx$ 3 m. So, for a range of [0, 100] mm, one should expect $\Delta N = 0$ or $\Delta N = -1$ for a $\Delta f = 25$ MHz.

5.2.1.1 Measurement Procedure

The experimental procedure to obtain an ADM for a [0, 100] mm range with a 10 mm step is:

1. Set the reference point by positioning the corner cube in the zero position of the translation stage;
2. Aligning the telescope with the corner cube;
3. Measure ten sets of phase measurements for a 1.8 GHz and 1.825 GHz modulation frequencies;
4. Displace the translation stage with a 10 mm magnitude;
5. Measure, for each modulation frequency, ten sets of phase measurements;
6. Repeat step 4 and 5 until the maximum range of the translation stage is achieved;

5.2.1.2 Results

For each position of the corner cube, ten sets of phase shift measurements were performed. This set of measurements were processed using the *Matlab 2017a* script D, and its ambiguity integer was determined for a modulation frequency of 1.8 GHz. Raw results can be found in figure 5.5.

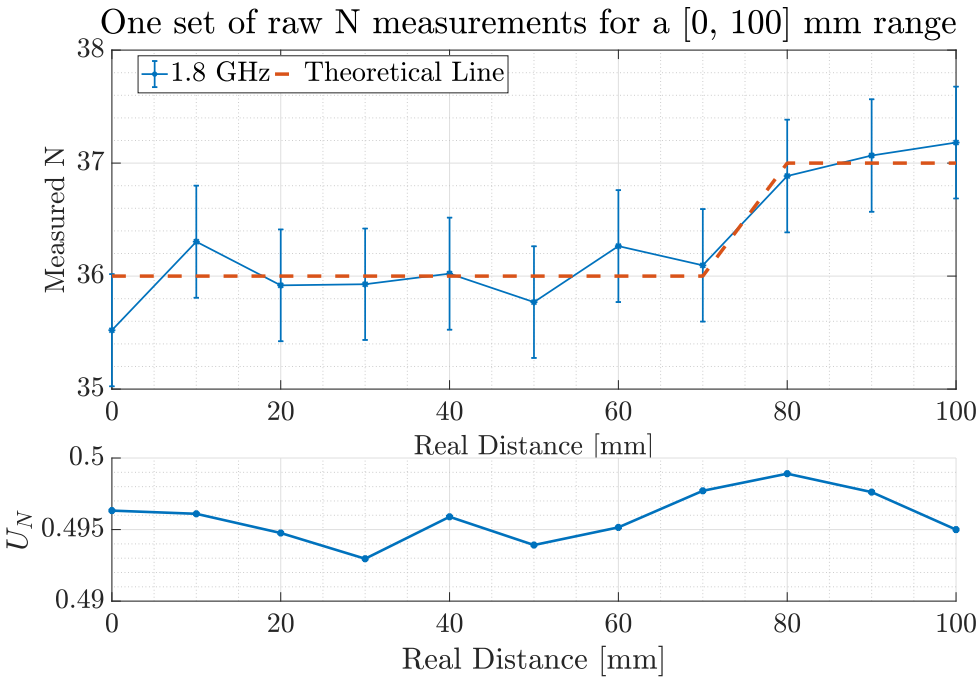

Figure 5.5: Experimental results for the ambiguity integer measurement for an ADM range of [0, 10] mm with a 1 mm step and an offset of $\approx$ 4.8 m. Additionally, it is presented the expanded uncertainty with a confidence interval of 95 % and a coverage factor of $k = 2$.

The processing script found the integer value within the confidence interval of the measured ambiguity integer. As seen in figure 5.5, due to the boundaries in the uncertainty limit of the ambiguity integer, there is only one possible integer value within its confidence interval. Hence, one considers it the measurement result and consequently, it has no uncertainty in its determination.

For each position, N_i and $\Delta\phi_i$ were determined and referenced to N_0 and $\Delta\phi_0$, respectively. The results for the processed set of ambiguity integer measurements can be found in figure 5.6. The obtained ADM for each modulation frequency can be found in figure 5.7.

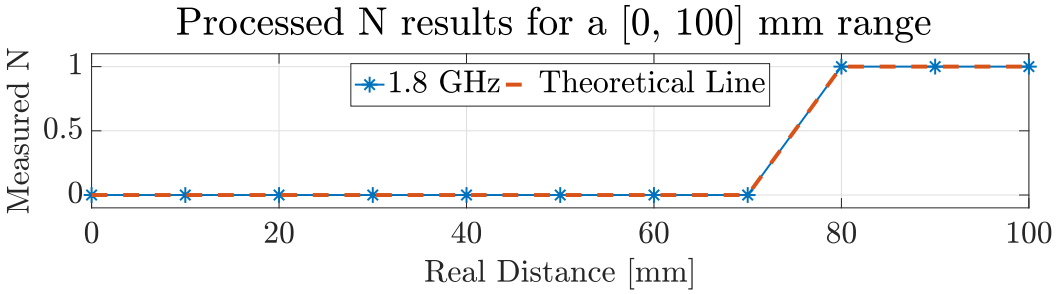

Figure 5.6: Processed ambiguity integer with a *Matlab 2017a* script, appendix D for an ADM range of [0, 100] mm.

Both results of the expanded uncertainties have been calculated based on the phase shift uncertainty budgets and the analytical model presented in chapter 3. The presented values show that the sensor can detect a change in the ambiguity integer and consequently measure the corresponding displacement within its uncertainty value.

The summarized results for the ambiguity integer and ADM, for the ten sets of measurements, can be found in figure 5.8 and figure 5.9. In all of the 110 ambiguity integer measurements, only 5 corresponded to an incorrect N measurement. This corresponds to a 95.5 % success rate in the measurements. Evidently, these incorrect measurements lead to an error in the resulting ADM. However, the majority of

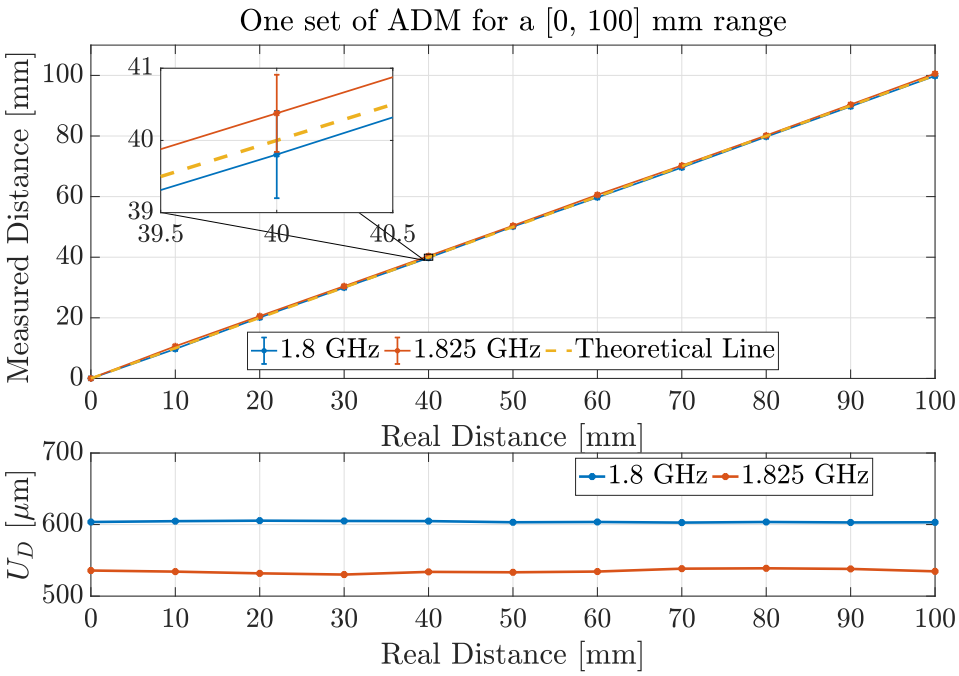

Figure 5.7: Experimental results for one set of ADM in range a of [0, 100] mm with a 10 mm step. Additionally, it is presented the expanded uncertainty with a coverage factor of $k = 2$, meaning a confidence interval of 95 %

the remaining distance measurements have the theoretical value for its measurement position within its 95 % confidence interval.

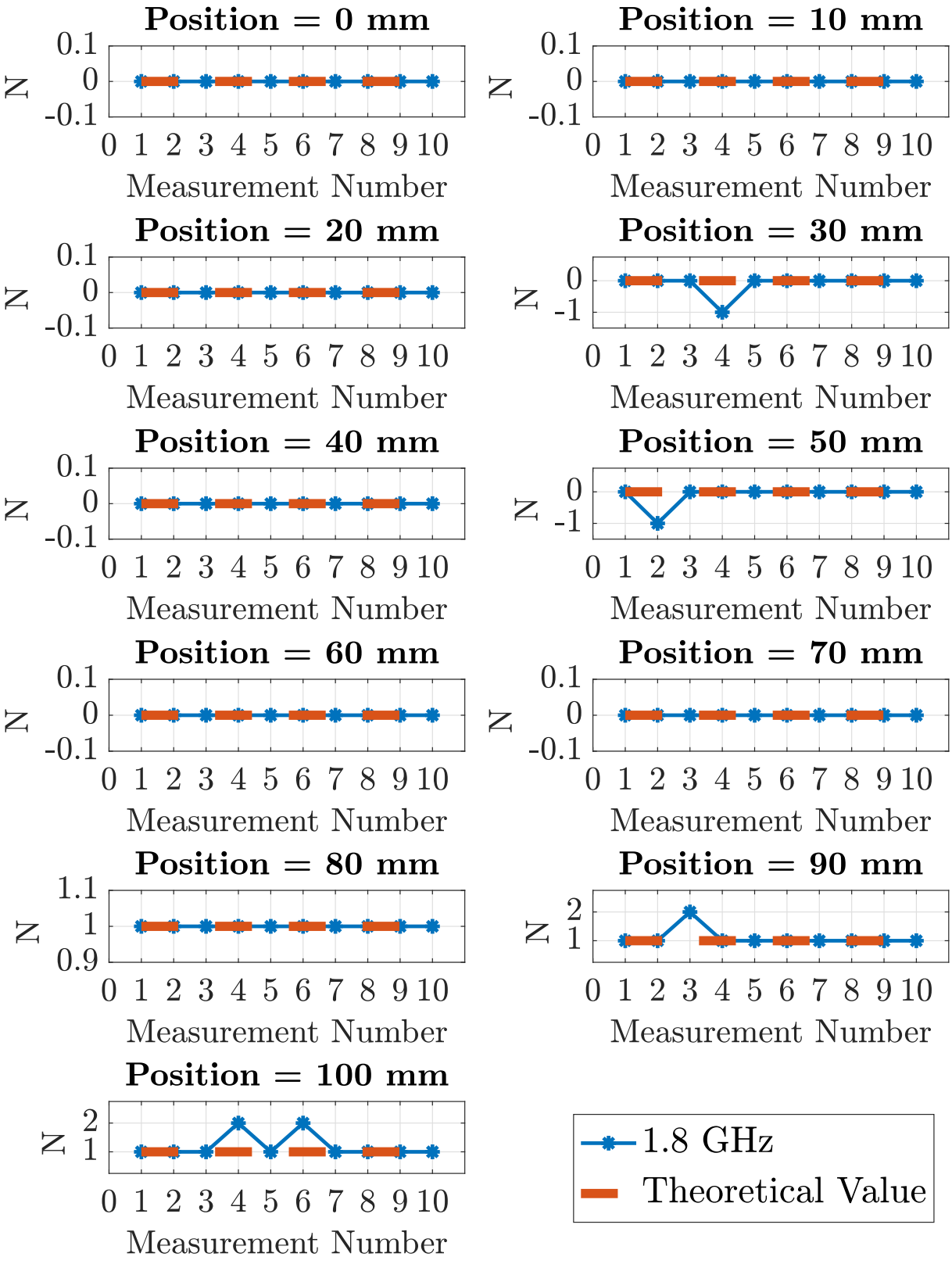

Figure 5.8: Experimental results of the ambiguity integer measurement for an ADM range of [0, 100] mm with a 10 mm step, accounting for 10 measurement sets per position.

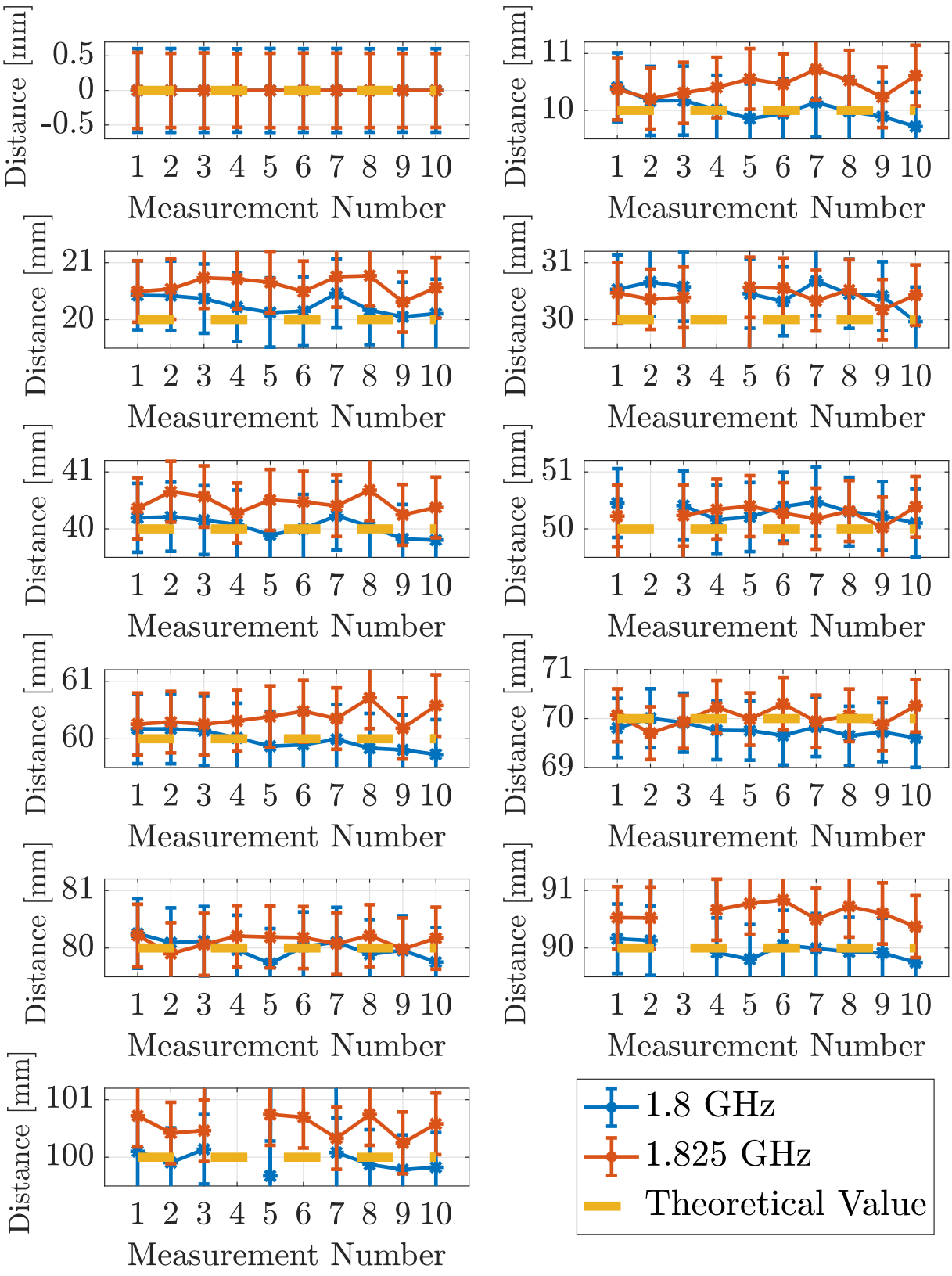

Figure 5.9: Experimental results of an ADM at a range of [0, 100] mm with a 10 mm step, accounting for 10 measurement sets per position. The error bars are the expanded uncertainty with a coverage factor of k = 2, meaning a confidence interval of 95 %

5.2.2 Mid Range

Afterwards, the sensor was tested in a mid range (greater than 4 m) by performing [0, 10] mm displacements with a 1 mm step. This range was achieved by extending the OPL from our reference, with the use of the fibre from a *Thor Labs FPC560* fibre polarization controller [65]. Despite using this instrument, the study of how the polarization correction could impact the SNR was not in the scope of this work.

Since one cannot open the instrument to measure the length of its optical fibre, the information of the datasheet was used to estimate it. With the required calculation, one figured that the fibre length is ≈ 3.2 m. This optical fiber has a refraction index of $n_{fiber} = 1.4682$ [46], which leads to an OPL of ≈ 4.8 m. It is not critical the degree of knowledge of the distance offset introduced by the fibre. Since one considers the translation table displacements exact, this measure intends to test the sensor's response for an ADM at a meter range.

Furthermore, by extending the measuring range by ≈ 4.8 m, and since one is using $\Delta f = 25$ MHz, it should be expect $\Delta N = -1$ or $\Delta N = -2$ for the ambiguity integer measurements. The fibre's offset is almost the same magnitude as the unambiguous range for this method (5.998 m). Since the reference of the setup is not in N = 0 and $\Delta\phi = 0$, the unambiguous operating range has an offset, as it was mentioned early, so this addition in the OPL is enough to surpass it. Due to the versatility of the developed method, the operating range was easily adjusted.

5.2.2.1 Measurement Procedure

The experimental procedure to obtain an ADM for a [0, 10] mm range with a 1 mm step and an offset of ≈ 4.8 m is:

1. Set the reference point by positioning the corner cube in the zero position of the translation stage;
2. Aligning the telescope with the corner cube;
3. Measure eleven sets of phase measurements for a 1.8 GHz and 1.825 GHz modulation frequencies;
4. Add the *Thor Labs FPC560* fibre controller to the light path;
5. Displace the translation stage with a 1 mm magnitude;
6. Measure, for each modulation frequency, eleven sets of phase measurements;
7. Repeat step 5 and 6 until a 10 mm displacement is complete;

5.2.2.2 Results

For each position of the corner cube, 11 sets of phase shift measurements were performed. This set of measurements were processed using the *Matlab 2017a* script D, and its ambiguity integers were determined for a modulation frequency of 1.8 GHz, figure 5.10.

In the processing script, the ambiguity integers for each position were measured and referenced to N_0, the results for this set can be found in figure 5.11. The obtained ADM for each modulation frequency can be found in figure 5.12.

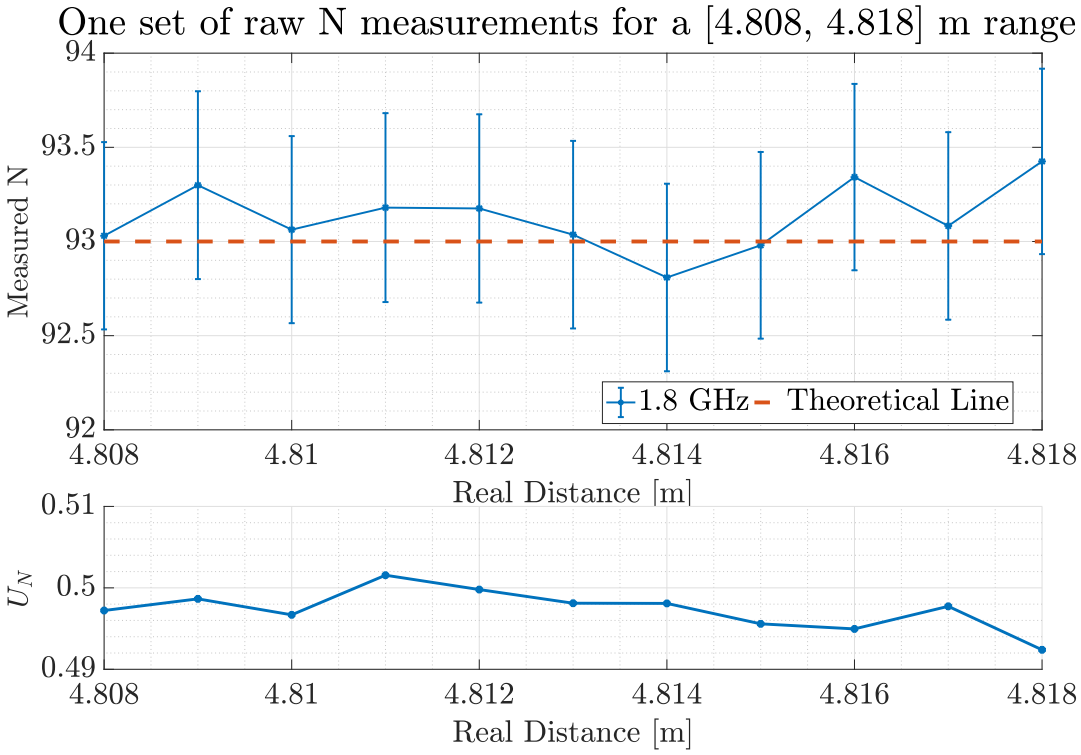

Figure 5.10: Experimental results for the ambiguity integer measurement for an ADM range of [0, 10] mm with a 1 mm step and an offset of $\approx$ 4.8 m. Besides the presented values the 0 m mark mesaured an N = [35.03 $\pm$ 0.49]. Additionally, it is presented the expanded uncertainty with a coverage factor of k = 2, meaning a confidence interval of 95 %

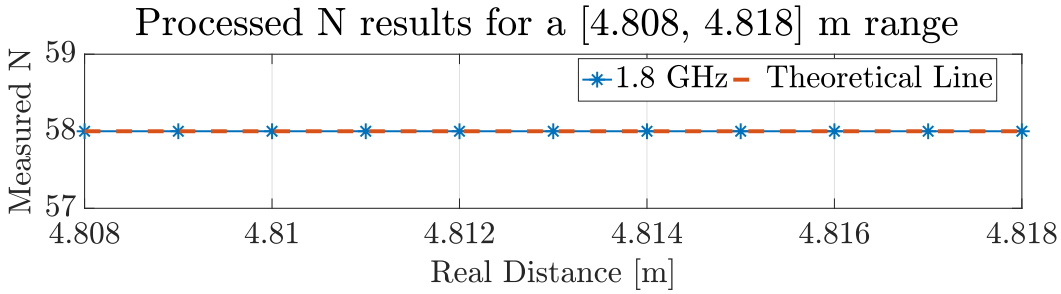

Figure 5.11: Processed ambiguity integer with a *Matlab 2017a* script, appendix D for an ADM range of [0, 10] mm with a 1 mm step and an offset of $\approx$ 4.8 m.

Due to the increase in the operating range by the fibre offset, the sensor's unambiguous range was expanded with $\Delta N = -1$ or $\Delta N = -2$. With this offset, an ambiguity integer of N = 58 was measured for the 10 mm range displacements. The measured fibre offset was [4.8080 $\pm$ 0.0006] m, this is the magnitude that was expected in our estimations. After analysing the performed displacements, we concluded

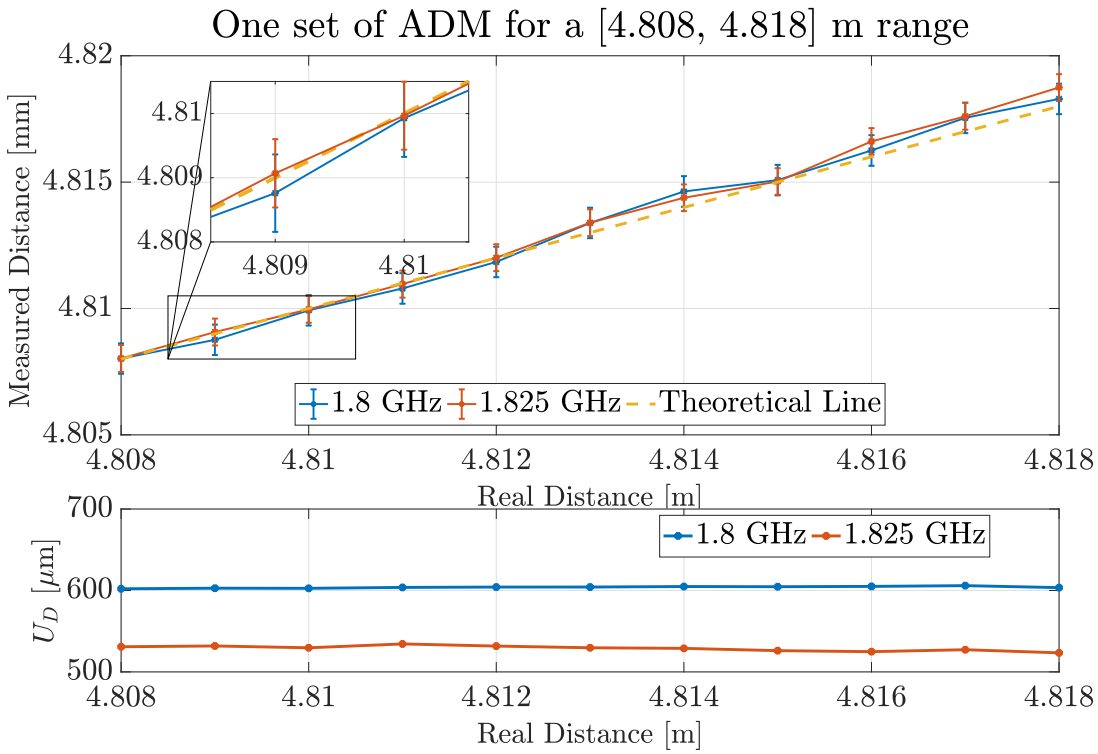

Figure 5.12: Experimental results for an ADM in a range of [0, 10] mm with a 1 mm step and an offset of $\approx$ 4.8 m . Additionally, it is presented the expanded uncertainty with a coverage factor of k = 2, meaning a confidence interval of 95 %

that the developed sensor could correctly measure the expected value for the ambiguity integer at that range.

The summarized results for the ambiguity integer and ADM for the eleven sets of measurements can be found in figure 5.13 and figure 5.14. In all of the 121 ambiguity integer measurements, only 9 corresponded to an incorrect N measurement. This corresponds to a 92.6 % success rate in the measurements. The most affected point by an incorrect N measurement was the 4.818 m, where only 6 out of 11 sets determined the correct ambiguity integer. However, the remaining distance measurements have the theoretical value for its measurement position within its 95 % confidence interval.

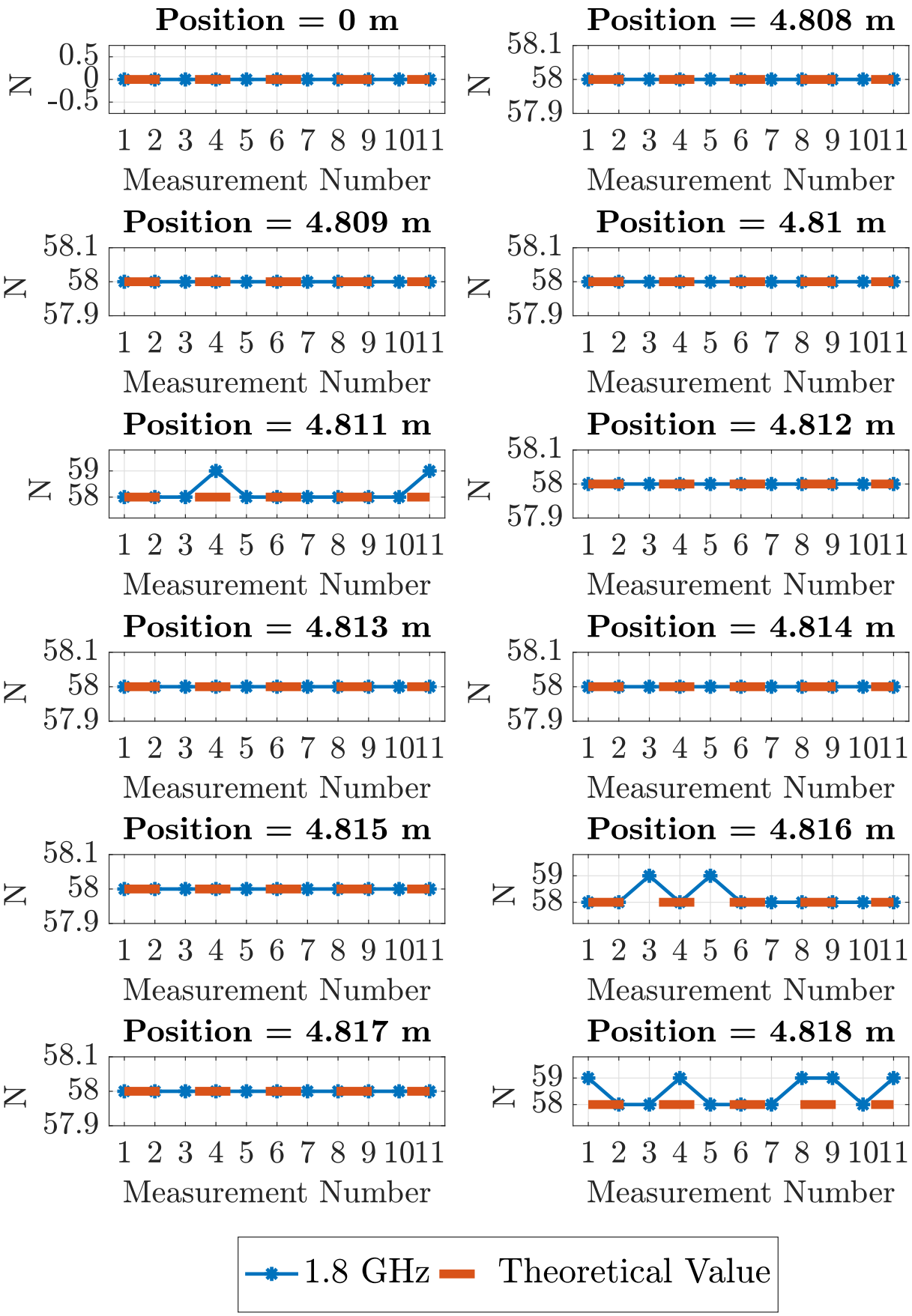

Figure 5.13: Experimental results for the ambiguity integer measurement for an ADM range of [0, 10] mm with a 1 mm step and with an offset of ≈ 4.8 m, accounting for 11 measurement sets per position.

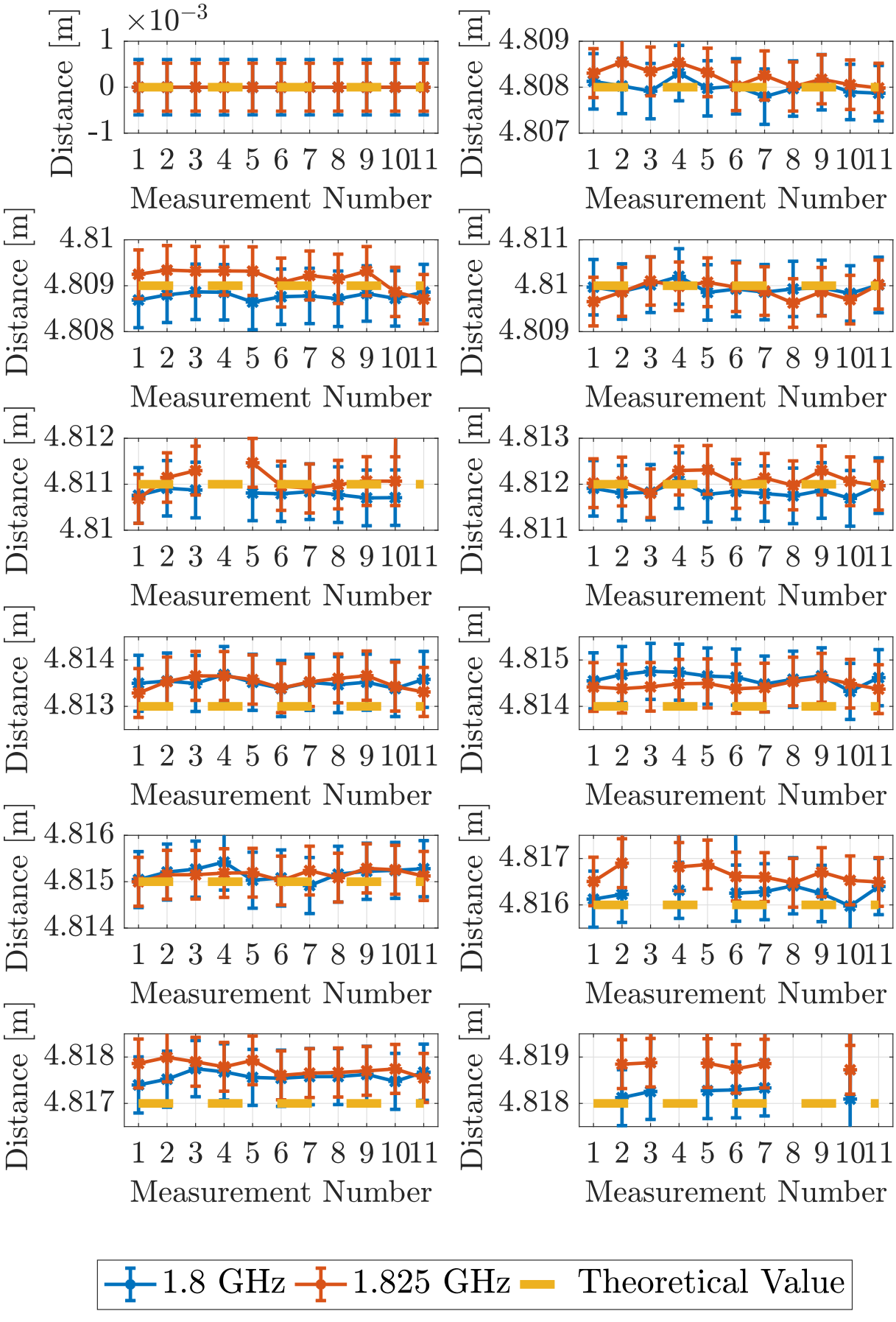

Figure 5.14: Experimental results for an ADM range of [0, 10] mm with a 1 mm step and with an offset of ≈ 4.8 m, accounting for 11 measurement sets per position. The error bars are the expanded uncertainty with a coverage factor of $k = 2$, meaning a confidence interval of 95 %.

5.2.3 Blind Measurement

Finally, one performed a blind measurement with the sensor. The corner cube was placed at ≈ 2 m from the sensor reference point. With this extension of the OPL and due to the offset in the unambiguous range, by using a $\Delta f = 25$ MHz one should expect $\Delta N = 0$ or $\Delta N = -1$.

Contrary to the previous measurements, the OPL is extended by physically separating the corner cube from the telescope. By increasing the distance between these two instruments the SNR is compromised. New issues regarding their optical alignment and signal reduction due to losses in the medium, increased the difficulty of performing an ADM. Further work needs to be done to overcome these difficulties.

To have a comparative ADM, one used a laser TOF range finder, *Leica D510* [60]. According to its datasheet, this device has a maximum range of 200 m with a 0.1 mm resolution and uncertainty of 1 mm. The latter is the biggest contributor for a distance measurement uncertainty with this device. So we considered that the corner cube position was measured with a 1 mm uncertainty. With this device fixed, we measured the target in its reference position and when displaced.

5.2.3.1 Measurement Procedure

The experimental procedure to an ADM for a target at an unknown distance, is:

1. Set the reference point by positioning the corner cube in the zero position of the translation stage;
2. Align the telescope with the corner cube;
3. Measure eleven sets of phase measurements for a 1.8 GHz and 1.825 GHz modulation frequencies;
4. Place the corner cube at ≈ 2 m from its reference;
5. Align the telescope with the corner cube;
6. Measure, for each modulation frequency, eleven sets of phase measurements;

5.2.3.2 Results

The position measurement result with the *Leica* range finder was a displacement of $[2.1391 \pm 0.0014]$ m. The comparison between the range finder measurement and the obtained results for eleven sets of phase measurements per position with the developed sensor, can be found in figure 5.15 and 5.16. Only one of the ambiguity integer measurements was not the expected value, having direct consequences on the distance measurements. Nevertheless, all of the other ADM and its expanded uncertainty was within the 95 $\%$ confidence interval of the laser range finder.

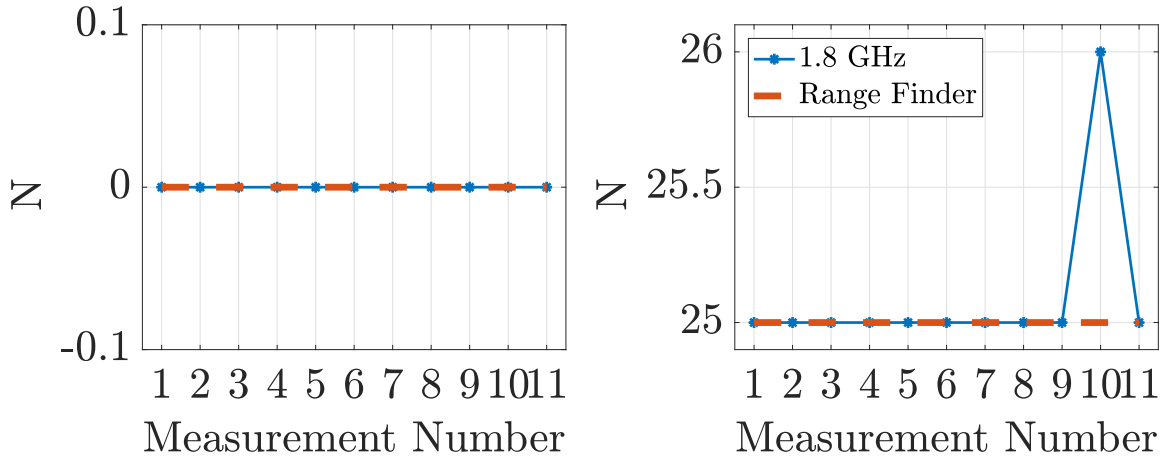

Figure 5.15: Experimental results for the ambiguity integer measurement for an ADM at a blind measurement of ≈ 2 m, accounting for 11 measurement sets per position. Additionally, it is presented the expanded uncertainty with a coverage factor of $k = 2$, meaning a confidence interval of 95 %.

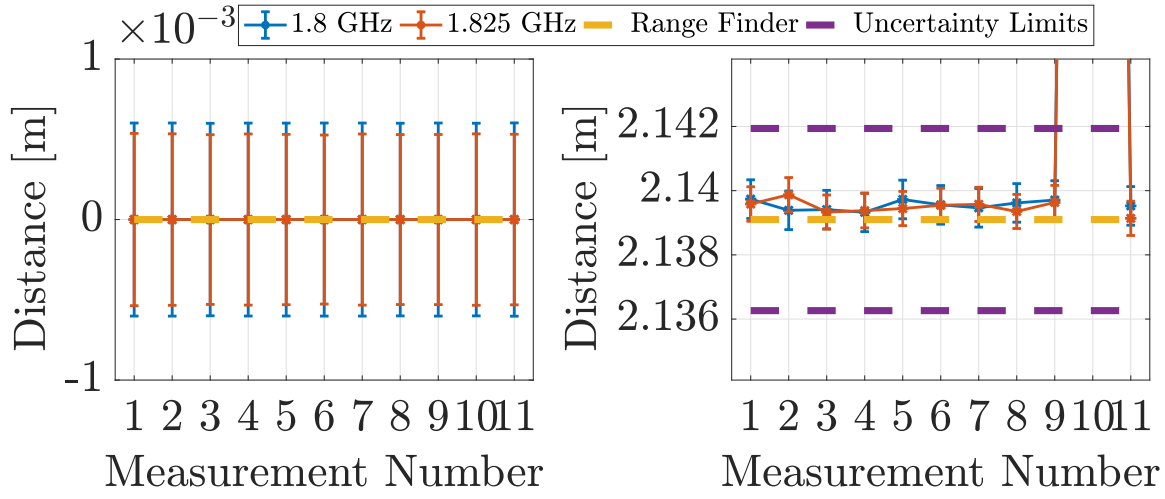

Figure 5.16: Experimental results for an ADM at a blind measurement of ≈ 2 m, accounting for 11 measurement sets per position. The error bars are the expanded uncertainty with a coverage factor of $k = 2$, meaning a confidence interval of 95 %. The measured ADM with the range finder is also represented with its uncertainty limits.

5.3 Result Analysis

With the obtained results for the different test ranges, one was able to accurately measure the ambiguity integer with the developed dual frequency PS CW TOF method. In the measurements at [0, 100] mm range, figure 5.8, it was possible to show that the sensor was able to detect the change in ambiguity integer and consequently measure the correct ADM. For a mid range target, we were also able to determine the correct ambiguity integer for most of the measurements, as showed by the results at a ≈ 4.8 m and the blind measurements, figure 5.13 and 5.15 respectively.

5.3.1 Ambiguity integer

The necessity for an accuracy $U_N < 0.5$ can be seen in the N transition between the 70 mm and 80 mm mark in figure 5.6. If the measurement uncertainty exceeds the imposed limit, the confidence interval might include two ambiguity integers, hence, not allowing a clear determination of the correct ambiguity.

To verify the reproducibility of the ambiguity integer determination with this sensor, we performed

several sets of measurements per position for each range and compared the obtained results, figure 5.8, 5.13 and 5.15. These revealed that in some situations the sensor was not able to measure the correct ambiguity for the test position. The incorrect measurements usually lead to the determination of the ambiguity in the next or previous integer value. This is due to the measurement of the incorrect phase shift. It is not clear the reason this effect might occur. However, it must be due to some optical or electric noise contribution for the equipment that deteriorates the SNR, leading to the incorrect measurement. Further work needs to be done to understand the origin and the contributors to this effect.

However, even without an in-depth analysis, there are still ways to overcome this problem. The easiest one is by doing a large number of phase measurement per position. Then, by calculating the corresponding N and performing statistical analysis of the obtained values, it would be possible to identify the outliers in the measurement and remove them. On the other hand, to acquire the required volume of samples it would be needed a large acquisition time per test position, which can be a limiting factor for some applications.

If the built sensor was not instrumentally constrained to perform a $\Delta f = 25$ MHz, one could have used a slightly different frequency shift to perform the same measurements. This measurement could be used to confirm the ambiguity integer obtained with the first frequency shift. At the same time, changing the operating frequency can remove any electrical resonance in the instruments connectors, that are typical noise contribution for a RF device. Removing these parasitic components could contribute to a more accurate set of phase shift measurement.

5.3.2 Absolute distance measurement

The ADM results for the tested ranges are directly related to the ambiguity integer measurement. The distances that are more deviated from the expected values are the ones corresponding to wrong ambiguity measurements, as seen in figure 5.9, 5.14 and 5.16. The incorrect N measurement for a given position leads to a distance measurement with an offset with a magnitude of an ambiguity range ($\approx$ 80 mm), consequently, ruining the sensor accuracy and precision.

By using the developed dual PS CW TOF method, one expected to obtain a distance uncertainty of ≈ 400 μm for the 1.8 GHz and 1.825 GHz frequencies, as seen in the simulation results in figure 4.16 in chapter 4. However, the resulting absolute distance measurement uncertainty is ≈ 600 μm for all test ranges. This unexpected increment in the distance uncertainty is due to the sensor needing a reference position to perform distance measurements relative to that point. This means that there is an uncertainty contribution from the degree of knowledge in the reference position of the system, as seen in eq. 5.8. The additional contribution lead to the disparity between the measured results and the Monte Carlo and analytical simulations.

Nevertheless, the error due to the reference can be reduced by performing a calibration with another ADM instrument with an uncertainty smaller than the presented sensor. For example, one could use a dual frequency interferometer as the calibration device. This instrument can operate in the intended range of [0, 5] m and achieve relative uncertainties in the magnitude of 1 ppm. The interferometer can be used to measure and calibrate the reference of the sensor. Hence, this distance would be determined with finer accuracy as before. So the contribution of the reference position in the sensors distance uncertainty budget is decreased, and the major contribution comes from the measurement of the point of interest.

5.3.3 Calibration Curves

Additional analysis can be performed to the short and mid range measurements. To have a representative value for each tested position, the corresponding results from figure 5.9 and 5.14, were averaged and $\overline{D_i}$, i= 1, 2, 3 ... obtained.

Since all of the different set of phase shifts are performed with the same conditions per position, then each ADM are correlated. According to [64], the expanded uncertainty of the average result is obtain through eq. 5.9, being k the number of measurements per position and U_{D_i} the expanded uncertainty for each individual measurement. The results for both the short and mid range can be found in figure 5.17 and 5.18, respectively.

$$\overline{U_D} = \sum_i \frac{U_{D_i}}{k}, i = 1, 2, ..., k \tag{5.9}$$

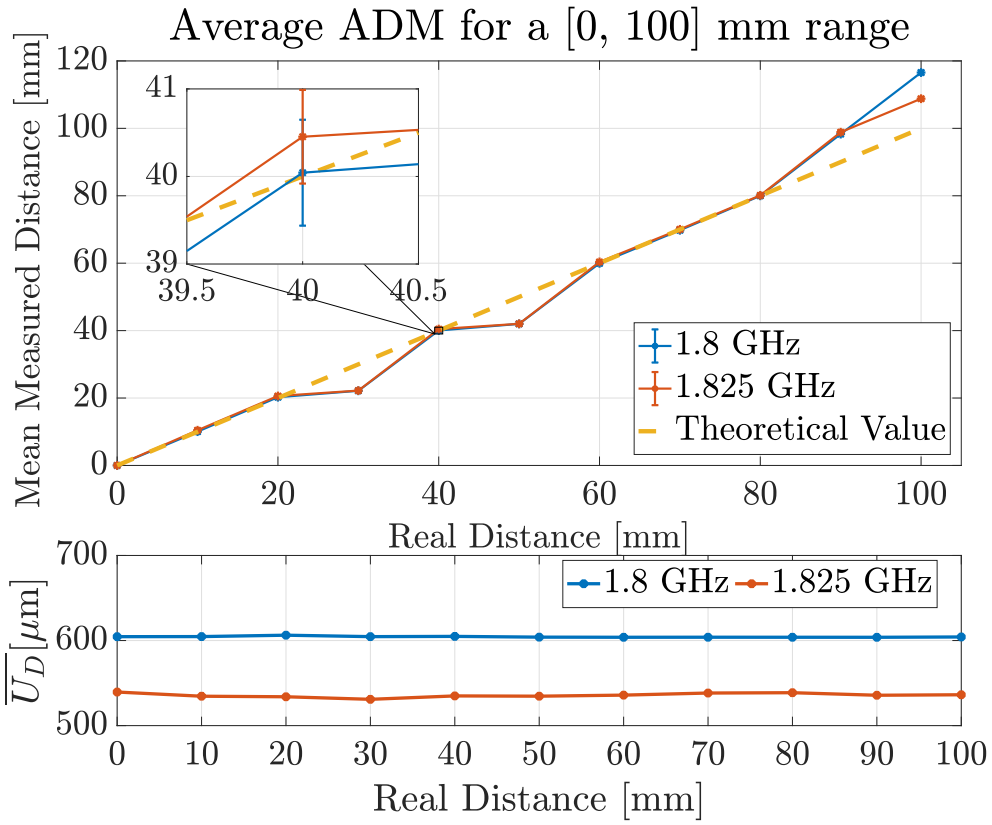

Figure 5.17: Average obtained ADM for each position in a [0, 100] mm range and its average expanded uncertainty with a coverage factor of k = 2, meaning a confidence interval of 95 %.

As it was mentioned before, the incorrect N measurement leads to an offset in the distance measurements. This extra contribution has a clear impact on the corresponding mean value of the measurement set. However, if the effect responsible for the wrong phase measurement could be repeatable within a given distance or interval, it could be corrected through a calibration curve. On the other hand, one did not perform ADM in a range wide enough to be able to conclude effectively anything regarding the sensor erroneous N measurements.

To perform a calibration curve for the measured ranges, the values of the incorrect N measurements were considered as outliers. Additionally, due to the small amplitude of the tested ranges, one figured that a linear fit was the best curve to represent the results. This fit intended to provide the information

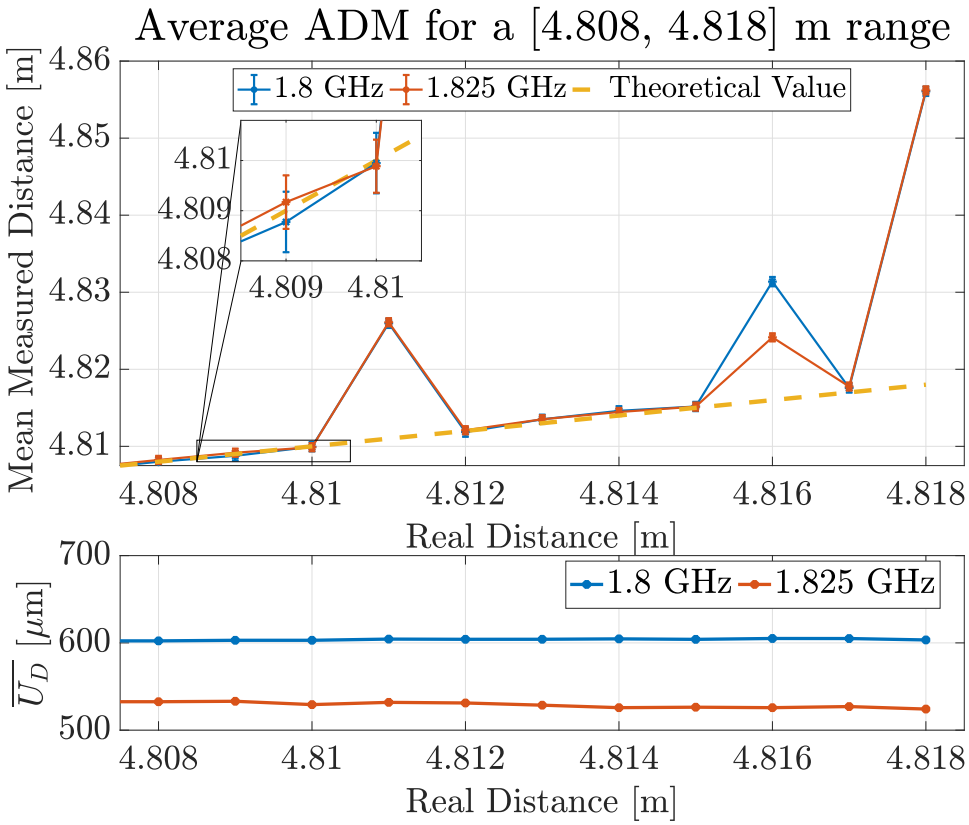

Figure 5.18: Average obtained ADM for each position in a [4.808, 8.818] m range and its average expanded uncertainty with a coverage factor of k = 2, meaning a confidence interval of 95 %.

regarding an offset, b and scale factor, α that are included in an ADM with the sensor, eq. 5.10.

$$D_M = \alpha D_{real} + b \tag{5.10}$$

Being D_M the average measured distance and D_{real} the corresponding real distance. The fit parameters for each frequency and range can be found in table 5.6. With the calibration curve results, one performed a correction to the mean measured values, using eq. 5.11, so that the experimental relative and absolute error could be reduced. For each frequency the calibration curves and corrected results for the short and mid ranges can be found in figure 5.19 and 5.20, respectively.

$$D_c = \frac{D_M - b}{\alpha} \tag{5.11}$$

Range	**Modulation Frequency**	**Scale Factor** α	**Standard Uncertainty**	**Offset** b	**Standard Uncertainty**
[0, 100] mm	1.8 GHz	0.997	0.001	1.9×10^{-4} m	0.8×10^{-4} m
	1.825 GHz	1.001	0.001	3.0×10^{-4} m	0.9×10^{-4} m
[4.808, 4.818] m	1.8 GHz	1.000	0.001	-1.4×10^{-6} m	0.006 m
	1.825 GHz	1.000	0.001	-1.7×10^{-6} m	0.006 m

Table 5.6: Calibration curve parameters for short and mid range for each frequency.

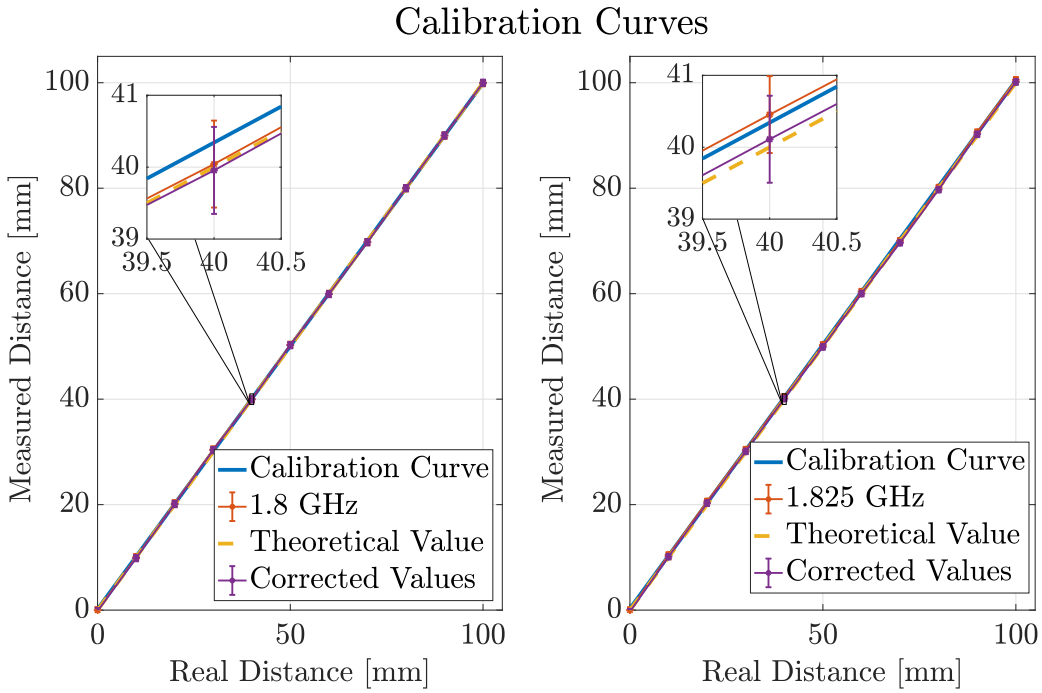

Figure 5.19: Calibration curves and corrected measured values for the [0, 100] mm range. The expanded uncertainty has a coverage factor of $k = 2$ with a confidence interval of 95 %.

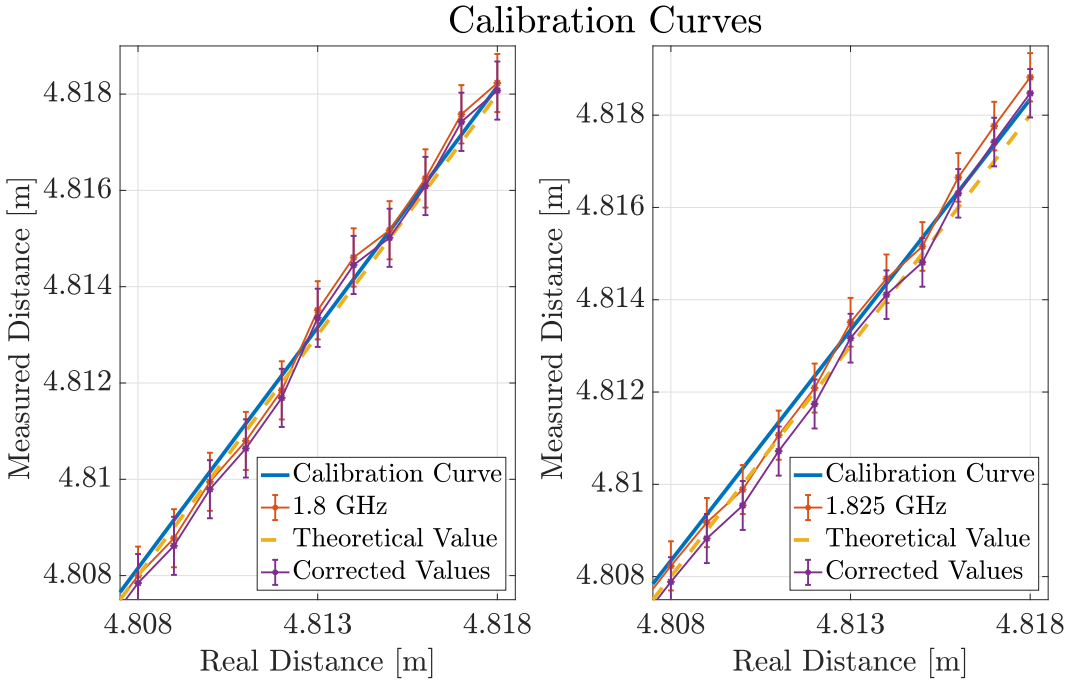

Figure 5.20: Calibration curves and corrected measured values for the [4.808, 4.818] m range. The expanded uncertainty has a coverage factor of $k = 2$ with a confidence interval of 95 %.

5.3.4 Error Analysis

To have a good idea of the sensor performance for the tested ranges, one verified the absolute and relative error for each position. The errors were calculated relative to the position in the translation stage, since we considered its displacements as exact. Only the results without the outlier ambiguity integer were considered. Not having this contribution for the average measured result has an impact on the experimental error obtained in an ADM by the sensor .

For example, the sensor average result for the blind measurement, accounting the erroneous N measurements is [2.1471 $\pm$ 0.0006] m and [2.1470 $\pm$ 0.0006] m, for a 1.8 GHz and 1.825 GHz modulation frequencies. This leads to an absolute error of $\approx$ 8 mm for both frequencies. When considering the measuring range, its relative error is $\approx$ 0.37 $\%$. However, by only accounting with the correctly obtained N, the distance result is similar for both frequencies [2.1395 $\pm$ 0.0006] m with a relative error of 0.02 $\%$. This means that when comparing absolutely to the measured value by the range finder its error is 446 μm and 385 μm for 1.8 GHz and 1.825 GHz, respectively. This set of measurements reveal that with the correct ambiguity integer, the sensor can improve its experimental error by an order of magnitude.

For the short and mid range test, one performed a correction with its calibration curve, as it was explained in the last subsection. To verify the effectiveness of this, a comparison between the error with and without it is presented. This evaluation can verify if the sensor performance is enhanced with the calibration curve corrections.

5.3.4.1 Short Range

The results for the short range relative and absolute experimental error can be found in figures 5.21 and 5.22. There is a noticeable difference in the magnitude of the experimental error for both frequencies. The obtained mean absolute errors with no corrections are 133 μm and 352 μm, for the 1.8 GHz and 1.825 GHz, respectively.

On the other hand, the average absolute error for the corrected values is 126 μm and 179 μm for the 1.8 GHz and 1.825 GHz frequency. The corrections impact is more notorious in the 1.825 GHz, where its error is reduced $\approx$ 49 $\%$ from its original value.

Considering the measuring range in the interval of [0, 100] mm, a relative error in the interval of [10^{-3}, 1] $\%$ was obtained for the corrected values. For some positions, this adjustment in the measured value allowed for a maximum reduction of the relative error by one order of magnitude for both frequencies.

With this correction, the experimental error for all of the tested positions is smaller than its uncertainty, $\approx$ 600 μm and $\approx$ 530 μm for 1.8 GHz and 1.825 GHz, respectively. This reveals that for this range the performed correction revealed effective in reducing the measurement error from its theoretical value and guaranteeing that the real value is within the 95 $\%$ confidence interval of the corrected value.

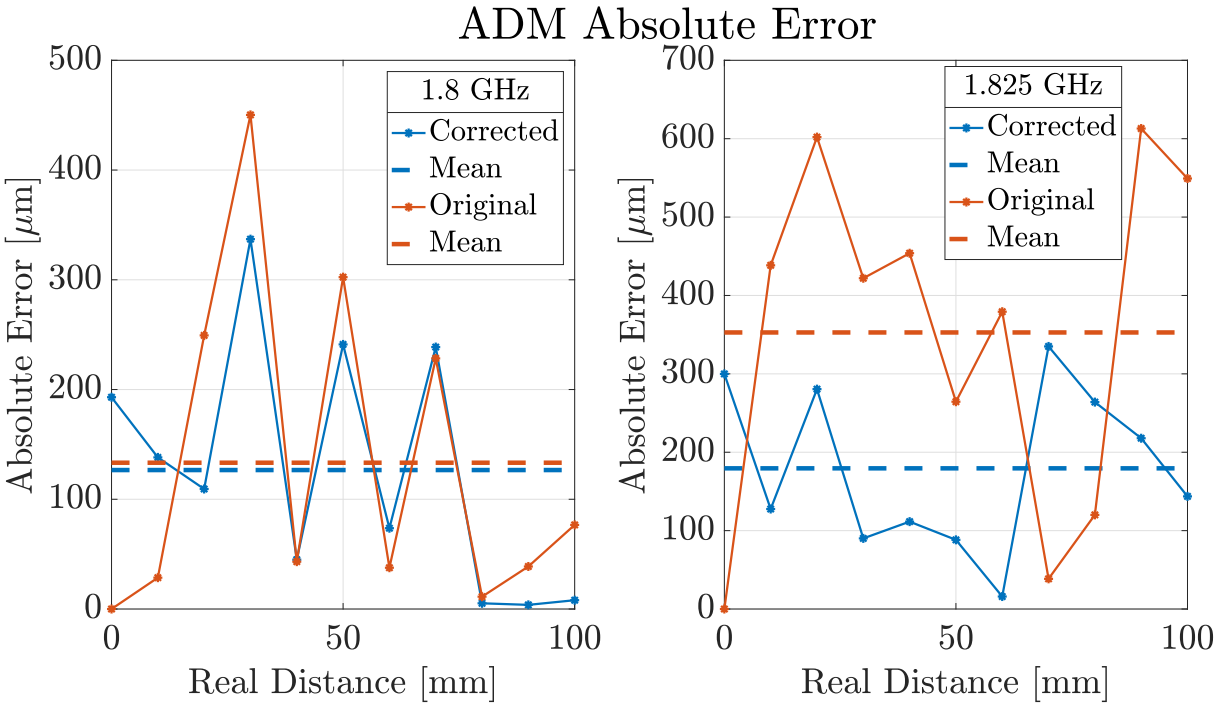

Figure 5.21: Comparison between the absolute experimental error of the corrected and averaged ADM results with the sensor for a range of [0, 100] mm.

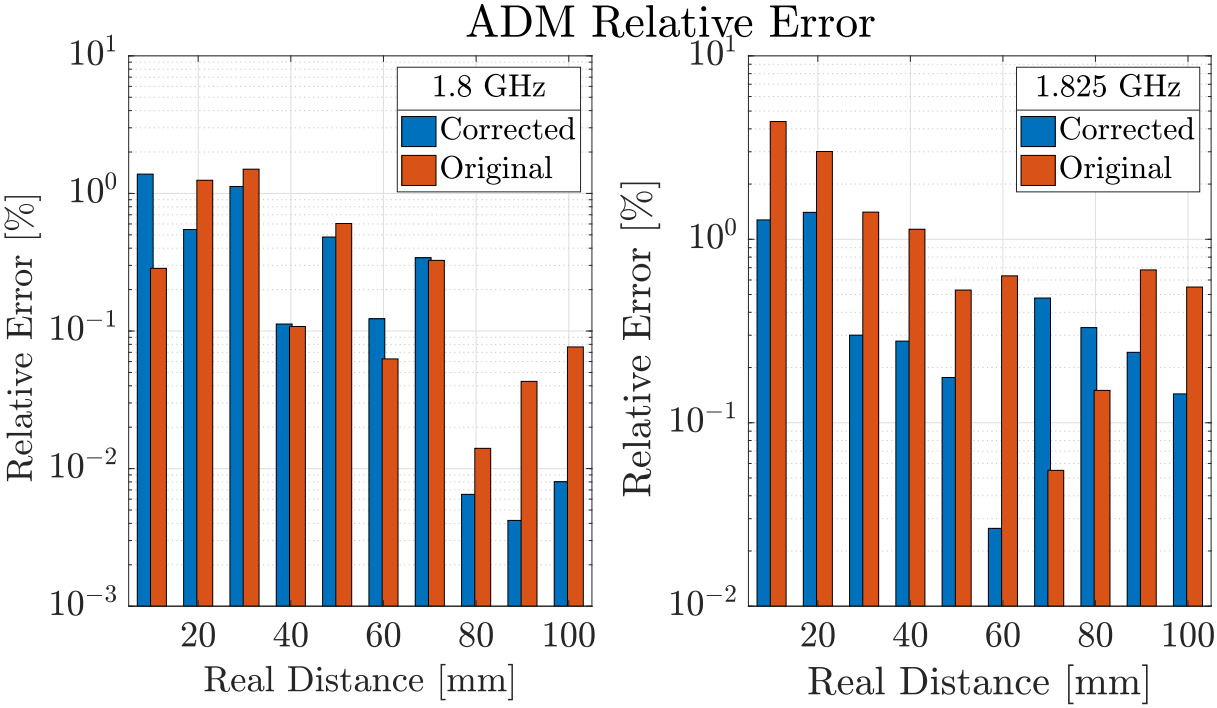

Figure 5.22: Comparison between the relative experimental error of the corrected and averaged ADM results with the sensor for a range of [0, 100] mm.

5.3.4.2 Mid Range

The results for the relative and absolute short range experimental error can be found in figures 5.23 and 5.24. Considering the average absolute error, its value with no correction is 270 μm and 365 μm, for the 1.8 GHz and 1.825 GHz, respectively.

Like for the other range, the corrected values have a smaller error than the original ones. In this case, the sensor achieved 256 μm and 268 μm for the 1.8 GHz and 1.825 GHz frequency. Despite the correction reducing the measurement experimental error for both frequencies, its impact is more notorious in the 1.825 GHz, where it is reduced in ≈ 27 % from the original value.

Considering that this measurement was in the meter range, impressive relative errors were achieved $[10^{-3}, 10^{-2}]$ %. Noticeably, for a 1.8 GHz in the 4.808 m mark, the original measurement have a relative error of 10^{-5} %. Despite it not being repeatable for the rest of the measurement range, it can foresee the result one might obtain after a more in-depth analysis of the purposed method and experimental setup.

Even though this set of measurements has an offset of [4.8080 $\pm$ 0.0006] m, its uncertainty is similar to the one obtained for the short range, $\approx$ 600 μm and $\approx$ 530 μm for 1.8 GHz and 1.825 GHz, respectively. Consequently, the experimental error is smaller than the expanded uncertainty of the corrected values. This reveals that also for this range the performed correction was effective in reducing the measurement error and guaranteeing that the real value is within the confidence interval of the corrected one.

Figure 5.23: Comparison between the absolute experimental error of the corrected and averaged ADM results with the sensor for a range of [4.808, 4.818] m.

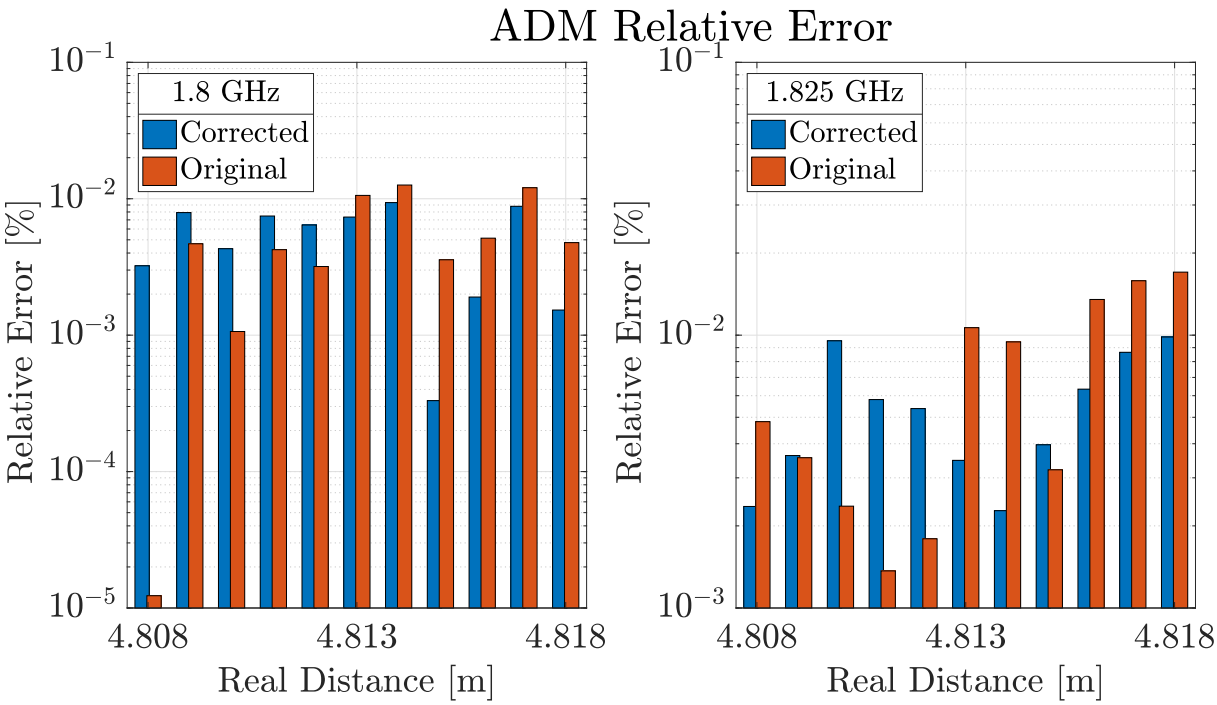

Figure 5.24: Comparison between the relative experimental error of the corrected and averaged ADM results with the sensor for a range of [4.808, 4.818] m.

5.3.4.3 Summary

The sensor's measurement uncertainty for a phase shift is smaller for 1.825 GHz than for 1.8 GHz, as seen in tables 5.4, 5.3 respectively. However, the experimental ADM results for both ranges reveal a smaller error in measurements at a modulation of 1.8 GHz. This reveals that the sensor is more accurate for the latter frequency than the shifted one. The measurement with the 1.825 GHz frequency has an evident noise contribution that was not considered in the uncertainty budget. This unwanted component leads to an ADM with a larger error for this frequency.

The best mean absolute error achieved in the short and mid range was of 126 μm and 256 μm for the 1.8 GHz modulation. This difference in the experimental error for the different ranges should be expected due to the millimetre and meter magnitude of the intervals. However, one notices that the relative error is in the same amplitude for both ranges.

However, one can not take any consideration regarding this sensor operation within this work's intended goal, a [0, 5] m range. For a more serious understanding of how it might operate, a full sweep of a [0, 5] m range would be needed. In a wider interval, the resulting calibration curves might not be linear approximations has one considered in this work. When testing the sensor in a wider range than the ones presented, this could reveal different operating regions. Consequently, a different correction could be applied to reduce even further the measurement error. Due to the technical limitations we encountered, this test was left undone. However, this would be the first test to perform in future work.

Chapter 6

Conclusion

The goal of the present dissertation was to develop and test a high accuracy absolute distance sensor, based on optical processes, that could perform ADM within a [10, 20] m range with an expanded uncertainty, $U_D < 100$ μm.

An evaluation of the state of the art of the different optical measuring techniques was conducted to evaluate which method allows reaching the established requirements. After this analysis, the PS CW TOF technique was chosen. To achieve the desired accuracies, this technique relies on amplitude modulating a light source with a GHz frequency. However, to perform an ADM with this frequency, the ambiguity in the phase measurement had to be removed.

In this context, we developed an adaptation of the Vernier method to remove the ambiguity in a phase shift measurement. It consists in performing a dual phase shift measurement for two different modulation frequencies. To measure its ambiguity integer correctly, one must determine it with an expanded uncertainty of $U_N < 0.5$.

We verified which were the uncertainty limits for a phase shift measurement and the modulation frequency, so that the required $U_N < 0.5$ and this work's goal $U_D < 100$ μm could be both achieved. We performed Monte Carlo and analytical simulations to verify these limits. This simulation results showed that in a [10, 20] m range with a modulation frequency of 3 GHz and $\Delta f = 14.8$ MHz a limit uncertainty of $u_{\Delta\phi} = 0.27$ º and $u_f = 3$ kHz would be needed to comply with the requirements.

To verify these assumptions, we developed an experimental setup that could be used to test the method and achieve the desired goals. Initially, one intended to use a calibrated air rail to test the sensor in a [10, 20] m range. However, in the course of this work, it was not possible to use this resource, so we opted to test our sensor in a [0, 5] m range with the available material in the laboratory.

In the process of building and characterizing this setup, an accident with *Laser 1*, the 3 GHz laser, occurred rendering it unusable. Consequently, the backup laser, *Laser 2* had to be used. However, the latter can only be modulated at 1.8 GHz, so the original setup had to be modified to comply with the lower modulation frequency.

This change in modulation frequency had a natural impact on the uncertainty limits that a phase shift measurement could attain. Additionally, the frequency shift was also limited by the operating bandwidths of each electrical device used in our setup. We figured that the best Δf was of 25 MHz, that with the correct signal amplification lead to a SNR ≈ 10 for measurements with both frequencies.

We performed the uncertainty budget for a phase shift measurement with the developed experimental setup and the resulting combined uncertainty was $u_{\Delta\phi} = 0.92$ º and $u_{\Delta\phi} = 0.82$ º for 1.8 GHz and 1.825 GHz, respectively. With the result of the frequency uncertainty of $u_f = 50$ Hz, these parameters allowed for an $U_N < 0.5$, satisfying this work's goal.

These uncertainty results are different from the obtained in the analytical simulation of chapter 4. In that scenario, the phase uncertainty for each modulation frequency was considered the same, which did not correspond to reality. Nevertheless, when combining both measurement uncertainties, the greatest uncertainty contributor in the ambiguity integer measurement, $e^N_{\Delta\Phi}$ eq. 3.22, did to not surpass the limit magnitude obtained in the simulation results. The requirements were met and N was determined with $U_N < 0.5$.

Finally, the method was tested by performing ADM at a short and mid range, [0, 100] mm and [4.808, 4.818] m, respectively and with a "blind measurement", where the target was placed at $\approx$ 2 m. We were able to verify that for the different test ranges, the developed sensor was able to correctly measure most of the ambiguity integer correspondent to the tested positions. The N measurements in the short range prove that the presented method can detect a change in the ambiguity integer.

These measurements reveal that in some situations the sensor was not able to determine the correct ambiguity integer for the tested position, which leads to an incorrect ADM. Further work must be done in order to understand the contributors for this effect.

As presented in chapter 5, these values can be conducted as an outlier, they are neglected in our evaluation. In that condition, it is possible to extract a calibration curve that allows to correct the scale and offset in our results.

By performing a correction of the measured values, we obtained an average experimental absolute error of 126 μm and 256 μm, which are within a confidence interval of $\approx$ 600 μm, computed for a 1.8 GHz modulation in the short and mid range tests.

The performed correction allowed for the relative error of the measured value to decrease one order of magnitude, compared when no correction is applied. Therefore, the performed linear correction proved to be effective for both test ranges and frequencies.

In brief, the main results of our work can be presented as follows:

- Evaluation of the state of the art of optical distance measurement techniques.
- Introduction of a Vernier variant to the PS CW TOF method used, to develop a mathematical model allowing to remove the ambiguity in an ADM.
- Project the uncertainty requirements necessary to achieve ADM within the desired range and with the predicted accuracy.
- Development of an experimental setup that allows the implementation of the proposed model for the ambiguity integer determination and ADM.

Further work must be done to fully conclude the characterization of the presented sensor. To do so, the following issues must be resolved:

- Incorrect N measurements

  It is not fully clear the reason incorrect measurements occur. However, it must be related to some instrumental error component that was not considered in the uncertainty budget. An intensive study of the error and uncertainty sources must be done, because the optical and electric noise contribution of the equipment can deteriorate the SNR, leading to the incorrect phase measurement.

- Improve ADM uncertainty

  The ADM uncertainty with this sensor did not match the one that was obtained through the computational simulations. Since we did not consider the contribution of the system reference for the

overall measurement uncertainty. This can be overcome by using another ADM instrument, with a better accuracy that the presented sensor, to measure and calibrate the system reference point. By doing so, the contribution of the reference position in the sensors distance uncertainty budget is decreased, and its major component comes from the measurement of the point of interest.

- Access full sensor operating range

  By performing a calibration curve for its intended operating range, [10, 20] m, one might find that the sensor has different responses for different regions in its range. Depending on the sensor's response, different calibration curves can be applied and consequently, corrections can be performed accordingly. This can contribute to the reduction of the measurement error.

Bibliography

[1] NIST, "Engineering Metrology Toolbox - Refractive Index of Air Calculator."

[2] S.-W. Kim, Y.-J. Kim, S. Hyun, B. J. Chun, and Y.-S. Jang, "Recent advances in absolute distance measurements using femtosecond light pulses," in *Ninth International Symposium on Precision Engineering Measurement and Instrumentation*, vol. 9446, p. 94464M, International Society for Optics and Photonics, 2015.

[3] C. V. M. Fridlund, "Darwin-the infrared space interferometry mission," *ESA Bulletin 103*, no. august, pp. 20–63, 2000.

[4] N. M. Gonçalves, M. Abreu, and D. Castro Alves, "Application of the Vernier method for absolute distance metrology with CW TOF phase shift technique," *EPJ Web of Conferences*, vol. 238, 2020.

[5] G. Berkovic and E. Shafir, "Optical methods for distance and displacement measurements," *Advances in Optics and Photonics*, vol. 4, p. 441, dec 2012.

[6] T. Bosch, "Laser ranging: a critical review of usual techniques for distance measurement," *Optical Engineering*, vol. 40, p. 10, jan 2001.

[7] F. Franceschini, M. Galetto, D. Maisano, and L. Mastrogiacomo, "Large-scale dimensional metrology (LSDM): From tapes and theodolites to multi-sensor systems," *International Journal of Precision Engineering and Manufacturing*, vol. 15, no. 8, pp. 1739–1758, 2014.

[8] G. N. Peggs and A. Yacoot, "A review of recent work in sub-nanometre displacement measurement using optical and X-ray interferometry," *Philosophical Transactions of the Royal Society A: Mathematical, Physical and Engineering Sciences*, vol. 360, no. 1794, pp. 953–968, 2002.

[9] J. A. S. D. Fonseca, A. Baptista, M. J. Martins, and J. P. N. Torres, "Distance Measurement Systems Using Lasers and Their Applications," *Applied Physics Research*, vol. 9, no. 4, p. 33, 2017.

[10] K.-E. Peiponen, R. Myllylä, and A. V. Priezzhev, eds., *Measurement of Positions, Distances, and Displacement*, pp. 67–101. Berlin, Heidelberg: Springer Berlin Heidelberg, 2009.

[11] Sick, "Distance Sensors - Product Catalog," 2020.

[12] M.-H. Lin, S.-K. Hung, S.-C. Huang, and L.-C. Fu, "Measuring the Deflection of the Cantilever in Atomic Force Microscope with an Optical Pickup System," *Proceedings of the IEEE Conference on Decision and Control*, pp. 592–596, 2007.

[13] B. D. Guenther, *Modern Optics Simplified*. No. 1, Great Clarendon Street, Oxford, OX2 6DP, United Kingdom Oxford: Oxford University Press, 1 ed., 2020.

[14] M. R. Pearlman, J. J. Degnan, and J. M. Bosworth, "The International Laser Ranging Service," *Advances in Space Research*, vol. 30, no. 2, pp. 135–143, 2002.

[15] I. Fujima, S. Iwasaki, and K. Seta, "High-resolution distance meter using optical intensity modulation at 28 GHz," *Measurement Science and Technology*, vol. 9, no. 7, pp. 1049–1052, 1998.

[16] S. Donati, *Electro-Optical Instrumentation (Sensing and Measuring with Lasers)*, vol. 7. Pearson Education, Inc, 2004.

[17] M. Norgia, F. Cavedo, A. Pesatori, and S. Merlo, "High-resolution optical rangefinder based on 2 GHz telecom transceiver," *4th IEEE International Workshop on Metrology for AeroSpace, MetroAeroSpace 2017 - Proceedings*, pp. 408–412, 2017.

[18] D. Xioli and S. Katuo, "High-accuracy absolute distance measurement by means of wavelength scanning heterodyne interferometry," *Measurement Science and Technology*, vol. 9, no. 7, pp. 1031–1036, 1998.

[19] A. Martelucci, Sergio, Chester, Arthur, Mignani, *Optical Sensors and Microsystems: New Concepts, Materials, Technologies*, vol. 32. KLUWER ACADEMIC / PLENUM PUBLISHERS NEW, 2000.

[20] R. Baldwin, G. Gordon, and A. Rudé, "Remote Laser interferometry," 1971.

[21] B. L. Swinkels, N. Bhattacharya, A. L. Verlaan, and J. J. M. Braat, "High accuracy absolute distance metrology," vol. 10567, no. June 2006, p. 23, 2017.

[22] A. Cabral, "Dual-frequency sweeping interferometry for absolute metrology of long distances," *Optical Engineering*, vol. 49, no. 8, p. 085601, 2010.

[23] A. Cabral and J. Rebordão, "Metrologia absoluta de comprimento por interferometria de varrimento de frequência," pp. 1–7, 2015.

[24] F. Pollinger, K. Meiners-Hagen, M. Wedde, and A. Abou-Zeid, "Diode-laser-based high-precision absolute distance interferometer of 20m range," *Applied Optics*, vol. 48, no. 32, pp. 6188–6194, 2009.

[25] S. Poujouly and B. Journet, "A twofold modulation frequency laser range finder," *Journal of Optics A: Pure and Applied Optics*, vol. 4, no. 6, 2002.

[26] C. Yu, W. Chunyang, G. Huan, and L. Huan, "Multi-Frequency Modulation Laser Range Finding System," *Modern Applied Science*, vol. 9, no. 4, pp. 328–334, 2015.

[27] F. E. Gueuning, M. Varlan, C. E. Eugène, and P. Dupuis, "Accurate distance measurement by an autonomous ultrasonic system combining time-of-flight and phase-shift methods," *IEEE Transactions on Instrumentation and Measurement*, vol. 46, no. 6, pp. 1236–1240, 1997.

[28] H. Yang, C. Zhao, H. Zhang, Z. Zhang, and K. Gui, "A novel hybrid TOF/phase-shift method for absolute distance measurement using a falling-edge RF-modulated pulsed laser," *Optics and Laser Technology*, vol. 114, no. May 2018, pp. 60–65, 2019.

[29] A. A. Dorrington, M. J. Cree, A. D. Payne, R. M. Conroy, and D. A. Carnegie, "Achieving sub-millimetre precision with a solid-state full-field heterodyning range imaging camera," *Measurement Science and Technology*, vol. 18, no. 9, pp. 2809–2816, 2007.

[30] A. D. Payne, A. P. P. Jongenelen, A. A. Dorrington, M. J. Cree, and D. A. Carnegie, "Multiple frequency range imaging to remove measurement ambiguity," *Proceedings of at 9th Conference on Optical*, pp. 1–3, 2009.

[31] A. P. Jongenelen, D. A. Carnegie, A. D. Payne, and A. A. Dorrington, "Maximizing precision over extended unambiguous range for TOF range imaging systems," *2010 IEEE International Instrumentation and Measurement Technology Conference, I2MTC 2010 - Proceedings*, pp. 1575–1580, 2010.

[32] A. P. Jongenelen, D. G. Bailey, A. D. Payne, A. A. Dorrington, and D. A. Carnegie, "Analysis of errors in ToF range imaging with dual-frequency modulation," *IEEE Transactions on Instrumentation and Measurement*, vol. 60, no. 5, pp. 1861–1868, 2011.

[33] W. Kent, *Mechanical engineers' handbook*. New York: Wiley, 1950.

[34] M. Rakhmanov, M. Evans, and H. Yamamoto, "An optical vernier technique for in situ measurement of the length of long Fabry-Pérot cavities," *Measurement Science and Technology*, vol. 10, no. 3, pp. 190–194, 1999.

[35] Joint Committee For Guides In Metrology, "Evaluation of measurement data — Guide to the expression of uncertainty in measurement," *International Organization for Standardization Geneva ISBN*, vol. 50, no. September, p. 134, 2008.

[36] P. R. Guimaraes Couto, J. Carreteiro, and S. P. de Oliveir, "Monte Carlo Simulations Applied to Uncertainty in Measurement," *Theory and Applications of Monte Carlo Simulations*, 2013.

[37] D. M. Pozar, *Microwave and Rf Design of Wireless Systems*. Wiley, 2000.

[38] Anritsu, "RF / Microwave Signal Generators," pp. 1–24, 2019.

[39] Atlantic Microwave, "Phased Locked Oscilator 2 GHz Internal CLock."

[40] Thorlabs, "Pigtailed Laser Diode LPS-1550-FC," 2013.

[41] C. S. T. G. Ltd, "1550nm RWG FP Laser 1550-FPL-2.5-X."

[42] F. R. Times, W. Ranges, and W. W. Ranges, "Ultrafast Photodetectors UPD-35-IR2-FC."

[43] Mini Circuits, "Mini Circuits - Frequency Mixer ZAM-42."

[44] Mini Circuits, "Low pass filter SLP-200+ DC to190 MHz."

[45] M. Circuits, "Power Splitter / Combiner ZN2PD2-63-S+."

[46] Corning Product Information, "SMF-28 Ultra Optical Fiber," 2014.

[47] Mini Circuits, "Bias-Tee 0.1 to 6000 MHz."

[48] Mini Circuits, "Low Noise Amplifiers ZX60-33LN+ 50 to 3000 MHz."

[49] Mini Circuits, “Coaxial Amplifier ZHL-6A+ 0.0025 to 500 MHz.”

[50] S. R. Systems, “Model Sr445a 4 Channel 350MHz.”

[51] Thorlabs, “Fiber optic circulators 6015-3-APC.”

[52] Thorlabs, “NRT Series Motorized Translation Stage User Guide,” pp. 1 – 20, 2016.

[53] Thorlabs, “BSC103 - Three-Channel APT Stepper Motor Controller.”

[54] Thorlabs, “BE20M-C 1050 - 1620 nm,” 2015.

[55] Newport, “Hollow Retroreflector, Broadband, 1.0 in, 5 arc sec, 450-10.000 nm UBBR1-5S.”

[56] Agilent, “Datasheet Agilent 53200A Series RF / Universal Frequency Counter / Timers Data Sheet.”

[57] Agilent, “Agilent MSO6000 Series Datasheet.”

[58] Mini Circuits, “Power Detector ZX47-60+ 10 to 8000 MHz ZX47-55+.”

[59] Melles Griot, “Universal Power Meter 13 PDC 001.”

[60] Leica Geosystems, “Leica DISTO D510.”

[61] A. S. Morris and R. Langari, *Measurement and instrumentation*. No. (ed.), Weinheim, Fed. Rep. Germany, VCH Verlagsgesellschaft mbH, 1985, Part 5, Chapter 29, p.763-786, Elsevier Ltd, 3 ed., 2015.

[62] U. L. Rohde and A. K. Poddar, “Electromagnetic interference and start-up dynamics in high frequency crystal oscillator circuits,” *33rd IEEE Sarnoff Symposium 2010, Conference Proceedings*, 2010.

[63] J. J. Laurin, S. G. Zaky, and K. G. Balmain, “EMI-Induced Failures in Crystal Oscillators,” *IEEE Transactions on Electromagnetic Compatibility*, vol. 33, no. 4, pp. 334–342, 1991.

[64] Joint Committee for Guides in Metrology (JCGM), *International vocabulary of metrology – Basic and general concepts and associated terms (VIM)*, vol. 58. 3º ed., 2008.

[65] Thorlabs, “Manual Fiber Polarization Controllers User Guide,” 2014.

[66] C. Robens and S. Brakhane, “Monte Carlo Error Propagation,” 2020.

Appendix A

Published Work

[4] - *"Application of the Vernier method for absolute distance metrology with CW TOF phase shift technique"*

Nuno M. Gonçalves, Manuel Abreu, D. Castro Alves

European Optical Society Annual Meeting, September of 2020

EPJ Web of Conferences 238, 06016 (2020)
https://doi.org/10.1051/epjconf/202023806016

EPJ Web of Conferences **238**, 06016 (2020) https://doi.org/10.1051/epjconf/202023806016
EOSAM 2020

Application of the Vernier method for absolute distance metrology with CW TOF phase shift technique

Nuno M. Gonçalves[1,2,*], *Manuel* Abreu[1,2,**], and *D.* Castro Alves[1,2,***]

[1]Instituto de Astrofísica e Ciências do Espaço, Universidade de Lisboa, Campo Grande, PT1749-016 Lisboa, Portugal
[2]Departamento de Física, Faculdade de Ciências, Universidade de Lisboa, Edifício C8, Campo Grande, PT1749-016 Lisbon, Portugal

Abstract. A phase shift time of flight technique determines a position by comparing the phase angle of a continuously modulated signal in the source and its reflection on a target. However, due to its cyclical properties, the position information is contained within an ambiguity interval. For an absolute measurement, this interval is repeated N times plus a residual part given by the phase shift. In this work we propose an application of the Vernier method to determine N and a setup for mid-range applications (10-20) m with a 3 GHz amplitude modulated source to allow accuracies $\leq 100\,\mu$m.

1 Introduction

Time of flight (TOF) is a very well established optical measuring technique that offer ways to determine absolute or relative distance measurements (ADM and RDM, respectively). In a phase shift (PS) continuous wave TOF (PS CW TOF) method, a coherent light source is continuously modulated in amplitude and directed to a target. The reflected signal will then have a phase shift, $\Delta\phi$, relative to the original, which will be related to the source-target distance by eq. 1.

$$D = \frac{cn}{2f}\left(\frac{\Delta\phi}{2\pi} + N\right) \tag{1}$$

$$\Lambda = \frac{cn}{2f} \tag{2}$$

Where f is the modulation frequency, D the source-target distance, c the speed of light and n the refractive index of the medium. Due to the cyclical properties of the phase, the position information is contained within an ambiguity distance, eq. 2. Therefore, for an absolute measurement, this interval is repeated N times plus a residual part given by the PS. Hence, it's crucial to determine N for absolute measurements. Different methods can be used for this purpose [1]. *Norgia, et al* [2] achieved 100 μm accuracy for a 2 GHz modulation using heterodyne down conversion (HdC), and solved the ambiguity by using a double Vernier method [3].

For a mid-range (10-20) m, by performing a 3 GHz modulation with HdC, one can achieve an accuracy of $<100\,\mu$m in an RDM, as long as the error of the frequency and PS are in the order of 1 kHz and 0.3 °, respectively. In this work, we propose a different approach to determine N, allowing this level of accuracy for ADM. Although, since N is an integer, it must be determined with an error < 0.5. In order to achieve the distance accuracy goal and N being properly determined, a trade off between both of this components must be done. However, the error analysis isn't in the scope of this document.

*e-mail: fc48080@alunos.fc.ul.pt
**e-mail: maabreu@fc.ul.pt
***e-mail: dmvalves@fc.ul.pt

2 Working Principle

In order to measure the source-target distance, the PS CW TOF technique employs the concept of a "ruler". This ruler has a primary and secondary mark, given by the ambiguity distance and by the PS (as it is referred in eq. 1), as shown by ruler A in figure 1.

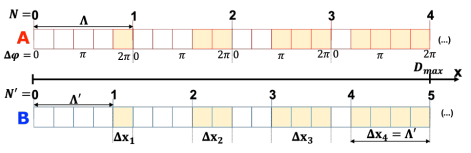

Figure 1. Comparison of two different rulers A and B. In A the distance between marks is determined by f and in B by $f' = f + \Delta f$.

It's possible to determine N by measuring the same distance with two different "rulers". The difference between primary markings of both rulers is defined as Δx_N:

$$\Delta x_N = N\Delta x_1 \quad ; \quad \Delta x_1 = \Lambda - \Lambda' = \frac{cn\Delta f}{2ff'} \tag{3}$$

Where N corresponds to the index of the primary mark of the ruler with biggest spacing between them and $f > \Delta f$ and $\Delta f = f' - f > 0$ since $f' > f$. This represents the difference in frequency for both scales and will rule the variation in position of the different primary marks.

Additionally, by considering the difference in phase shifts between rulers for the same distance, $\Delta\Phi$=$\Delta\ \phi' - \Delta\phi$, one gets eq. 4. By rearranging it, the absolute distance can be written as eq. 5.

$$\frac{\Delta\Phi}{2\pi} = D\frac{2\Delta f}{cn} + \Delta N \tag{4}$$

$$D = \frac{cn}{2\Delta f}\left(\frac{\Delta\Phi}{2\pi} - \Delta N\right) \tag{5}$$

Where $\Delta N = N - N' \leq 0$ and an integer, since $f' > f$ then $\Lambda > \Lambda'$ and consequently $N' \geq N$. Additionally, by rearranging eq. 1 we obtain eq. 6. By inserting eq. 5 in eq. 6 and solving for N, eq. 7 is obtained.

$$\frac{\Delta\phi}{2\pi} = \frac{2D}{cn}f - N \tag{6}$$

$$N = \frac{\left(\frac{\Delta\Phi}{2\pi} - \Delta N\right)}{\Delta f}f - \frac{\Delta\phi}{2\pi} \tag{7}$$

Considering a target at a fixed distance D, one can measure a pair of different phase shifts corresponding to known modulation frequencies spaced by Δf, by using eq. 7 it's possible to determine the value of N.

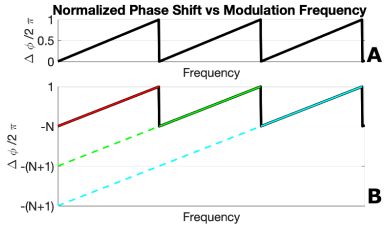

Figure 2. Normalized phase shift for a fixed distance. The colored lines in B are a fit of eq. 6 in the positive slope region of the normalized phase shift.

Very briefly, if one plots eq. 6 for a fixed distance the result is a saw-tooth profile as seen on figure 2A. For a single and arbitrary frequency-PS point in this profile, the corresponding N can be found as the intercept in the normalized PS axis, as shown in figure 2B. However, for a pair of arbitrary and different frequency-PS points, the ΔN between them can be 0,-1,-2,-3... depending on the Δf spacing. More generally, for any given $D \leq D_{max}$, by constraining Δf one can ensure that for a pair of different frequency-PS points, $\Delta N = 0 \bigvee \Delta N = -1$. The maximum distance at which this condition is fulfilled is when D_{max} is an integer multiple of the ambiguity distances of both frequencies, i.e. the marking of both rulers match and consequently $\Delta\Phi$= 0. However, as seen in figure 1, D_{max} will be reached when $\Delta x_N = \Lambda'$, which mathematically implies that $\Delta N = -1$. By using eq. 5 one can find D_{max}:

$$D_{max} = \frac{cn}{2\Delta f}(0 - (-1)) = \frac{cn}{2\Delta f_{max}} \tag{8}$$

Meaning that for $D \leq D_{max}$ by doing spacings of Δf_{max}, as long as $f > \Delta f_{max}$ for any modulation frequency one can find $\Delta N = 0 \bigvee \Delta N = -1$. This is consistent with the results of *S. Donati* [1], that with a different approach showed it was possible to measure unambiguously for $D \leq D_{max}$.

Additionally, through mathematical analysis of eq. 5, one can conclude that if $\Delta\Phi < 0 \rightarrow \Delta N = -1$ and $\Delta\Phi > 0 \rightarrow \Delta N = 0$. Hence, by measuring a pair of different PS and modulation frequencies spaced at most by Δf_{max} one can know if $\Delta N = 0$ or $\Delta N = -1$ if the difference in PS between them is positive or negative.

$$slope = \frac{\frac{\Delta\phi' - \Delta\phi}{2\pi}}{\Delta f} = \frac{\Delta\Phi/2\pi}{\Delta f} \tag{9}$$

In conclusion, with eq. 9 and a pair of frequency-PS measurements, one can determine N through eq. 7. Therefore, by knowing N and applying eq. 1 with a GHz modulation frequency it's possible to achieve the desired accuracy.

3 Future work

In order to show that this principle is valid to obtain absolute distances with high accuracy, we intend to build the setup showed in figure 3. One must ensure that given the instrumental limitation, we can measure for a mid-range distance, (10-20) m, with accuracies $\leq$ 100 μm. For that purpose the knowledge of the frequency and PS must be in the order of 1 kHz and 0.3 °, respectively. Additionally, since N is an integer, its measurement error must be smaller than 0.5, to determine the exact integer number of phase cycles to reach the distance D.

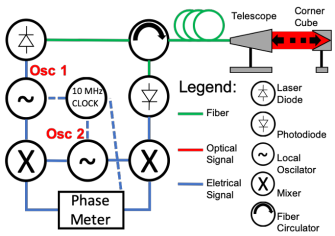

Figure 3. Sensor scheme with *Osc 1* at 3 GHz + Δf and *Osc 2* at 3 GHz.

This work was supported by Fundação para a Ciência e a Tecnologia (FCT) through the research grants UIDB/04434/2020 and UIDP/04434/2020. We also recognize the support of SPOF on the participation of this conference.

References

[1] S. Donati, *Electro-Optical Instrumentation* (Pearson Education, New Jersey, 2004) 61-63
[2] M. Norgia, F. Cavedo, A. Pesatori, *Proc. IEEE MetroAeroSpace*, 408-412 (2017)
[3] M. Rakhmanov, M. Evans, H. Yamamoto, Meas. Sci. Technol. **10**, 190-194 (1999)

Figure A.1: Article presented in the proceedings volume of the *European Optical Society Annual Meeting* in September of 2020.

Appendix B

Monte Carlo Simulations

The Monte Carlo simulations were based on the functions of *Matlab 2017a* developed by [66]. This is composed of two different functions *"generateMCparameters"* and *"propagateErrorWithMC"*. The first one was applied for all of the tested variables, $\Delta\phi$ and f, and it generates a Gaussian distribution with a center value and a standard deviation defined by the user. This distribution was performed via the Monte Carlo method with 200 000 random generated points. For example, the simulated phase shift measurement for a 20 m target with a standard deviation of 0.27 ° can be seen in figure B.1.

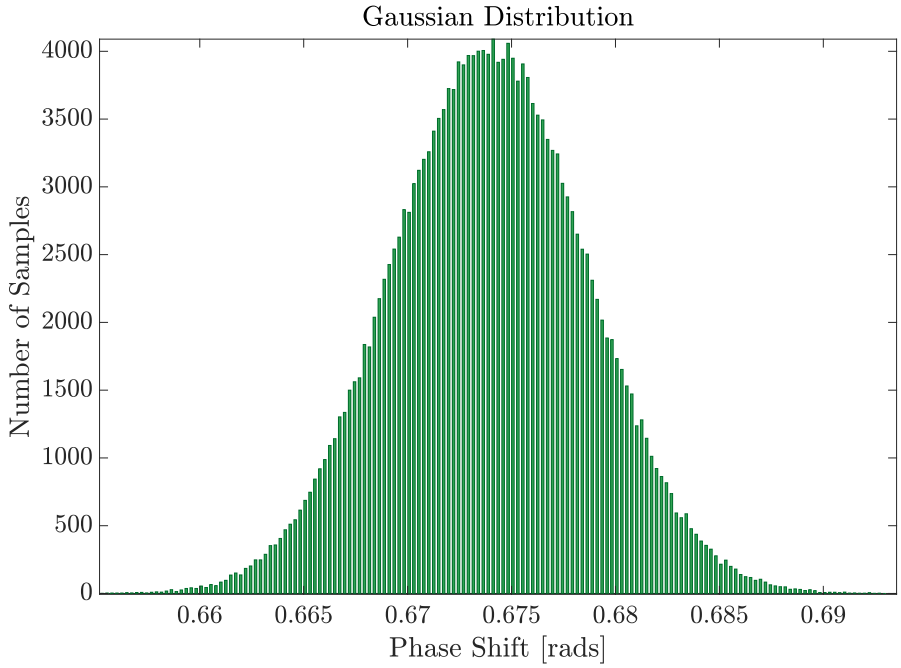

Figure B.1: Gaussian distribution for a phase shift measurement at 20 m centred in 0.6739 rads with a standard deviation of 0.0047. This distribution was generated with the Monte Carlo method with 200 000 samples.

By performing this Gaussian distribution for the phase shift and the frequency stability, we propagate the uncertainty with the function *"propagateErrorWithMC"*. In this function we would input the mathematical model of interest and its different distributions. These would be convoluted through the mathematical model and the output returns a probability distribution of the distance and ambiguity integer, figures B.2 and B.3, respectively.

We fixed a target distance of 20 m and swept the standard deviation of the frequency and the phase shift as described in chapter 3. The expanded uncertainty of the output probability distributions corre-

sponds to its standard deviation with a coverage factor of $k = 2$. By defining in the function *"propagateErrorWithMC"* the confidence interval threshold of 95 % the expanded uncertainty is directly obtained.

With the *Matlab 2017a* code in figure B.4 a .txt file was generated containing the simulation results. The plots in chapter 3 were done with the code in figure B.5.

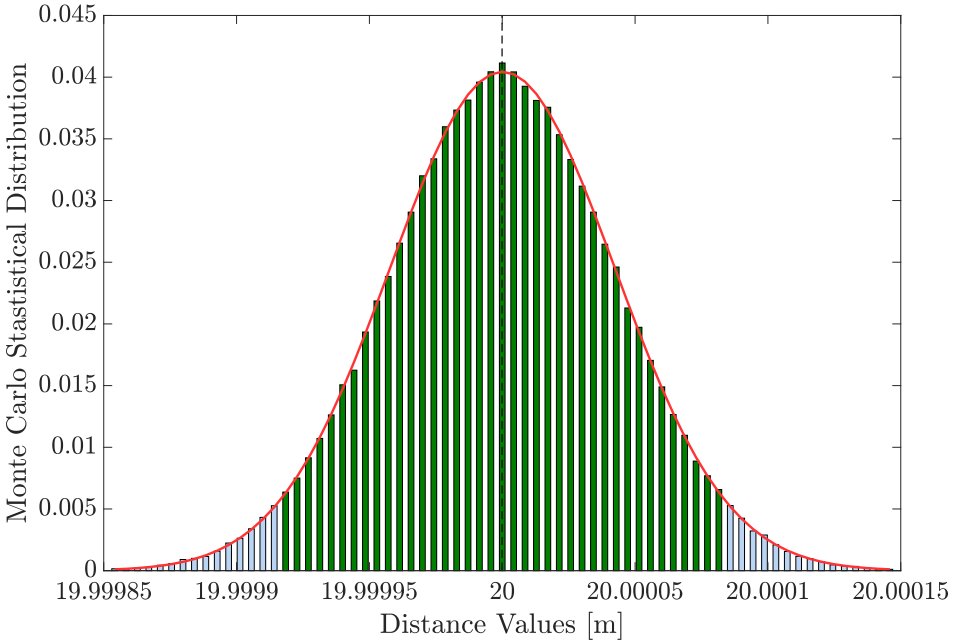

Figure B.2: Distance probability distribution output obtained for a frequency of 3 GHz, with the convolution of the Gaussian distributions for the phase shift and frequency stability. The green region corresponds to a coverage factor of $k = 2$, meaning a coverage factor of 95 %.

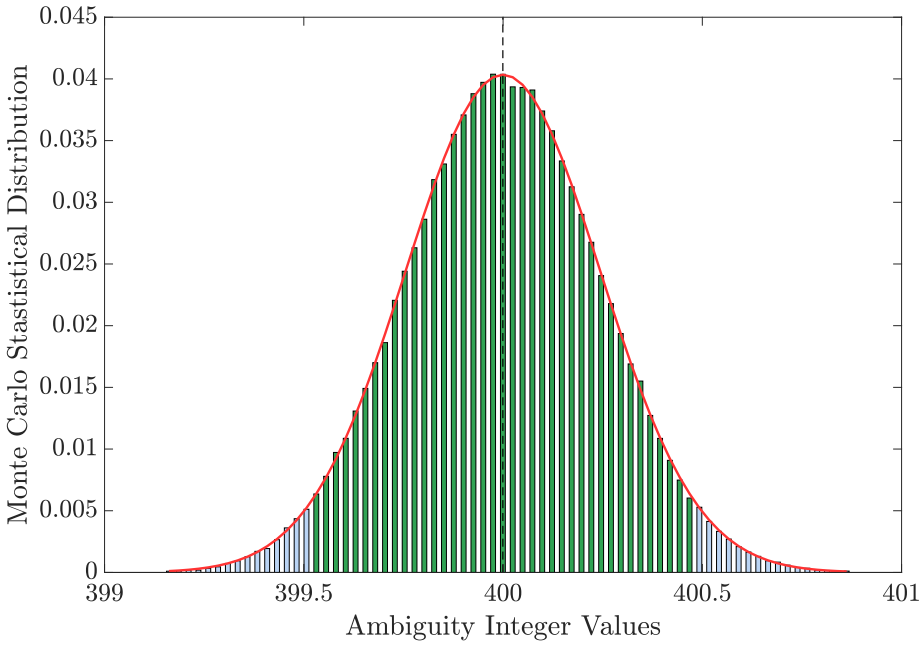

Figure B.3: Ambiguity integer probability distribution output obtained for a frequency of 3 GHz, with the convolution of the Gaussian distributions for the phase shift and frequency stability for the modulation frequencies of 3 GHz and 3.0148 GHz . The green region corresponds to a coverage factor of $k = 2$, meaning a coverage factor of 95 %.

```
%%%%%%%%%%%%%%%%%%%%%%%%%%%%%%%%%%%%%%%%%%%%%%%%%%%%%%%%%%%%%%%%%%%%%%%%%%%%%%%%
% Program name: Monte Carlo Uncertainty Analysis                                 % ...
                                                                                   %
%                                                                                 %
% Author: Nuno Miguel Cabecinhas Goncalves                                        %
%                                                                                 %
% Date : 13/11/2020                                                               %
%                                                                                 %
% Purpose: This code has the purpose to apply a Monte Carlo computational         %
% method in order to simulate an uncertainty budget of an absolute               %
% distance measurement with the dual phase shift time of lfight method            %
%                                                                                 %
% Version: V1 - 13/11/2020                                                        %
%%%%%%%%%%%%%%%%%%%%%%%%%%%%%%%%%%%%%%%%%%%%%%%%%%%%%%%%%%%%%%%%%%%%%%%%%%%%%%%%
clear;
close all;
tic;

%%%%%%%%Initial Parameters %%%%%%%%%%%%%%%%%%%%%%%%%%%%%%%%%%%%%%%%%%%%%%%%%%%%
c = 3 * 10.^8; %m/s - Speed of light
n = 1.000268148;% Refractive Index
CI = 0.95;  %Confidence Interval
LimN = 0.500; % Ambiguity integer Uncertainty Limit
LimD = 100.00; %um - Distance Uncertainty Limit
samples = 2e5; %Sample number for Monte Carlo Simulations

D=20.0; %m - Test distance
fcentral= 3e9;%Hz - Test modulation frequency
dfteste = 0.0148*10^9;%Hz - Frequency Shift
fteste=[fcentral fcentral + dfteste];

if CI ≥ 0.95
    h = 2;
else
    h=1;
end



%% Frequency and phase uncertainty parameters %%%%%%%%%%%%%%%%%%%%%%%%%%%%%%%%


Rpp= 0.01:0.01:0.35; %deg - Phase shift Uncertainty
Max=9;
Min=6;
Rf= zeros(Max-Min,2);
for i= Min:1:Max
Rf(i-Min+1,:) = (fteste/(10^i)); %%Hz - Frequency uncertainty
end

Rp = ((Rpp*pi)/180); %rads
RDP = sqrt(2)*Rp;


```

```
%%%%%%%%%%%%%%%%%%%%%%%%%%%%%%%%%%%%%%%%%%%%%%%%%%%%%%%%%%%%%%%%%%%%%%%%%%%%%%%%

%%%Prelocating variables
pt=zeros(size(fteste));
p1t=pt;
Nt = pt;
%%% Phase Calculation
p1t = 2*pi*(D*2*n*fteste./(c));
Nt= floor(p1t./(2*pi)); %%It will store the integer part of the phase in
                        %order to retrieve N
pt = p1t/(2*pi) - Nt; %normalized phase shift

%%%Prelocating variables
dif_pt = zeros(size(fteste,1),1);
DNt =dif_pt;
RDf =dif_pt;

%%% Distance and N uncertainties parameters
dif_pt = pt(2) - pt(1);
DNt =  Nt(1) -Nt(2) ;
RDf = zeros(1,size(Rf,1));
for t =1:1:size(Rf,1)
RDf(t) = sqrt(Rf(t,1).^2 + Rf(t,2).^2);
end
%%%%%%%%%%%%%%%%%%%%%%%%%%%%%%%%%%%%%%%%%%%%%%%%%%%%%%%%%%%%%%%%%%%%%%%%%%%%%%%%
%% Paralel Computation for the Monte Carlos Uncertainty Analysis with
% diferent parameters
%%$ Distance and ambiguity integer mathematical formulations
 funcDist = @(x) (c*((x(1)/(2*pi))+Nt(1)))/(2*x(3)*x(2));
 funcN = @(y) ( ( ((y(3)-y(1))/(2*pi))-DNt(1))*(y(2)/(y(4)-y(2)))  - ...
     (y(1))/(2*pi) );

%%% Pre locating variables
freq=[];
phase=[];
PT1 = pt(1);
PT2 = pt(2);
phase1=phase;
ValueD = zeros(size(Rp,2),size(Rf,1));
CID_max = ValueD;
DumbDumb_freq = zeros(size(Rf,1),samples);
DumbDumb_freq1 = zeros(size(Rf,1),samples);

ValueN = zeros(size(RDP,2),size(RDf,2));
CIN_max = ValueN;

%%% Generate the refraction index measurement as a gaussian  probability
nMC= generateMCparameters('gaussian',[n,0.000000023],'numSamples',samples);
%x(3)

parfor i = 1:1:size(Rp,2)
      DumbValueD = zeros(1,size(Rf,1));
      DumbCID_max = DumbValueD;
      DumbValueN = DumbValueD;
      DumbCIN_max = DumbValueN;
```

```
108     %%% Generate the phase shift measurement as a gaussian  probability
109     %%% distribution
110     phase(i,:) = ...
            generateMCparameters('gaussian',[2*pi*PT1,Rp(i)],'numSamples',samples); ...
            %x(1) and y(1)
111     phase1(i,:) = ...
            generateMCparameters('gaussian',[2*pi*PT2,Rp(i)],'numSamples',samples); ...
            % y(3)
112     %%% Generate the frequency stability as a gaussian  probability
113     %%% distribution
114     for j = 1:1:size(Rf,1)
115     freq = ...
            generateMCparameters('gaussian',[fteste(1),Rf(j,1)],'numSamples',samples, ...
            'plot', false); %x(2) e y(2)
116     freq1 = ...
            generateMCparameters('gaussian',[fteste(2),Rf(j,1)],'numSamples',samples, ...
            'plot', false); %x(2) e y(4)
117
118     %%% Distance Monte Carlo Simulation
119     paramDist = [phase(i,:);freq;nMC];
120     [funValue,funCI,funSamples] = propagateErrorWithMC(funcDist, ...
            paramDist,'CIthreshold', CI, 'plot', false,'method','median');
121     DumbValueD(j) = funValue;
122     DumbCID_max(j) = funCI(2);
123
124     %%% N Monte Carlo Simulation
125     paramN = [phase(i,:); freq; phase1(i,:); freq1];
126     [funValueN,funCIN,funSamplesN] = propagateErrorWithMC(funcN, ...
            paramN,'CIthreshold', CI, 'plot', false);
127     DumbValueN(j) = funValueN;
128     DumbCIN_max(j) = funCIN(2);
129
130     end
131
132     ValueN(i,:)=DumbValueN;
133     CIN_max(i,:)= DumbCIN_max;
134     ValueD(i,:) = DumbValueD;
135     CID_max(i,:) = DumbCID_max;
136
137 end
138
139 %% Filter Unwanted Distance results
140
141 sigma= (CID_max - ValueD)*10^6; %um
142 sigmaOK =[];
143 IdxSigOK = find(LimD > sigma);
144 [rowD, colD] = ind2sub(size(sigma),IdxSigOK);
145
146 sigmaOK(:,:)=sigma(IdxSigOK);
147
148 %% Filter Unwanted Ambiguity integer results
149 h_p = zeros(size(sigmaOK));
150 h_p(:,:) = h;
151
152 sigmaN= (CIN_max-ValueN);
```

```
153 sigmaNOK =[];
154 IdxSigNOK = find(sigmaN < LimN);
155 sigmaNOK(:,:)=sigmaN(IdxSigNOK);
156
157 [row,col]=ind2sub(size(sigmaN),IdxSigNOK);
158 FF = string(fcentral/10^9);
159 RF1 = string(Rf(1,1)/10^3);
160 RF2 = string(Rf(end,1)/10^3);
161
162 %% Prepares the simulation output in a file
163 distFile = ...
        fopen('Dist_andN_at_'+FF+'GHz_df_'+string(dfteste/10^6)+'MHz_uf_'+RF1+'_'+RF2+'kHz.txt','w'
164
165 fprintf(distFile,'Frequency = %.1f GHz. \n', fcentral/10^9);
166 fprintf(distFile,'Distance = %.2f with %.0fsigma <100um. \n', ValueD(1),h_p(1));
167 fprintf(distFile,'df = %.3f MHz. \n', dfteste/10^6);
168 fprintf(distFile,'uf = [%.1f ; %.1f]kHz. \n',RF1,RF2);
169 fprintf(distFile,'N = %.4f with %.0fsigma <0.5. \n', ValueN(1),h_p(1));
170 fprintf(distFile,'u_p(deg) \t u_f (Hz) \t u_D(um) \t u_N(um)\n');
171
172 for j = 1:1:size(IdxSigOK,1)
173
174      for i = 1:1:size(IdxSigNOK,1)
175         if IdxSigOK(j) == IdxSigNOK(i)
176         fprintf(distFile,'%.3f \t %.3f \t %.6f \t %.6f ...
                \n',Rpp(rowD(j)),Rf(colD(j)),sigma(rowD(j),colD(j))',sigmaN(row(i),col(i))');
177         end
178
179      end
180  end
181 fclose(distFile);
182
183 toc;
```

Figure B.4: Script for the Monte Carlo distance and ambiguity integer uncertainty simulations in *Matlab 2017a*

```
1
2  %%%%%%%%%%%%%%%%%%%%%%%%%%%%%%%%%%%%%%%%%%%%%%%%%%%%%%%%%%%%%%%%%%%%%%%%%%%%
3  % Program name: Monte Carlo Uncertainty Plot Creation                        % ...
                                                                                  %
4  %                                                                            %
5  % Author: Nuno Miguel Cabecinhas Goncalves                                   %
6  %                                                                            %
7  % Date : 13/11/2020                                                         %
8  %                                                                            %
9  % Purpose: This code has the purpose to construct the plots presented in    %
10 % the dissertation work regarding the Monte Carlo simulations               %
11 %                                                                            %
12 % Version: V1 - 13/11/2020                                                  %
13 %%%%%%%%%%%%%%%%%%%%%%%%%%%%%%%%%%%%%%%%%%%%%%%%%%%%%%%%%%%%%%%%%%%%%%%%%%%%
14
15 clear;
16 close all;
17 titlefont=40;
18 font = 32;
19 set(0,'defaultTextInterpreter','latex');
20 set(0, 'defaultAxesTickLabelInterpreter','latex');
21 set(0, 'defaultLegendInterpreter','latex');
22
23 %%%%%%%%%%%%%%%%%%%%%%Initial Parameters%%%%%%%%%%%%%%%%%%%%%%%%%%%%%%%%%%%%
24 freq = 3; %GHz
25 Dist = 20; %m
26
27 fid = fopen('Dist_andN_at_3GHz_df_7.4MHz_uf_3_0.003kHz.txt','r');
28
29 %%% Uncoment for plots with f = 3GHz and df =[8,14]MHz
30 %  fid = fopen('Dist_andN_at_3GHz_df_14.8MHz_uf_3_0.003kHz.txt','r');
31
32 D = textscan(fid,'%f %f %f %f','HeaderLines',6) ;
33 D = cell2mat(D);
34 fclose(fid);
35
36
37 DIST = string(Dist);
38 FF = string(freq);
39 %%% Find the identifier for each of the tested frequency
40 idx3k=find(D(:,2)==3000);
41 idx300=find(D(:,2)==300);
42 idx30=find(D(:,2)==30);
43 idx3=find(D(:,2)==3);
44
45 %% Plots %%%%%%%%%%%%%%%%%%%%%%%%%%%%%%%%%%%%%%%%%%%%%%%%%%%%%%%%%%%%%%%%%%%
46 figure('Renderer', 'painters', 'Position', [1 1 1087 608])
47
48 h1=subplot(211);
49 set(h1,'Position', [0.13 0.595 0.775 0.309])
50 plot(D(idx3k,1),D(idx3k,3),'-*', 'LineWidth', 2, 'MarkerSize',8)
51 hold on; plot(D(idx300,1),D(idx300,3),'-*', 'LineWidth', 2, 'MarkerSize',8)
52 hold on; plot(D(idx30,1),D(idx30,3),'-*', 'LineWidth', 2, 'MarkerSize',8)
53 hold on; plot(D(idx3,1),D(idx3,3),'-*', 'LineWidth', 2, 'MarkerSize',8)
```

```
set(gca,'FontSize',font);
title('Monte Carlo Simulation', 'fontsize', titlefont);
xlabel("$u_{\Delta \phi}$ [$^\circ$]",'fontsize',font, 'position',[0.155 ...
    -21.907 -1]);
ylabel("$U_{D}$ [$\mu$m]", 'fontsize',font);

%ylim([0 75]) %For 7.4 MHz
ylim([0 100]) %For 14.8 MHz

yticks(0:20:100);
xlim([0 0.32]);


grid on;

hold off;
% [plo,z, p]=zoomPlot(D(idx3k,1),D(idx3k,3),[0.139990 0.14001],[37.9 ...
    38.3],[.563 .77 .166 .124]); %For 7.4 MHz
[plo,z, p]=zoomPlot(D(idx3k,1),D(idx3k,3),[0.139990 0.14001],[38.265 ...
    38.455],[.718 .650 .166 .124]); %For 14.8 MHz
p.LineStyle='-.';
p.LineWidth=2;
p.MarkerSize=8;
hold on; plot(D(idx300,1),D(idx300,3),'-*', 'LineWidth', 2, 'MarkerSize',8)
hold on; plot(D(idx30,1),D(idx30,3),'-*', 'LineWidth', 2, 'MarkerSize',8)
hold on; plot(D(idx3,1),D(idx3,3),'-*', 'LineWidth', 2, 'MarkerSize',8)
 set(gca,'FontSize', font-4)
 yticks(38.3:0.1:38.4);
grid on;

h2=subplot(2,1,2);%,
set(h2,'Position', [0.13 0.15 0.775 0.311])
plot(D(idx3k,1),D(idx3k,4),'-*', 'LineWidth', 2, 'MarkerSize',8)
hold on; plot(D(idx300,1),D(idx300,4),'-*', 'LineWidth', 2, 'MarkerSize',8)
hold on; plot(D(idx30,1),D(idx30,4),'-*', 'LineWidth', 2, 'MarkerSize',8)
hold on; plot(D(idx3,1),D(idx3,4),'-*', 'LineWidth', 2, 'MarkerSize',8)

set(gca,'FontSize',font)

xlabel("$u_{\Delta \phi}[^\circ]$",'fontsize',font, 'position', [0.155 -0.133 ...
    -1]);

ylabel("$U_{N}$", 'fontsize',font);
ylim([0 0.55]);
yticks(0:0.1:0.5);
  xlim([0 0.32]);
grid on;
lgd=legend('3 kHz','300 Hz', '30 Hz', '3 Hz');
    lgd.FontSize= font-6;
    lgd.Location = 'southoutside';
    lgd.Orientation= 'horizontal';
    lgd.Position= [0.073 0.01 0.385 0.069];

%%% Inlets
hold off;
```

```
105
106 % [plo1,z1, p1]=zoomPlot(D(idx3k,1),D(idx3k,4),[0.139990 0.14001],[0.4392
107 % 0.4422 ],[.733 .204 .166 .124]); %For 7.4 MHz
108 [plo1,z1, p1]=zoomPlot(D(idx3k,1),D(idx3k,4),[0.139990 0.14001],[0.2207 ...
        0.2224],[.733 .204 .166 .124]); %For 14.8 MHz
109 p1.LineStyle='-.';
110 p1.LineWidth=2;
111 p1.MarkerSize=8;
112 hold on; plot(D(idx300,1),D(idx300,4),'-*', 'LineWidth', 2, 'MarkerSize',8)
113 hold on; plot(D(idx30,1),D(idx30,4),'-*', 'LineWidth', 5, 'MarkerSize',10)
114 hold on; plot(D(idx3,1),D(idx3,4),'-*', 'LineWidth', 2, 'MarkerSize',8)
115  set(gca,'FontSize', font-4)
116   yticks(0.221:0.001: 0.222);
117 grid on;
```

Figure B.5: Script in *Matlab 2017a* for plotting the obtained results in the Monte Carlo simulations.

Appendix C

Analytical Simulations

The analytical uncertainty simulations were done with the *Matlab 2017a* code in figure C.1. In this code we defined the combined uncertainty for the phase shift and frequency stability and its values were calculated for a given fixed distance. With this information and using the law of uncertainty propagations the contributions of the phase shift and frequency uncertainty are then propagated for the ambiguity integer and distance.

```

%%%%%%%%%%%%%%%%%%%%%%%%%%%%%%%%%%%%%%%%%%%%%%%%%%%%%%%%%%%%%%%%%%%%%%%%%%%%
% Program name: Analytical Simulations                                     % ...
                                                                             %
%                                                                          %
% Author: Nuno Miguel Cabecinhas Goncalves                                 %
%                                                                          %
% Date : 13/11/2020                                                        %
%                                                                          %
% Purpose: This code has the purpose to simulate the uncertainty of an     %
% absolute distance measurement and ambiguity integer by simulating both   %
% quantities analytical model                                              %
%                                                                          %
% Version: V1 - 13/11/2020                                                 %
%%%%%%%%%%%%%%%%%%%%%%%%%%%%%%%%%%%%%%%%%%%%%%%%%%%%%%%%%%%%%%%%%%%%%%%%%%%%
clear;
close all;
titlefont=40;
font = 32;
plots =2;
set(0,'defaultTextInterpreter','latex');
set(0, 'defaultAxesTickLabelInterpreter','latex');
set(0, 'defaultLegendInterpreter','latex');

%%%%%%%%%%%%%%%%%%%%%%Initial Parameters%%%%%%%%%%%%%%%%%%%%%%%%%%%%%%%%%%%%
D = 0:0.1:20; %%m - Distance sweep
n = 1.000268148;% Refractive Index
c = 3 * 10.^8; %m/s - Speed of light
N = 0;
sig= 2; % For a coverage factor k = 2 with a 95% Confidence Interval

%%% For 1.8 GHz modulation %%%%%%%%%%%%%%%%%%%%%%%%%%%%%%%%%%%%%%%%%%%%%%%%%
```

```
fcentral= 1.8; %GHz - Modulation Frequency
dfteste = 0.025; %GHz - Frequency shift magnitude
Rpp= 0.87;%deg - Phase Uncertainty

%%% For 3 GHz modulation with df = 7.4 MHz %%%%%%%%%%%%%%%%%%%%%%%%%%%%%%%%
% fcentral= 3; %GHz
% dfteste = 0.0074; %GHz
% Rpp = 0.06; %deg

%%% For 3 GHz modulation with df = 14.8 MHz %%%%%%%%%%%%%%%%%%%%%%%%%%%%%%%%
% fcentral= 3; %GHz
% dfteste = 0.0148; %GHz
 %Rpp = 0.27; %deg

fteste= ((fcentral) : dfteste : (fcentral+dfteste))*10.^9 ;

%% Uncertainty contributors
%%% Frequency uncertainty
Rff = 10^6;
Rf = fteste/Rff; %%Hz

R_n = 0.000000023 ;

Rp = (Rpp*pi)/180; %%rad Phase uncertainty
RDP = sqrt(2)*(Rpp*pi/180);
%% Phase Calculation %%%%%%%%%%%%%%%%%%%%%%%%%%%%%%%%%%%%%%%%%%%%%%%%%%%%%%

pt=[];
p1t=[];
dif_pt = [];
DNt = [];

for j =1:1:length(D)
    p1t(j,:) = 2*pi*(D(1,j)*2*n*fteste./(c));
    Nt(j,:)= floor(p1t(j,:)./(2*pi));
    pt(j,:) = p1t(j,:)/(2*pi) - Nt(j,:);
end


for j =1:1:length(D)
    for t = 1:1:(size(pt,2)-1)
       w =t+1;
       F_dif_pt(j,t) = pt(j,w) - pt(j,t);
       DNt(j,t) =  Nt(j,t) -Nt(j,w) ;
       RDf(t) = sqrt(Rf(t)^2 + Rf(w)^2);
    end
end


%% Distance Uncertainty Calculation  %%%%%%%%%%%%%%%%%%%%%%%%%%%%%%%%%%%%%%

ef = ((c./(2*n*(fteste).^2)).*(pt+Nt)).*Rf.*10.^(6); %%um
en = ((c./(2*fteste.*(n)^2)).*(pt+Nt)).*(R_n/2).*10.^(6); %%um
ep = (Rp*c./(4*pi*n*fteste))*10.^(6); %%um
et = sig*sqrt(ef.^2 + ep.^2 + en.^2); %%um
```

```
%% N Uncertainty Calculation  %%%%%%%%%%%%%%%%%%%%%%%%%%%%%%%%%%%%%%%%%%%%%

eDf =[];
eDp= [];
eff = ((F_dif_pt - DNt).*Rf(1:end-1))./(dfteste.*10^9);
epp = (Rp/(2*pi));


for j =1:1:(size(fteste,2)-1)
   w =j+1;
  eDf(:,j) = ((F_dif_pt(:,j) - DNt(:,j)).*fteste(1,w)*RDf)./(dfteste.*10^9)^2;
  eDp(:,j) = (RDP*fteste(1,w))./(2*pi*dfteste.*10^9);
end

eN = sig*sqrt(eff.^2 + eDp(1,:).^2+ epp.^2 + eDf.^2);


%% Plot %%%%%%%%%%%%%%%%%%%%%%%%%%%%%%%%%%%%%%%%%%%%%%%%%%%%%%%%%%%%%%%%%%

MAX = floor(max(max(et)))+1;
MIN = floor(min(min(et)));
figure('Renderer', 'painters', 'Position', [1 1 1324 619]);

%% Distance uncertainty %%%%%%%%%%%%%%%%%%%%%%%%%%%%%%%%%%%%%%%%%%%%%%%%%%%
h1=subplot(121);

set(h1,'Position', [0.09 0.18 0.374 0.723])
plot(D,et','-','LineWidth',4);
set(gca,'FontSize', font);
title("Analytical Simulation",'FontSize',titlefont, 'Position', [25 132 0]);
lgd11=legend(FF + ' GHz');
lgd11.FontSize= font-10;
lgd11.Location = 'northwest';
lgd11.Orientation= 'vertical';
xlim([min(D) max(D)]);
ylim([MIN MAX]);

yticks(MIN: 2 :MAX);

xlabel("Distance [m]",'FontSize',font);
ylabel("$U_{D}$ [$\mu$m]",'FontSize',font);
grid on;
xlim([10 20]);

%%% Components plot %%%%%%%%%%%%%%%%%%%%%%%%%%%%%%%%%%%%%%%%%%%%%%%%%%%%%%%
ax2 = axes('Position',[.239 .274 .213 .239]);
box on;
ep_dumb = ep(1)*ones(1,length(D));
plot(D, abs(2*ep_dumb),'-','LineWidth', 3,'MarkerSize',12, 'Color', 'k');
grid on;
hold(ax2,'on');
plot(D, abs(2*ef(:,1)),'-', 'LineWidth', 3, 'Color', 'magenta');
hold(ax2,'on');
plot(D, abs(2*en(:,1)),'-', 'LineWidth', 3);
```

```
title("Uncertainty Components (2$\sigma$) ",'FontSize',font-10);
lgd1=legend( '$|e^D_{\Delta \phi}|$','$|e^D_{f}|$','$|e^D_{n}|$');
lgd1.FontSize= font-8;
lgd1.Location = 'best';
lgd1.Orientation= 'horizontal';
set(gca,'FontSize', font-10); %Changes axis size
xlim([10 20]);

%% Ambiguity integer uncertainty %%%%%%%%%%%%%%%%%%%%%%%%%%%%%%%%%%%%%%%%%%%%%%%%
h2=subplot(122);

set(h2,'Position', [0.607 0.18 0.356 0.723])
plo1= plot(D, eN,'-','LineWidth',4);
lgd.Location = 'west';
lgd.Orientation= 'vertical';
set(gca,'FontSize', font);
xlabel("Distance [m]",'FontSize',font);
ylabel("$U_{N}$  ",'FontSize',font);
grid on;
lgd=legend(FF(1:end-1) + ' GHz');
lgd.FontSize= font-10;
lgd.Location = 'southeast';
lgd.Orientation= 'horizontal';
 xlim([10 20]);

%%% Components plot %%%%%%%%%%%%%%%%%%%%%%%%%%%%%%%%%%%%%%%%%%%%%%%%%%%%%%%%%%%%%
ax2 = axes('Position',[.638 .600 .213 .239]);
box on;
plot(D, abs(2*epp_dumb),'*-','LineWidth', 3,'MarkerSize',12);
hold(ax2,'on');
plot(D, abs(2*eff(:,1)),'-', 'LineWidth', 3);
hold(ax2,'on');
plot(D, abs(2*eDf(:,1)),'-','LineWidth', 3);
hold(ax2,'on');
plot(D, abs(2*eDp_dumb),'-','LineWidth', 3);
xlim([10 20]);
title("Uncertainty Components (2$\sigma$)",'FontSize',font-10);
set(gca,'FontSize', font-10); %Changes axis size
lgd=legend('$|e^N_{f}|$','$|e^N_{\Delta \phi}|$', '$|e^N_{\Delta ...
    f}|$','$|e^N_{\Delta \Phi}|$');%%
lgd.FontSize= font-8;
lgd.Location = 'best';
lgd.Orientation= 'vertical';
grid on;
```

Figure C.1: Script for the analytical distance and ambiguity integer uncertainty simulations in *Matlab 2017a*.

Appendix D

Phase shift processing

The raw phase shift measurements obtained through the *Agilent 53230A* were processed with a *Matlab 2017a* function that we developed, *"Distancia"*, figure D.1 and a script, figure D.2.

The raw files are comma separated files (.csv) identified through its name in the format *MediXXXmm_YY* where XXX is the position of the translation stage, and YY the number of the measurement set. The function *"Distancia"* would analyse a given measurement set, by setting its set number *YY* and determining the ambiguity integer and ADM with their respective expanded uncertainties for the different measured positions XXX.

By using the script in figure D.1 we could consider simultaneously the output result of the *"Distancia"* function for the measured positions per sets. It is in this code where the analysis presented in chapter 5 is performed.

```
function [DT, Nt1, eD, eN, DT_f0, Nt1_f0, eD_f0, eN0] = Distancia(files)
%%%%%%%%%%%%%%%%%%%%%%%%%%%%%%%%%%%%%%%%%%%%%%%%%%%%%%%%%%%%%%%%%%%%%%%%%%%%%%%%
% Function name: Distance Measurements Processing                              %
%                                                                              %
% Author: Nuno Miguel Cabecinhas Goncalves                                     %
%                                                                              %
% Date : 13/11/2020                                                            %
%                                                                              %
% Purpose: This function has the purpose to process a single set of ADM        %
%                                                                              %
% Version: V1 - 13/11/2020                                                     %
%                                                                              %
% INPUT - files - Integer in [0, 11], it is the identifier for each set of%
% measurements                                                                 %
%                                                                              %
% OUTPUT - DT - Measured distance for a 1.8 GHz modulation [m]                 %
%          Nt1 - Measured ambiguity integer for a 1.8 GHz modulation           %
%          eD - Measured distance expanded uncertainty for a 1.8 GHz           %
%          modulation with a coverage factor of k = 2, meaning a               %
%          confidence interval of 95% [um]                                     %
%          eN - Measured ambiguity integer expanded uncertainty for a          %
%          1.8 GHz with a coverage factor of k = 2, meaning a confidence       %
%          interval of  95% [um]                                               %
%          DT_f0 - Measured distance for a 1.825 GHz modulation [m]            %
%          Nt1_f0 - Measured ambiguity integer for a 1.825 GHz modulation      %
%          eD_f0 - Measured distance expanded uncertainty for a 1.825 GHz      %
```

```
%          modulation with a coverage factor of k = 2, meaning a          %
%          confidence interval of 95% [um]                                %
%          eN0 - Measured ambiguity integer expanded uncertainty for a    %
%          1.825 GHz with a coverage factor of k = 2, meaning a confidence%
%          interval of  95% [um]                                          %
%%%%%%%%%%%%%%%%%%%%%%%%%%%%%%%%%%%%%%%%%%%%%%%%%%%%%%%%%%%%%%%%%%%%%%%%%%%
set(0,'defaultTextInterpreter','latex');
set(0, 'defaultAxesTickLabelInterpreter','latex');
set(0, 'defaultLegendInterpreter','latex');

%%%%%%%%%%%%%%%%%%%%%%%%Initial Parameters%%%%%%%%%%%%%%%%%%%%%%%%%%%%%%%%%%%%
c = 3e08; %m/s - speed of light
n = 1.000264409;% Air refractive index
f0 = 1.825e09;% Hz
f1=1.8e09; % Hz
f=[f0,f1];
df=f0-f1;
Rf = [50 50];% Hz Frequency uncertainty
%%%%%%%%%%%%%%%%%%%%%%%%%%%%%%%%%%%%%%%%%%%%%%%%%%%%%%%%%%%%%%%%%%%%%%%%%%%


if files == 10
    index = string(files);
else
    index = "0" +string(files);
end


%% Extracting the Phase Shift information from the raw files
%%% Reference position D0
FILE0 = "100mm/Medi100mm_f0_"+ string(index)+".csv";
D0_f0 = csvread(FILE0);
FILE0 = "100mm/Medi100mm_f1_"+ string(index)+".csv";
D0_f1 = csvread(FILE0);

%%% Measured Positions
contador = 0;
 for i = linspace(90,0,10)
    contador= contador +1;
    if i == 100
    FILE1 =  string(i)+"mm/Medi"+ string(i)+"mm_f0_"+ string(index)+".csv";
    FILE11 =  string(i)+"mm/Medi"+ string(i)+"mm_f1_"+ string(index)+".csv";
    elseif (0 < i) && (i < 10)
    FILE1 =  string(i)+"0mm/Medi0"+ string(i)+"0mm_f0_"+ string(index)+".csv";
    FILE11 =  string(i)+"0mm/Medi0"+ string(i)+"0mm_f1_"+ string(index)+".csv";
    elseif i == 0
    FILE1 =  string(i)+"mm/Medi0"+ string(i)+"0mm_f0_"+ string(index)+".csv";
    FILE11 =  string(i)+"mm/Medi0"+ string(i)+"0mm_f1_"+ string(index)+".csv";
    else
    FILE1 = string(i)+"mm/Medi0"+ string(i)+"mm_f0_"+ string(index)+".csv";
    FILE11 =  string(i)+"mm/Medi0"+ string(i)+"mm_f1_"+ string(index)+".csv";
    end
    D1_f0(:,contador) = csvread(FILE1);
    D1_f1(:,contador) = csvread(FILE11);
end

```

```
%% Correct a data set when the measurement is close to 360 deg
d1_f1_out =find(std(D1_f1)>10);
d1_f0_out =find(std(D1_f0)>10);

if size(d1_f1_out,2) ≠ 0
    idx = find(D1_f1(:,d1_f1_out) <  mean(D1_f1(:,d1_f1_out))- ...
        std(D1_f1(:,d1_f1_out)));
    D1_f1(idx,d1_f1_out) = 0;
    idx1=find(D1_f1(:,d1_f1_out) ≠ 0);
    DMean =  mean(D1_f1(idx1,d1_f1_out));
    D1_f1(idx,d1_f1_out) = DMean;
end

if size(d1_f0_out,2) ≠ 0
    for i = 1:size(d1_f0_out,2)
        N360= find(D1_f0(:,d1_f0_out(i)) > 300);
        N000 = find(D1_f0(:,d1_f0_out(i)) ≤ 20);
        if length(N000) > length(N360)
            idx = find(D1_f0(:,d1_f0_out(i)) >  mean(D1_f0(:,d1_f0_out(i))));
        else
            idx = find(D1_f0(:,d1_f0_out(i)) <  mean(D1_f0(:,d1_f0_out(i))));
        end
    D1_f0(idx,d1_f0_out(i)) = 0;
    idx1=find(D1_f0(:,d1_f0_out(i)) ≠ 0);
    DMean =  mean(D1_f0(idx1,d1_f0_out(i)));
    D1_f0(idx,d1_f0_out(i)) = DMean;
    end
end

%% Calculate the ambiguity integer
Mean0_f0 = mean(D0_f0);
Mean0_f1 = mean(D0_f1);%- 23;
Mean1_f0= mean(D1_f0);
Mean1_f1= mean(D1_f1);%-23;

phase_f0= (([Mean0_f0,Mean1_f0]).*(pi/180))./(2*pi);%Normalized phase shift
% for 1.8 GHz frequency
phase_f1= (([Mean0_f1,Mean1_f1]).*(pi/180))./(2*pi);%Normalized phase shift
% for 1.825 GHz frequency

Dphase=zeros(size(phase_f0));
dN = Dphase;
Ds= Dphase;
Dm = Dphase;
for j = 1:size(phase_f0,2)
Dphase(j) = phase_f0(j) - phase_f1(j);
[s, m, b,sb, rx]= linreg(f, [phase_f0(j),phase_f1(j)]); %Linear fit
Ds(j) = s;
Dm(j)= b;
if s > 0
    dN(j) = 0;
else
    dN(j) = -1;
end
end
```

```
136
137 N0_f1 = (((Ds(1)- (dN(1)./df)).*f1)) - phase_f1(1);
138 N0_f0= N0_f1 - dN(1);
139
140 N1_f1 = (((Ds(2:end)- (dN(2:end)./df)).*f1)) - phase_f1(2:end);
141 N1_f0= N1_f1 - dN(2:end);
142
143 N_f1 =[N0_f1,N1_f1];
144 N_f0 =[N0_f0,N1_f0];
145 %%%%%% Frequency Counter Uncertainty %%%%%%%%%%%%%%%%%%%%%%%%%%%%%%%%%%%%%%
146
147 sig = 2;
148 df0 = (2e9 -f0);
149 df1= df0 +df;
150 % For IF = 200 MHz
151 SR_f0 = 2*pi*df0*5; % V/Hz
152 TE_f0 = sqrt((500e-6)^2 + (223.607e-6)^2)/SR_f0;% s
153 RU_f0 = sqrt((20e-12)^2 + TE_f0^2)*df0*360;% deg
154 SU_f0 = (5e-12 + 2*10e-12)*df0*360;% deg
155 % For IF = 175 MHz
156 SR_f1 = 2*pi*df1*5; %V/Hz
157 TE_f1 = sqrt((500e-6)^2 + (223.607e-6 )^2)/SR_f1;% s
158 RU_f1 = sqrt((20e-12)^2 + TE_f1^2)*df1*360; % deg
159 SU_f1 = (5e-12 + 2*10e-12)*df1*360; % deg
160
161 %% Phase shift combined uncertainty %%%%%%%%%%%%%%%%%%%%%%%%%%%%%%%%%%%%%%%
162
163 u_f1 = sqrt(([std(D0_f1),std(D1_f1)]./sqrt(100)).^2 + (RU_f1./sqrt(100))^2 + ...
        (SU_f1/2)^2); %deg for a 1.8 GHz modulation
164 u_f0 = sqrt(([std(D0_f0),std(D1_f0)]./sqrt(100)).^2 + (RU_f0./sqrt(100))^2 + ...
        (SU_f0/2)^2); %deg for a 1.825 GHz modulation
165
166 Rp=u_f1*(pi/180); %rads for a 1.8 GHz modulation
167 Rp_f0=u_f0*(pi/180); %rads for a 1.825 GHz modulation
168
169 %% Ambiguity integer expanded uncertainty calculation %%%%%%%%%%%%%%%%%%%%%%
170
171 RDp = sqrt((u_f0*pi/180).^2 + (u_f1.*pi/180).^2);%rads Phase shift difference ...
        uncertainty
172 RDf = sqrt((f1/10^6)^2 + (f0/10^6)^2 ); %Hz Frequency shift uncertainty
173
174 % For 1.8 GHz
175 ef1 = ((Dphase(1:end) - dN(1:end)).*Rf(2))./(df);
176 ep1 = (Rp(1:end)/(2*pi));
177 eDf1 = ((Dphase(1:end) -dN(1:end)).* f1 *RDf)./(df)^2;
178 eDp1 = (RDp(1:end)*f1)./(2*pi*df);
179 eN = sig*sqrt(ef1.^2 + eDp1.^2+ ep1.^2 + eDf1.^2);
180 % For 1.825 GHz
181 ef0 = ((Dphase - dN).*Rf(1))./(df);
182 ep0 = (Rp_f0/(2*pi));
183 eDf0 = ((Dphase -dN).* f0 *RDf)./(df)^2;
184 eDp0 = (RDp*f0)./(2*pi*df);
185 eN0 = sig*sqrt(ef0.^2 + eDp0.^2+ ep0.^2 + eDf0.^2);
186
187 %% Algorithm for ambiguity integer determination%%%%%%%%%%%%%%%%%%%%%%%%%%%%
```

```
%Searches within the confidence interval of the  measured N for an integer
%value

% For 1.8 GHz %%%%%%%%%%%%%%%%%%%%%%%%%%%%%%%%%%%%%%%%%%%%%%%%%%%%%%%%%%%%%%%%
Up_lim = N_f1 + eN;
Down_lim = N_f1 - eN;
FUp_lim = round(Up_lim);
FDown_lim = round(Down_lim);
Nt = zeros(size(N_f1));
intervalo_N=[Down_lim' , Up_lim'];
for i = 1:1:size(intervalo_N,1)
int=round(intervalo_N(i,1),4):1e-4:round(intervalo_N(i,2),4);
if floor(find(round(int(:)) == (int(:)) ==1)) == find((round(int(:)) == ...
    int(:)) ==1)
    dumbN = int(round(int(:)) == int(:));
    if length(dumbN) ≠ 1
    Nt(i) =  dumbN(1);
    else
        Nt(i) = dumbN;
    end
else
    dUp = FUp_lim(i) - N_f1(i);
    dDown = FDown_lim(i) - N_f1(i);
    if abs(dUp) < abs(dDown)
        Nt(i) = FUp_lim(i);
    else
         Nt(i) = FDown_lim(i);
    end
end
end

% For 1.825 GHz %%%%%%%%%%%%%%%%%%%%%%%%%%%%%%%%%%%%%%%%%%%%%%%%%%%%%%%%%%%%%%%%
Up_lim = N_f0 + eN0;
Down_lim = N_f0 - eN0;
FUp_lim = round(Up_lim);
FDown_lim = round(Down_lim);
Nt_f0 = zeros(size(N_f0));
intervalo_N=[Down_lim' , Up_lim'];
for i = 1:1:size(intervalo_N,1)
int=round(intervalo_N(i,1),4):1e-4:round(intervalo_N(i,2),4);
if floor(find(round(int(:)) == (int(:)) ==1)) == find((round(int(:)) == ...
    int(:)) ==1)
    dumbN = int(round(int(:)) == int(:));
    if length(dumbN) ≠ 1
    Nt_f0(i) =  dumbN(1);
    else
        Nt_f0(i) = dumbN;
    end
else
    dUp = FUp_lim(i) - N_f0(i);
    dDown = FDown_lim(i) - N_f0(i);
    if abs(dUp) < abs(dDown)
        Nt_f0(i) = FUp_lim(i);
    else
         Nt_f0(i) = FDown_lim(i);
```

```
    end
end
end

%% Distance determination%%%%%%%%%%%%%%%%%%%%%%%%%%%%%%%%%%%%%%%%%%%%%%%%%%%%

% For 1.8 GHz
 NormPH_f1 = phase_f1(1:end)-phase_f1(1);% deg - Remove the sensor's
 % reference in the phase measurement
 Nt1 = Nt -Nt(1); % Remove the sensor's reference in the ambiguity integer
 % measurement
 DT  = ((c)/(2*n*f1))*(NormPH_f1(1:end)+Nt1(1:end)); %m - Determine the ADM

 % For 1.825 GHz
 NormPH_f0 = phase_f0(1:end)-phase_f0(1);% deg - Remove the sensor's
 % reference in the phase measurement
 Nt1_f0 = Nt_f0 -Nt_f0(1);% Remove the sensor's reference in the ambiguity
 % integer measurement
 DT_f0  = ((c)/(2*n*f0))*(NormPH_f0(1:end)+ Nt1_f0(1:end));%m - Determine
 %the ADM

%% ADM expanded uncertainty calculation %%%%%%%%%%%%%%%%%%%%%%%%%%%%%%%%%%%%

Dif_Rp= sqrt(Rp(1)^2 + Rp.^2); %deg - Combined uncertainty of the reference
% and interest position phase shifts for 1.8 GHz
Dif_Rp_f0= sqrt(Rp_f0(1)^2 + Rp_f0.^2);%deg - Combined uncertainty of the
%reference and interest position phase shifts for 1.825 GHz

% Expanded uncertainty ADM for 1.8 GHz
eff = ((c./(2*n*f1.^2)).*(NormPH_f1+Nt1)).*Rf(2).*10.^(6); %um
epp = ((Dif_Rp.*c)./(4*pi*n*f1))*10.^(6); %um
eD = sig*sqrt(eff.^2 + epp.^2); %um

% Expanded uncertainty ADM for 1.825 GHz

eff_f0 = ((c./(2*n*f0.^2)).*(NormPH_f0+Nt1_f0)).*Rf(1).*10.^(6); %um
epp_f0 = ((Dif_Rp_f0.*c)./(4*pi*n*f0))*10.^(6); %um
eD_f0 = sig*sqrt(eff_f0.^2 + epp_f0.^2); %um
```

Figure D.1: Function in *Matlab 2017a* for processing a single set of phase shift measurements.

```
%%%%%%%%%%%%%%%%%%%%%%%%%%%%%%%%%%%%%%%%%%%%%%%%%%%%%%%%%%%%%%%%%%%%%%%%%%%%
% Program name:Distance Measurements Processing (Example for the           %
%[0, 100] mm )                                                             %
%                                                                          %
% Author: Nuno Miguel Cabecinhas Goncalves                                 %
%                                                                          %
% Date : 13/11/2020                                                        %
%                                                                          %
% Purpose: This code has the purpose to process the multiple sets of phase%
% shift measurements in order to obtain an ambiguity integer measurement  %
% and absolute distance measurement                                        %
%                                                                          %
% Version: V1 - 13/11/2020                                                 %
```

```
%%%%%%%%%%%%%%%%%%%%%%%%%%%%%%%%%%%%%%%%%%%%%%%%%%%%%%%%%%%%%%%%%%%%%%%%%%%%%%%%
clear;
close all;
plots= 1;
titlefont=40;
font = 32;
set(0,'defaultTextInterpreter','latex');
set(0, 'defaultAxesTickLabelInterpreter','latex');
set(0, 'defaultLegendInterpreter','latex');

%%%%%%%%%%%%%%%%%%%%%%%%Initial Parameters%%%%%%%%%%%%%%%%%%%%%%%%%%%%%%%%%%%%%%%

L_real = 0:10:100;%mm
DT = zeros(10,11);
Nt=DT;
eD=DT;
DT_f0 =DT;
eD_f0=DT;
Nt1_f0=DT;
eN0=DT;
eN=DT;
contador = 0;

%% Extract the different necessary quantities with the function "Distancia"
for i = 0:1:10
    if i == 6
        continue
    else
        contador = contador +1;
    [DT(contador,:), Nt(contador,:), ...
        eD(contador,:),eN(contador,:),DT_f0(contador,:),Nt1_f0(contador,:),eD_f0(contador,:),eN
        = Distancia(i);

    end

end
%% Expected ambiguity integer for the [0, 100] mm range %%%%%%%%%%%%%%%%%%%%

Ntdumb= [0 0 0 0 0 0 0 0 1 1 1]; % For 1.8 GHz
Nt_f0dumb= [0 0 0 0 1 1 1 1 1 1 1]; % For 1.825 GHz

%%%%%%%%%%%%%%%%%%%%%%%%%%%%%%%%%%%%%%%%%%%%%%%%%%%%%%%%%%%%%%%%%%%%%%%%%%%%%%%%

meanDT =zeros(1,11);
meanDT_f0 = meanDT;

%% Remove the outlier N measurements %%%%%%%%%%%%%%%%%%%%%%%%%%%%%%%%%%%%%%%%%%
for i = 1:1:size(DT,2)

    id = find(Nt(:,i) == Ntdumb(i));
    meanDT(i) = mean(DT(id,i)); % For 1.8 GHz
    id0 = find(Nt1_f0(:,i) == Nt_f0dumb(i));
    meanDT_f0(i) = mean(DT_f0(id0,i)); % For 1.825 GHz

end
```

```
67 %% Linear fit of the measured distances  %%%%%%%%%%%%%%%%%%%%%%%%%%%%%%%%%%%%
68
69 x =(0:0.01:100);
70 [s, m, b,sb, rx] = linreg(L_real, meanDT*10^3); % For 1.8 GHz
71 y = x.*s +b;
72 [s0, m0, b0,sb0, rx0] = linreg(L_real,meanDT_f0*10^3); % For 1.825 GHz
73 y0 = x.*s0 +b0;
74
75 %% Correction of the Distance measurements %%%%%%%%%%%%%%%%%%%%%%%%%%%%%%%%%%%%
76
77 DT_fit = (meanDT*10^3-b)./s; % For 1.8 GHz
78 DT_fitf0 = (meanDT_f0*10^3-b0)./s0; % For 1.825 GHz
79
80 %% Absolute and relative error %%%%%%%%%%%%%%%%%%%%%%%%%%%%%%%%%%%%%%%%%%%%%%%
81
82 mDT = mean(DT)*10^3; % For 1.8 GHz
83 mDTf0= mean(DT_f0)*10^3; % For 1.825 GHz
84
85 ErroAbs_f1C = abs(DT_fit(1:end) -L_real(1:end)); % For 1.8 GHz
86 ErroAbs_f0C = abs(DT_fitf0(1:end) -L_real(1:end)); % For 1.825 GHz
87
88 ErroRel_f1C = ErroAbs_f1C./L_real; % For 1.8 GHz
89 ErroRel_f0C = ErroAbs_f0C./L_real; % For 1.25 GHz
90
91 ErroAbs_f1 = abs(meanDT*10^3-L_real);  % For 1.8 GHz
92 ErroAbs_f0 = abs(meanDT_f0*10^3-L_real); % For 1.825 GHz
93
94 ErroRel_f1 = ErroAbs_f1./L_real; % For 1.8 GHz
95 ErroRel_f0 = ErroAbs_f0./L_real; % For 1.825 GHz
96
97
98 %% Plots %%%%%%%%%%%%%%%%%%%%%%%%%%%%%%%%%%%%%%%%%%%%%%%%%%%%%%%%%%%%%%%%%%%%%
99
100 if plots ==1
101
102 %%%%%%%%%%%%%%%%%%%%%%%%%%%%%%%%%%%%%%%%%%%%%%%%%%%%%%%%%%%%%%%%%%%%%%%%%%%%
103
104 f1= figure('Renderer', 'painters', 'Units', 'centimeters', 'Position', [1 1 ...
        21 28.5]);
105
106 for i = 1:1:size(DT,2)
107     lim=(i-1)*10;
108
109     subplot(6,2,i)
110
111     errorbar(1:1:size(DT,1),DT(:,i)*10^3,eD(:,i)*10^-3,'vertical','-*', ...
            'LineWidth', 2, 'MarkerSize',8);
112     hold on; ...
            errorbar(1:1:size(DT,1),DT_f0(:,i)*10^3,eD_f0(:,i)*10^-3,'vertical','-*', ...
            'LineWidth', 2, 'MarkerSize',8);
113     hold on; plot(lim*ones(1,size(DT,1)),'--','LineWidth',5);
114
115     set(gca,'FontSize', font-14)
116     xlabel("Measurement Number",'fontsize',font-14);
117     ylabel("Distance [mm] ", 'fontsize',font-16);
```

```
118
119 if lim == 0
120         ylim([-0.7 0.7])
121 elseif lim == 70
122      ylim([(lim -1) (lim +1)]);
123 else
124     ylim([(lim -0.5) (lim +1.2)]);
125 end
126
127
128 xlim([0 11]);
129     grid on;
130     xticks(1 :1: 10);
131 end
132
133 lgd=legend('1.8 GHz','1.825 GHz', 'Theoretical Value');
134     lgd.FontSize= font-12;
135     lgd.Location = 'bestoutside';
136     lgd.Orientation= 'vertical';
137  lgd.Position = [0.616 0.113 0.223 0.106]; % position is an array of [x y l h ]
138   set(gcf, 'PaperUnits', 'centimeters');
139 set(gcf, 'PaperType', 'A4');
140 print(f1,'ADMmeasurement_100mm_Rep','-depsc')
141 movefile('ADMmeasurement_100mm_Rep.eps', ...
        '/Users/nunogonc/Desktop/Tese/TESE_LATEx/Figuras/CH5');
142
143
144 %%%%%%%%%%%%%%%%%%%%%%%%%%%%%%%%%%%%%%%%%%%%%%%%%%%%%%%%%%%%%%%%%%%%%%%%%%%%%%%
145
146 f=figure('Renderer', 'painters', 'Units', 'centimeters', 'Position', [1 1 21 ...
        28.5]);
147 for i = 1:1:size(DT,2)
148     subplot(6,2,i)
149     plot(1:1:size(DT,1),Nt(:,i),'-*', 'LineWidth', 2, 'MarkerSize',8);
150     hold on; plot(Ntdumb(i)*ones(1,size(DT,1)),'--','LineWidth',5);
151
152    set(gca,'FontSize', font-14)
153     xlabel("Measurement Number",'fontsize',font-14);
154     ylabel(" N ", 'fontsize',font-14);
155     title("\textbf{Position = "+string(L_real(i))+" mm}",'fontsize',font-14)
156  if i == 9
157      ylim([0.9 1.1]);
158
159  elseif i == 4 || i == 6
160          ylim([-1.5 0.75]);
161           yticks(-1:1:1);
162  elseif i > 9
163      ylim([0.25 2.75]);
164       yticks(1:1:2);
165
166  else
167         ylim([-0.1 0.1]);
168
169  end
170
```

```
171
172 xlim([0 11]);
173     grid on;
174     xticks(0 :1: 10);
175 end
176
177 lgd=legend('1.8 GHz', 'Theoretical Value');
178     lgd.FontSize= font-12;
179     lgd.Location = 'bestoutside';
180     lgd.Orientation= 'vertical';
181    lgd.Position = [0.616 0.113 0.223 0.073];
182
183 set(gcf, 'PaperUnits', 'centimeters');
184 set(gcf, 'PaperType', 'A4');
185 print(f,'Nmeasurement_100mm_Rep','-depsc')
186 movefile('Nmeasurement_100mm_Rep.eps', ...
        '/Users/nunogonc/Desktop/Tese/TESE_LATEx/Figuras/CH5');
187
188 %%%%%%%%%%%%%%%%%%%%%%%%%%%%%%%%%%%%%%%%%%%%%%%%%%%%%%%%%%%%%%%%%%%%%%%%%%%%
189
190 elseif plots == 2
191
192 %%%%%%%%%%%%%%%%%%%%%%%%%%%%%%%%%%%%%%%%%%%%%%%%%%%%%%%%%%%%%%%%%%%%%%%%%%%%
193 figure('Renderer', 'painters', 'Position', [1 1 992 752]);
194 subplot(3,1,[1 2],'Position',[0.13,0.435,0.775,0.49]);
195 errorbar(L_real,mean(DT)*10^3,mean(eD)*10^-3,'vertical','-*', 'LineWidth', 2, ...
        'MarkerSize',8)
196 hold on;  errorbar(L_real,mean(DT_f0)*10^3,mean(eD_f0)*10^-3,'vertical','-*', ...
        'LineWidth', 2, 'MarkerSize',8)
197 hold on;  plot(L_real,L_real,'--', 'LineWidth', 4)
198
199 ylim([0 100]);
200 set(gca,'FontSize', font)
201 title("Average ADM for a [0, 100] mm range",'fontsize',titlefont);
202
203     xlabel("Real Distance [mm]",'fontsize',font);
204     ylabel("Mean Measured Distance [mm] ", 'fontsize',font);
205
206 lgd=legend('1.8 GHz','1.825 GHz', 'Theoretical Value');
207     lgd.FontSize= font;
208     lgd.Location = 'southeast';
209     lgd.Orientation= 'vertical';
210
211 grid on;
212 hold off;
213 [plo,z, p]=zoomPlot(L_real,L_real,[39.5 40.5],[39 41.0],[.194 .679 .213 .212]);
214 p.LineStyle='--';
215 p.LineWidth=4;
216 p.Color= [0.9290 0.6940 0.1250];
217 hold on;errorbar(L_real,mean(DT)*10^3,mean(eD)*10^-3,'vertical','-*', ...
        'LineWidth', 2, 'MarkerSize',8, 'Color' ,[0 0.4470 0.7410]);
218 hold on;errorbar(L_real,mean(DT_f0)*10^3,mean(eD_f0)*10^-3,'vertical','-*', ...
        'LineWidth', 2, 'MarkerSize',8, 'Color' ,[0.8500 0.3250 0.0980]);
219  set(gca,'FontSize', font-2)
220 grid on;
```

```

subplot(313);
plot(L_real,mean(eD),'-*','LineWidth',3,'MarkerSize',8);
hold on; plot(L_real,mean(eD_f0),'-*','LineWidth',3,'MarkerSize',8);
 lgd=legend('1.8 GHz','1.825 GHz');
    lgd.FontSize= font;
    lgd.Location = 'best';
    lgd.Orientation= 'horizontal';

xticks(0 :10: 100);
xlabel("Real Distance [mm]",'fontsize',font);
ylabel(" $\overline{U_D}$[$\mu$m]", 'fontsize',font);
set(gca,'FontSize', font)
grid on;


%%%%%%%%%%%%%%%%%%%%%%%%%%%%%%%%%%%%%%%%%%%%%%%%%%%%%%%%%%%%%%%%%%%%%%%%%%%

figure('Renderer', 'painters', 'Position', [1 1 1275 724])
subplot(121)
plot(x,y,'-','LineWidth', 4);
hold on;  errorbar(L_real,meanDT.*10^3,mean(eD)*10^-3,'vertical','-*', ...
    'LineWidth', 2, 'MarkerSize',8)
hold on;  plot(L_real,L_real,'--', 'LineWidth', 4)
 hold on; errorbar(L_real,DT_fit,mean(eD)*10^-3,'vertical','-*', 'LineWidth', ...
     2, 'MarkerSize',8)
 set(gca,'FontSize', font)
title("Calibration Curves",'fontsize',titlefont, 'position', [117.726 100.691 ...
    0]);
ylim([0 100]);

    xlabel("Real Distance [mm]",'fontsize',font);
    ylabel(" Measured Distance [mm] ", 'fontsize',font);

lgd=legend('Calibration Curve ','1.8 GHz', 'Theoretical Value','Corrected ...
    Values');
    lgd.FontSize= font;
       lgd.Location = 'best';
    lgd.Orientation= 'vertical';

grid on;

%%% Inlets
hold off;
[plo,z, p]=zoomPlot(L_real,L_real,[39.5 40.5],[39 41.0],[0.171 0.659 0.111 ...
    0.209]);
p.LineStyle='--';
p.LineWidth=4;
p.Color= [0.9290 0.6940 0.1250];
hold on;plot(x,y0,'-','LineWidth', 4,'Color' ,[0, 0.4470, 0.7410]);
hold on;errorbar(L_real,meanDT.*10^3,mean(eD)*10^-3,'vertical','-*', ...
    'LineWidth', 2, 'MarkerSize',8, 'Color' ,[0.8500, 0.3250, 0.0980]);

hold on;errorbar(L_real,DT_fit,mean(eD)*10^-3,'vertical','-*', 'LineWidth', ...
    2, 'MarkerSize',8,'Color' ,[0.4940, 0.1840, 0.5560]);
```

```
 set(gca,'FontSize', font-2)
grid on;

subplot(122)

plot(x,y0,'-','LineWidth', 4);
hold on;  errorbar(L_real,meanDT_f0.*10^3,mean(eD_f0)*10^-3,'vertical','-*', ...
    'LineWidth', 2, 'MarkerSize',8)
hold on;  plot(L_real,L_real,'--', 'LineWidth', 4)
hold on; errorbar(L_real,DT_fitf0,mean(eD_f0)*10^-3,'vertical','-*', ...
    'LineWidth', 2, 'MarkerSize',8)

ylim([0 100]);
set(gca,'FontSize', font)
xlabel("Real Distance [mm]",'fontsize',font);
ylabel(" Measured Distance [mm] ", 'fontsize',font);

lgd=legend('Calibration Curve ','1.825 GHz', 'Theoretical Value','Corrected ...
    Values');
    lgd.FontSize= font;
    lgd.Location = 'best';
    lgd.Orientation= 'vertical';

%%% Inlets
grid on;
hold off;
[plo,z, p]=zoomPlot(L_real,L_real,[39.5 40.5],[39 41.0],[0.63 0.688 0.111 ...
    0.209]);
p.LineStyle='--';
p.LineWidth=4;
p.Color= [0.9290 0.6940 0.1250];
hold on;plot(x,y0,'-','LineWidth', 4,'Color' ,[0, 0.4470, 0.7410]);
hold on;errorbar(L_real,meanDT_f0.*10^3,mean(eD_f0)*10^-3,'vertical','-*', ...
    'LineWidth', 2, 'MarkerSize',8, 'Color' ,[0.8500, 0.3250, 0.0980]);
hold on;errorbar(L_real,DT_fitf0,mean(eD)*10^-3,'vertical','-*', 'LineWidth', ...
    2, 'MarkerSize',8,'Color' ,[0.4940, 0.1840, 0.5560]);
set(gca,'FontSize', font-2)
grid on;

%%%%%%%%%%%%%%%%%%%%%%%%%%%%%%%%%%%%%%%%%%%%%%%%%%%%%%%%%%%%%%%%%%%%%%%%%%%%

elseif plots==3

%%%%%%%%%%%%%%%%%%%%%%%%%%%%%%%%%%%%%%%%%%%%%%%%%%%%%%%%%%%%%%%%%%%%%%%%%%%%

ErrorRelPlo=figure('Renderer', 'painters', 'Position', [1 1 1236 620]);

subplot(121)
bar1= bar(L_real(1:end),[(ErroRel_f1C*10^2)' (ErroRel_f1*10^2)'],'BarWidth',1.2);
bar1(1).FaceColor= [0 0.4470 0.7410];
bar1(2).FaceColor= [0.8500 0.3250 0.0980];
set(gca,'FontSize', font)
lgd=legend('Corrected', 'Original');
title(lgd,'1.8 GHz')
    lgd.FontSize= font-4;
```

```
318      lgd.Location = 'northeast';
319      lgd.Orientation= 'vertical';
320  xlim([5 105]);
321  xticks(0 :20: 100);
322  set(gca, 'YScale', 'log')
323  xlabel("Real Distance [mm]",'fontsize',font);
324  ylabel("Relative Error [$\%$] ", 'fontsize',font);
325  title("ADM Relative Error",'fontsize',titlefont, 'position', [121.971 10.479 0]);
326
327  grid on;
328
329  subplot(122)
330
331  bar1= bar(L_real(1:end),[(ErroRel_f0C*10^2)' (ErroRel_f0*10^2)'],'BarWidth',1.2);
332  bar1(1).FaceColor= [0 0.4470 0.7410];
333  bar1(2).FaceColor= [0.8500 0.3250 0.0980];
334
335  lgd=legend('Corrected', 'Original');
336  title(lgd,'1.825 GHz')
337      lgd.FontSize= font-4;
338      lgd.Location = 'northeast';
339      lgd.Orientation= 'vertical';
340   xlim([5 105]);
341    xticks(0 :20: 100);
342
343  xlabel("Real Distance [mm]",'fontsize',font);
344  ylabel("Relative Error [$\%$] ", 'fontsize',font);
345  set(gca,'FontSize', font)
346  set(gca, 'YScale', 'log')
347  grid on;
348
349  set(gcf, 'PaperUnits', 'centimeters');
350  set(gcf, 'PaperType', 'A4');
351  print(ErrorRelPlo,'RelativeError_100mm','-depsc')
352  movefile('RelativeError_100mm.eps', ...
         '/Users/nunogonc/Desktop/Tese/TESE_LATEx/Figuras/CH5');
353
354
355  %%%%%%%%%%%%%%%%%%%%%%%%%%%%%%%%%%%%%%%%%%%%%%%%%%%%%%%%%%%%%%%%%%%%%%%%%%%%%%%%
356  else
357
358  ErrorAbsPlo=figure('Renderer', 'painters', 'Position', [1 1 1236 620]);
359
360  subplot(121)
361  plot(L_real(1:end),(ErroAbs_f1C).*10^3, '-*', 'LineWidth', 2, 'MarkerSize',8, ...
         'Color',[0 0.4470 0.7410]);
362  hold on; plot(L_real(1:end), ones(1,11).*mean(ErroAbs_f1C).*10^3, '--', ...
         'LineWidth', 4, 'Color',[0 0.4470 0.7410]);
363  hold on;plot(L_real(1:end), (ErroAbs_f1).*10^3, '-*', 'LineWidth', 2, ...
         'MarkerSize',8, 'Color',[0.8500 0.3250 0.0980]);
364  hold on; plot(L_real(1:end), ones(1,11).*mean(ErroAbs_f1).*10^3, '--', ...
         'LineWidth', 4, 'Color',[0.8500 0.3250 0.0980]);
365
366  lgd=legend('Corrected','Mean', 'Original','Mean');
367  title(lgd,'1.8 GHz')
```

```
368      lgd.FontSize= font-5;
369      lgd.Location = 'northeast';
370      lgd.Orientation= 'vertical';
371
372  set(gca,'FontSize', font)
373  xlabel("Real Distance [m]",'fontsize',font);
374  ylabel("Absolute Error [$\mu$m]", 'fontsize',font);
375  title("ADM Absolute Error",'fontsize',titlefont, 'position', [120 505 0]);
376
377  grid on;
378
379  subplot(122)
380
381  plot(L_real(1:end),(ErroAbs_f0C).*10^3, '-*', 'LineWidth', 2, 'MarkerSize',8, ...
         'Color',[0 0.4470 0.7410]);
382  hold on; plot(L_real(1:end), ones(1,11).*mean(ErroAbs_f0C).*10^3, '--', ...
         'LineWidth', 4, 'Color',[0 0.4470 0.7410]);
383  hold on;plot(L_real(1:end), (ErroAbs_f0).*10^3, '-*', 'LineWidth', 2, ...
         'MarkerSize',8, 'Color',[0.8500 0.3250 0.0980]);
384  hold on; plot(L_real(1:end), ones(1,11).*mean(ErroAbs_f0).*10^3, '--', ...
         'LineWidth', 4, 'Color',[0.8500 0.3250 0.0980]);
385  lgd=legend('Corrected','Mean', 'Original','Mean');
386  title(lgd,'1.825 GHz')
387      lgd.FontSize= font-5;
388      lgd.Location = 'north';
389      lgd.Orientation= 'vertical';
390      lgd.Position=[0.732 0.641 0.121 0.273];
391  set(gca,'FontSize', font)
392  xlabel("Real Distance [m]",'fontsize',font);
393  ylabel("Absolute Error [$\mu$m]", 'fontsize',font);
394  grid on;
395  set(gcf, 'PaperUnits', 'centimeters');
396  set(gcf, 'PaperType', 'A4');
397  print(ErrorAbsPlo,'AbsoluteError_100mm','-depsc')
398  movefile('AbsoluteError_100mm.eps', ...
         '/Users/nunogonc/Desktop/Tese/TESE_LATEx/Figuras/CH5');
399
400
401  end
```

Figure D.2: Script in *Matlab 2017a* for processing the multiple set of phase shift measurements and perform its correction and error analysis.